Stony Brook University

Organic/Biological Hybrid Nanomaterials for Biosensing and Energy Conversion: from Fundamentals to Applications

A Dissertation presented

by

Zhongwei Liu

to

The Graduate School

in Partial Fulfillment of the

Requirements

for the Degree of

Doctor of Philosophy

in

Materials Science and Engineering

Stony Brook University

December 2014

Stony Brook University

The Graduate School

Zhongwei Liu

We, the dissertation committe for the above candidate for the

Doctor of Philosophy degree, hereby recommend

acceptance of this dissertation

Mircea Cotlet - Dissertation Advisor
Adjunct Professor, Materials Science and Engineering at Stony Brook University
Scientist, Center for Functional Nanomaterials, Brookhaven National Laboratory

Dillip Gersappe - Chairperson of Defense
Professor, Materials Science and Engineering at Stony Brook University

T. A. Venkatesh - Committe Member of Defense
Associate Professor, Materials Science and Engineering at Stony Brook University

Helmut Strey - Outside Committe Member of Defense
Associate Professor, Biomedical Engineering at Stony Brook University

This dissertation is accepted by the Graduate School

Charles Taber
Dean of the Graduate School

Abstract of the Dissertation

Organic/Biological Hybrid Nanomaterials for Biosensing and Energy Conversion: from Fundamentals to Applications

by

Zhongwei Liu

Doctor of Philosophy

in

Materials Science and Engineering

Stony Brook University

2014

Water-soluble conjugated polymers have emerged as cost-effective, light harvesting materials for the development of highly sensitive and selective biosensing platforms where the detection of a target is recognized through changes in the spectroscopic properties of the conjugated polymer. My dissertation describes fundamental studies of interaction in water-soluble conjugated polymers/DNA organic/biological hybrids and the application of such hybrids in DNA sensing and energy conversion. In particular, I demonstrated a conjugated poly(phenylene vinylene (PPV)/DNA hybrid with sequence dependent photoluminescence and chiroptical properties, for which the PPV's photoluminescence was found to be enhanced as high as seven fold upon binding with DNA. These sequence specific spectroscopic and structural changes resulted from hydrophobic interactions in the form of π-π stacking between the PPV's backbone and DNA bases. In this study I also demonstrated the importance of electrostatic interactions between PPV's charged side groups and DNA phosphate backbone in promoting hydrophobic interactions leading to sequence specific properties of the hybrid. I then developed a label-free DNA sensor based on F*ö*rster Resonant Energy Transfer (FRET) between a water soluble PPV and an intercalating dye, malachite green chloride where

the detection of target DNA is read through FRET sensitized fluorescence of the intercalated dye. In the proposed sensor, the PPV bound to DNA experiences photoluminescence enhancement due to a chain conformation change induced by DNA and this enhancement provides improved FRET efficiency and increased FRET sensitized fluorescence from the intercalated dye, the transducing signal for the DNA sensor. Moreover, the particular small dye used by me intercalates hybridized DNA at a maximum, one-to-one dye-to-base pair ratio, which in combination with the FRET sensitization provides a wide range for base pair mismatch detection, from one up to five base pair mismatches for 25 mer single stranded DNA probe and target. Finally, I demonstrated the ability of DNA to promote photoinduced charge transfer between same-charge sign, cationic donor and acceptor moieties, here PPV and fullerene, with efficiencies approaching those observed for oppositely charged donor and acceptor molecules with similar backbones and without DNA. In this same study I also demonstrated the ability to tune the charge transfer rate between same charge type donor and acceptor molecules by replacing single stranded DNA with double stranded (hybridized) DNA and I provided a detailed description of the mechanisms of quenching by charge transfer for the studied donor-acceptor hybrids.

Dedication

To my family

Table of Contents

List of Figures

List of Tables

List of Abbreviations

PL	Photoluminescence
FRET	Förster resonant energy transfer
ssDNA	Single stranded DNA
dsDNA	Double stranded DNA
PPy	Polypyrrole
PANI	Polyanilines
PEDOT	Poly(3,4-thylenedioxythiophene)
PT	Polythiophene
PA	Polyacetylene
PP	Poly(phenylene)
PF	Polyfluorene
OPV	Organic photovoltaic
OFET	Organic field effect transistor
OLED	Organic light emitting diode
WSCP	Water soluble conjugated polymer
ACP	Anionic conjugated polymer
CCP	Cationic conjugated polymer

NCP	Nonionic conjugated polymer
PPE	Poly(p-phenylene ethynylene)
PCR	Polymerase chain reaction
GMR	Giant magneto resistance
PCT	Photo-induced charge transfer
QTL	Quench-tether-ligand
PPi	Pyrophosphate
SPR	Surface plasmon resonance
BP	Base pair
PNA	Peptide nucleic acid
EB	Ethidium bromide
DLS	Dynamic light scattering
FCS	Fluorescence correlation spectroscopy
C_{60}	Fullerene
C-C_{60}	Cationic fullerene
A-C_{60}	Anionic fullerene
HOMO	Highest occupied molecular orbital
LUMO	Lowest unoccupied molecularorbital
D-A	Donor-acceptor
MGC	Malachite green chloride
LMG	Leuco malachite green
UV-vis	Ultra violate-visible
CD	Circular dichroism
TCSPC	Time-correlated single photon counting

PM	Photomultiplier
CFD	Constant function discriminator
TAC	Time-to-amplitude converter
PGA	Programmable gain amplifier
ADC	Analog-to-digital converter
WD	Window discriminator
C-PPV	Cationic poly(p-phenylene vinylene)
A-PPV	Anionic poly(p-phenylene vinylene)
N-PPV	Nonionic poly(p-phenylene vinylene)
PVSA	Poly(vinylsulfonic acid, sodium salt)
PBS	Phosphate buffered saline
QY	Quantum yield
A	Adenine
C	Cytosine
G	Guanine
T	Thymine
SV	Stern-Volmer

Acknowledgments

First of all, I would like to express my sincere gratitude to my advisor, Dr. Mircea Cotlet. Without his kind guidance, I would not achieve where I am today. From his mentorship, I learned how research work should be carried out. Thanks to his passion and encouragement, I can keep motivated to solve problems in my research. I feel lucky to have him as my Ph.d advisor.

I would thank Dr. Hsing-Lin Wang in Los Alamos National Laboratory for generously providing water soluble conjugated polymers and fullerenes, which are critical for my research.

I appreciate Dr. Paul I. Freimuth's kind help on expression and purification of proteins.

I would thank my groupmates: Drs. Zhihua Xu, Huidong Zang and Mr. Prahlad Kumar Routh for their helpful advice and discussion, especially for Mr. Prahlad Kumar Routh's assistance for modeling and fitting in my research.

I also thank Soft/Bio Materials Group: Dr. Oleg Gang, Dr. Cheng Chi, Dr. Fang Lu, Dr. Dmytro Nykypanchuk, Dr. Kevin Yager, Dr. Yugang Zhang, Dr. Wenyan Liu, Mr. Ye Tian. I enjoyed being a member of such a brilliant group.

I would thank all my friends, with whom I carpool to lab, play tennis, go to skiing, hang out and have a lot of fun. Thank you, guys! You know who you are.

Research carried out in part at the Center for Functional Nanomaterials, Brookhaven National Laboratory, which is supported by the U.S. Department of Energy, Office of Basic Energy Sciences, under Contract No. DE-AC02-98CH10886.

Chapter 1

Introduction

1.1 Water Soluble Conjugated Polymers

Conjugated polymers (CPs) have been widely used in plastic optoelectronic devices, such as organic photovoltatics (OPVs), organic field effect transistors (OFETs) and organic light emitting diodes (OLEDs), owing to their efficient absorption and emission properties, easy and cost-effective synthesis, and their esy mechanical processability. [1–5] Structurally, CPs contain two parts, a conjugated backbone and side groups. (Figure1.1) After light absorption, CPs can generate delocalized excitons, or Coulombically bound electron/hole pairs formed in the π-conjugation system of the backbone. Such excitons can readily move in the conjugation system along the polymer chain (intra-chain) and/or among stacks of polymer chains (inter-chain). Upon reaching an energy trap, excitons can decay by various paths such as thermal vibrations, photoluminescence (PL) emission, F*ö*rster resonance energy transfer (FRET) to energy acceptors, or charge transfer to electron/hole acceptors. Similar to the doping of semiconductive materials, CPs of n-type or p-type can be produced by reduction or oxidation of π-system electrons. [2,4,5] With relatively good charge mobility and good mechanical properties, CPs are expected to substitute the more expensive materials such as monocrystalline silicon in solar panels. The opto-electronic properties of a CP strongly depend on the chain conformation and aggregation state of the polymer. [6–8]To satisfy different application requirements, CPs with different designs of backbones and side chains have been synthesized and some examples of organic soluble CPs are

shown in Figure 1.1. Organic light emitting diodes have been built with CPs with

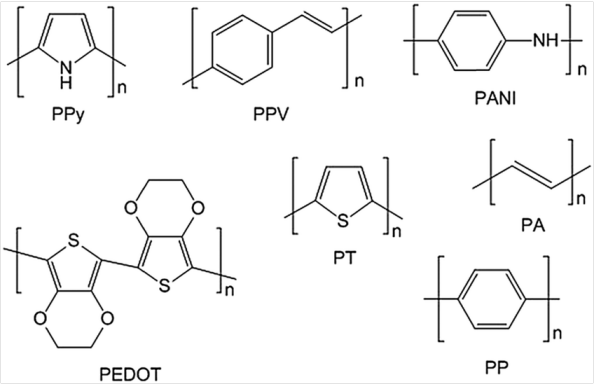

Figure 1.1. Examples of Conjugated Polymers: polypyrrole (PPy), Poly(p-phenylene vinylene)(PPV), polyanilines (PANI), poly(3,4-ethylenedioxythiophene) (PEDOT), polythiophenes (PT), polyacetylenes (PA), poly(phenylene) (PP), polyfluorene (PF). Reprinted with permission from Ref [9] Copyright (2014) The Royal Society of Chemistry.

emission colors covering the entire visible spectrum while CP-based photovoltaic devices have achieved over 11% light-to-energy conversion efficiency. [3–5,10] There are comprehensive reviews on the utilization of various types of CPs both in solar cell and in light emitting diode applications, exemplifying synthetic and morphological approaches taken at improving the performance of such devices as well spectroscopic characterization of charge transport in such materials. [8, 11, 12]To enhance the efficiency of energy conversion in OPVs and OLEDs, detailed studies have been performed on light absorption, charge generation and separation, and collection of charge carriers at electrodes. [6, 7] The exciton migration and charge mobility have been studied either along single polymer chains by single particle methods or in solvent-casted polymer films incorporated in devices. [13–17]

Functionalization of CPs with hydrophilic side groups renders water solubility, opening the possibility to develop various chemical/biological sensors. [18–21] Among other applications, CPs have been prepared into nanoparticles/dots (CPNs/CP-dots) for in vivo/vitro imaging assays. [22] Compared to organic dyes and quantum dots, CPNs and CP-dots possessed higher photostability and lower toxicity. [23–27]

The CPs used in the fabrication of organic optoelectronic devices are usually dispensable in non-polar organic solvents and insoluble in polar solvents like water.

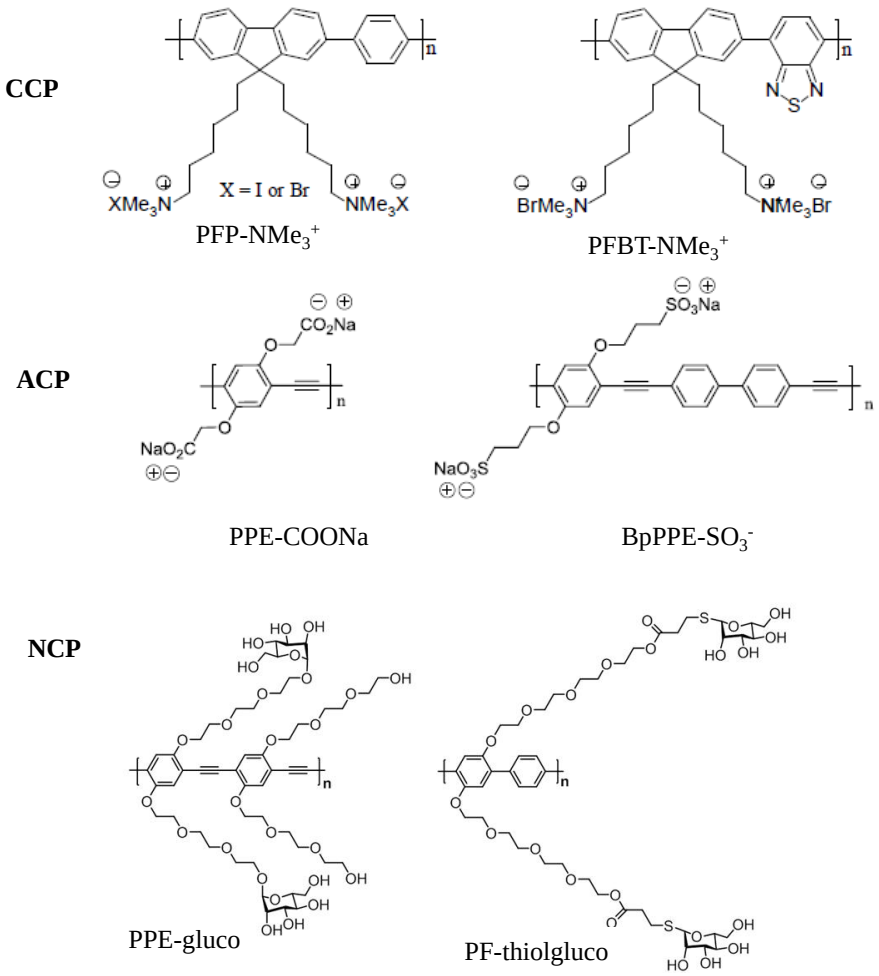

Figure 1.2. Examples of Water Soluble Conjugated Polymers: cationic conjugated polymer (CCP): poly(fluorene phenylene)-NMe^{3+} (PFP-NMe^{3+}), Poly(fluorene-co-benzothiadiazole)-NMe^{3+}(PFBT-NMe^{3+}); anionic conjugated polymers: poly(phenylene ethynylene)-carboxl sodium (PPE)-COO_2^-, bipoly(phenylene ethynylene)-sulforic sodium (PPE)-SO_3^-; non-ionic conjugated polymer(NCP): poly(phenylene ethynylene)-gluocose(PPE-gluco); polyfluorene-thiolated gluocose (PF-thiogluco). Reprinted with permission from Ref [28] Copyright (2012) National University of Singapore.

To develop chemical/biological sensors based on CPs, researchers have synthesized water soluble CPs (WSCPs) by introducing hydrophilic side groups to CPs. [21, 27–33] According to the charge existent on the side groups in aqueous solution, WSCPs can be of three types: cationic CPs (CCPs), anionic CPs (ACPs), and nonionic CPs (NCPs) and some examples are shown in 1.2.

Like their organic soluble counterparts, WSCPs have also attracted interests for the development of organic opto-electronic devices, such as OPVs, OLEDs and OFETs. [4, 34, 34–36] Compared with their organic soluble counterparts, WSCPs possess three advantages for the development of opto-electronic devices: 1) the spincoating of WSCPs only needs high polar solvents like water or alcohols, as opposed to the spincoating of hydrophobic CPs where orthogonal solvents are needed in order to avoid dissolution of the underlying layers; 2) Owing to their water solubility and charged side groups, WSCPs can be combined with oppositely charged acceptor materials by employing layer-by-layer assembly methods to realize devices; 3) WSCPs also show higher charge injection leading to enhanced device performance. [34–36] For example, Schanze and coworkers fabricated an organic solar cell utilizing layer-by-layer electrostatic assembly of oppositely charged anionic poly(p-phenylene ethynylene)s (PPEs) and cationic fullerene. [37] This WSCPs based solar cell showed 5.5 % energy conversion efficiency at maximum absorption of the PPEs. It should be noted that, from previous reports and from our own

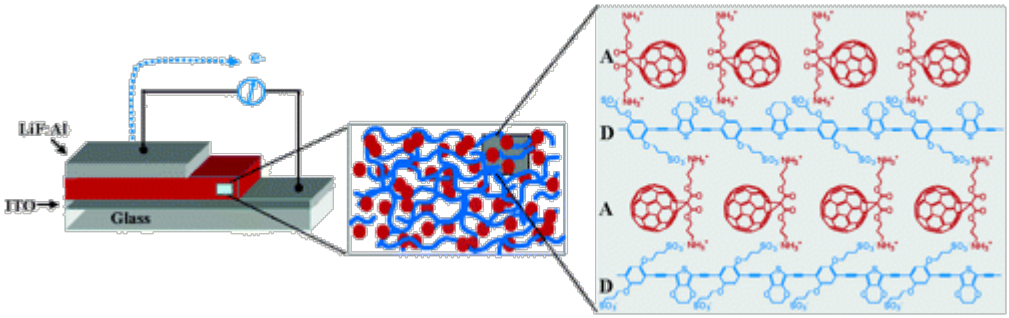

Figure 1.3. Scheme of the WSCPs based solar cell structure fabricated by layer-by-layer assembly of water soluble PPEs and fullerene. Reprinted with permission from Ref [37] Copyright (2005) American Chemical Society

experience, WSCPs also have some obvious disadvantages for fabrication of opto-electronic devices: 1) the solubility of many WSCPs is still too low in polar solvents when compared that of hydrophobic CPs in organic solvents. As a result, after spun on substrate, WSCPs cannot form uniform and thick enough layers, which are required for high performance organic opto-electronic devices. 2) as previously shown by others and from our own results, WSCPs can form micelle-like aggregates with self-quenched defects leading to lower PL quantum yield, which can hamper the performance of OLED or OPVs. Although the field of WSCP-based OLED

and OPV is relatively recent, there exists already several comprehensive reviews about the utilization of such materials in optoelectronic devices. [34–36, 38, 39]

WSCPs have been intensively studied for the development of biological/chemical sensors. [21, 29, 32]The research described in this thesis includes fundamental studies on the mechanism of interaction between biomolecules like DNA and WSCPs and the development of a WSCP-based DNA sensor. Therefore, in the following sections, a brief literature review is given on WSCPs based sensors.

1.2 Sensors based on Water Soluble Conjugated Polymers

Cost-effective sensors play a crucial role in clinical diagnosis, forensics and pathogen detection. [40–42] Traditional detection methods for biomolecules, like polymerase chain reaction (PCR) or enzyme-linked immune-sorbent assay (ELISA) require expensive instruments, highly skilled operators and many hours of laborious work. [18, 41–43] WSCPs have attracted intense research interests as potential candidate materials for the development of cost-effective chemical/biological sensors since late 1990s. [31, 44]

After binding with oppositely charged biomolecules like DNA or proteins, WSCPs can undergo chain conformation/aggregation changes resulting in changes of their optical properties (absorption, PL). This allows the detection of target biomolecules to be transduced into measurable optical signals from WSCPs. Compared with organic dyes, WSCPs have higher photostability and brightness due to their multi-chromophoric π-conjugated system. WSCPs have been applied in various sensors: detection of metal ions, [45] small molecules [46, 47] and large biomolecules like proteins and DNA, [48, 49] and more recently in cellular imaging, photothermal-therapy, drug delivery and release, gene delivery, or disease-related biomarkers. [22, 27] Sensors based on WSCPs are classified into: 1)turn-off, [50–53] 2)turn-on, [54, 55] 3)colorimetric, [21, 56] 4)FRET-based. [49, 57]

Turn-off biological/chemical sensors were first developed based on the quenching of WSCP's PL induced by binding with target molecules. The concentra-

tion of target molecules could be quantified from Stern-Volmer PL quenching plots. [51–53, 58] Quenching in such WSCPs based turn-off sensors was achieved either by photo- induced charge transfer (PCT) with the target molecule or by formation of self-quenched WSCP aggregates by the target molecules. In a PCT based sensor, the target molecules act as charge acceptor and quench the PL of WSCPs. For example, an anionic PPV was used to detect cytochrome C a heme-protein known to act as an electron acceptor. The concentration of cytochrome C was quantified from a Stern-Volmer plot of the anionic PPV's PL quenched by charge transfer with cytochrome C and occurring as a result of electrostatic binding between the polymer and protein. [50] The second type of WSCP-based turn-off sensor exploits formation of target-induced self-quenched WSCP aggregates. After binding with oppositely charged target molecules, aggregates of WSCPs/target complex form due to the decrease of surface charge resulting from charge neutralization. These aggregates contain more defects, which facilitate self quenching by inter/intra-chain energy transfer. For example, a WSCP-based protein sensor based on such a principle used a cationic poly(p-phenyleneethynylene) (PPE) for the detection of Concanavalin A from bacteria. [51] After binding with Concanavalin A, the cationic PPE chains were induced to form more self-quenched aggregates due to surface charge neutralization. The concentration of Concanavalin A could be read through a Stern-Volmer plot of the cationic PPE.

Turn-on sensors detect target molecules by the increased PL of WSCPs binding with target molecules. [54–56] Two mechanisms for the PL enhancement are reported: quench-tether-ligand (QTL) [60] and chain conformation/aggregation state change. For example, Schanze proposed a specific pyrophosphate (PPi) detection based on QTL utilizing an anionic PPE, PPE-COO_2^-. [59]The PL of the anionic CP was first quenched by copper ions, which bind with the side groups of anionic CP by relatively weak metal-coordination force.('off' step in scheme Figure.1.4) Upon addition of pyrophosphate, copper ions were taken away by the stronger association with PPi, and the PL of the anionic CP would be restored.('on' step in scheme and PL spectrum Figure.1.4)

With respect to turn-on sensors based on chain conformation/aggregation change of WSCPs, the self-quench defects in WSCPs chain/aggregation are reduced after binding with target molecules. For example, Liu developed a

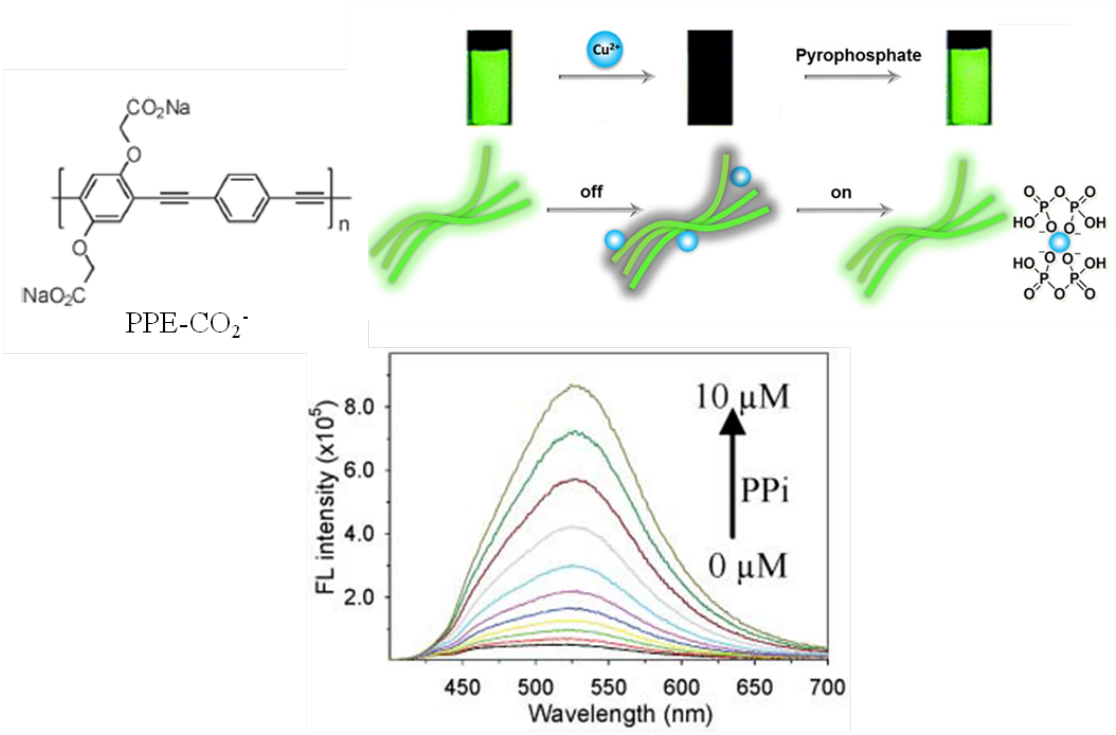

Figure 1.4. Chemical structure of PPE-COO_2^-; Schematic illustration of indicator displacement mechanism for pyrophosphate detection; PL spectra of PPE-COO_2^-/copper solution with increasing PPi concentration. Reprinted with permission from Ref [59] Copyright (2007) The Royal Society of Chemistry.

turn-on heparin sensor based on a cationic polyfluorene. [61] After binding with heparin, the PL showed enhancement of over 20 times. They attributed the PL enhancement to 'aggregation-induced emission' in WSCP/heparin complex. In a more recent work, [48] they further studied the 'aggregation-induced emission' from WSCP/protein complex and found out that electrostatic and hydrophobic interaction contribute together to the PL enhancement. As discussed in Chapter 2, our experimental results also showed that hydrophobic interaction between DNA and a cationic PPV contributed to PL enhancement of the cationic conjugated polymer.

Besides changes in PL intensity in the case of turn-on and turn-off sensors, colorimetric changes, that is, peak position shift in Uv-vis absorption and/or PL spectra, could also be induced by the binding of WSCPs and target molecules and utilized as a transduction mechanism. Based on this mechanism, researchers built label free biological/chemical sensors. [21, 56, 62] As shown in Figure.1.6, Leclerc

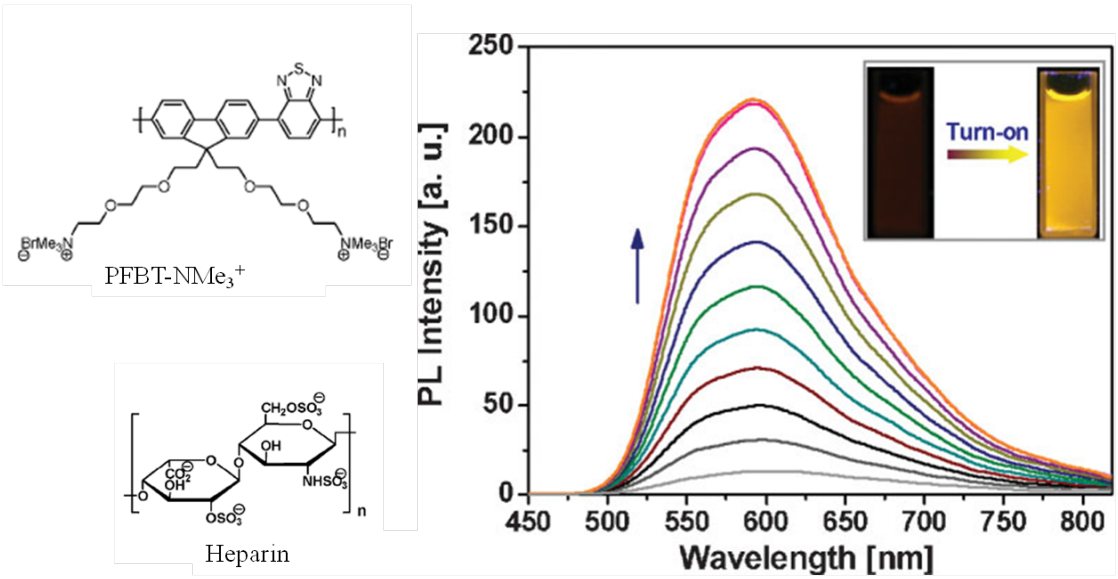

Figure 1.5. Left: Chemical structures of PFBT-NMe_3^+ and heparin. Right: PL spectra of PFBT-NMe_3^+ with increasing heparin concentration, the PL quantum yield of PFBT-NMe_3^+ was enhanced over 20 times at highest heparin concentration. Reprinted with permission from Ref [61] Copyright (2009) Wiley and Sons.

reported a specific potassium ions sensing based on a cationic polythiophene's chain conformational change induced by guanine rich single stranded DNA (G-rich ssDNA). [63] (Figure.1.6) In presence of single valent ions other than potassium ions, like lithium, sodium and rubidium ions, the G-rich ssDNA could not fold into a specific G-quadruplex secondary structure. In turn, the cationic polythiophene chain would only follow identical conformations and result same spectral redshift after binding with the G-rich(Figure.1.6,Path A and b,c,e curves in absorption spetrum) In contrast, with the stabilization of potassium ions (Figure.1.6,Path B), the guanine (G) rich ssDNA takes a specific secondary structure, G-quadruplex. After binding with the G-quadruplex, the cationic polythiophene chain will follow the conformation of G-quadruplex, resulting in a specific redshift in absorption spetrum (Figure.1.6 Path B and curve d in absorption spectrum).

Owing to the multi-chromphoric π-conjugated system, WSCPs have high extinction coefficient and are efficient light harvesting materials capable to enhance PL signals of acceptor molecules (dyes) by FRET. The energy transfer process is initiated by the biding between oppositely charged WSCPs and the complex formed by acceptor dyes and target molecules. Researchers have built sensors based on

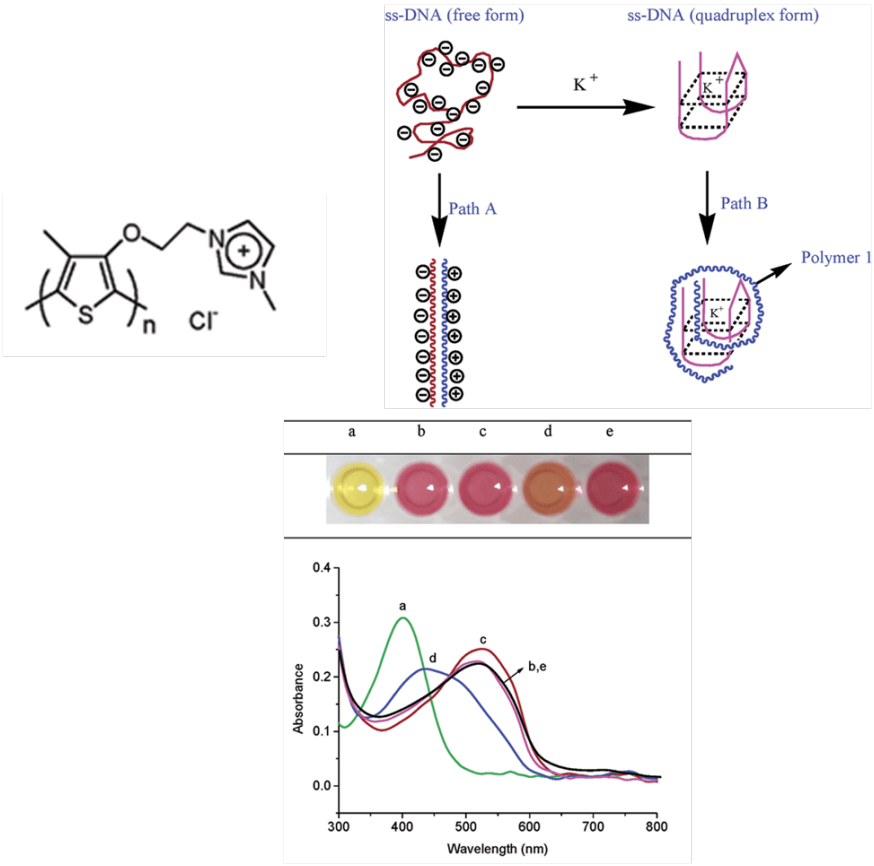

Figure 1.6. Chemical structure of a cationic polythiophene derivative; Scheme of a color-change based potassium ions detection utilizing the chain conformational change of the cationic polythiophene derivative induced by G-quadruplex; Uv-vis absorption of the cationic polythiophene alone (a) and in presence of lithium (b), sodium (c), potassium (d), rubidium (e) ions and G-rich ssDNA. Reprinted with permission from Ref [63] Copyright (2004) American Chemical Society.

FRET for the detection of metal ions, small molecules, large biomolecules, enzymatic activity. [21, 29–32, 43] As shown in Figure.1.7, a FRET-based potassium detection was developed based on using a cationic polyfluorene (PF) as donor and a dye labeled on guanine rich (G-rich) ssDNA as acceptor. [45] Without potassium ions in presence, very weak FRET occurs due to the relatively weak electrostatic interaction between the random coiled G-rich ssDNA and the cationic PF. Upon addition of potassium ions, efficient FRET would occur assisted by stronger electrostatic attraction in the tetraplex structure formed by the cationic PF and potassium ions induced G-quadruplex. As a result, higher FRET sensitized signal from the dye could be observed in the presence of potassium ions than other

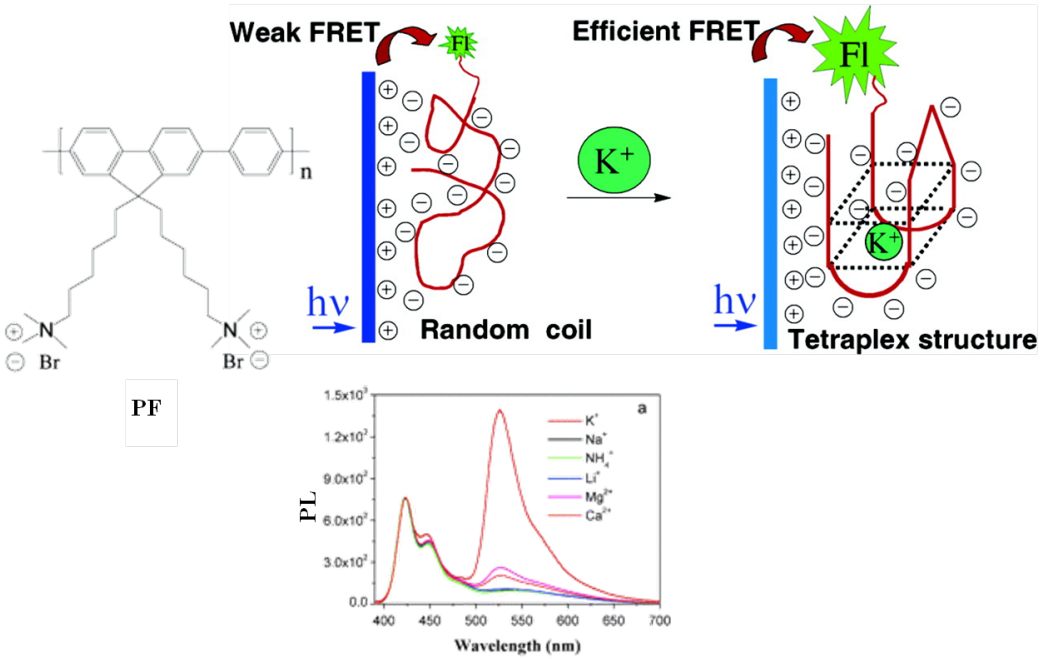

Figure 1.7. Chemical structure of cationic polyfluorene (PF); Schematic illustration of a potassium ions assay based on FRET from the cationic PF to the dye labeled on G-quadruplex; Normalized PL spectra of the cationic PF/G-rich ssDNA complex in presence of different ions. Reprinted with permission from Ref [45] Copyright (2005) American Chemical Society

ions. [45, 64–66]

Since chapters 2 and 3 report results on the fundamental interaction of a WSCP and DNA and a DNA sensor based on this particular WSCP, the next paragraphs in this current chapter provide a detailed literature review on current DNA sensors. Comprehensive reviews about WSCPs based biosensors and optoelectronic devices can be found in [21, 29–32, 44].

1.3 A brief review of DNA Sensors

Maxam and Gilbert reported the first DNA sensor based on chemical modification of DNA and subsequent cleavage at specific bases in 1977. [67] Target DNA was radioactive labeled and chemically treated to generate DNA segments which were detected in gels with X-ray radiation. Frederick Sanger optimized Maxam-Gilbert method by using less toxic chemicals and radioactive labeling and

developed Sanger sequencing. [68]

Polymerase chain reaction (PCR) is still the most popular DNA detection technique. [69] First, target double stranded DNA (dsDNA) is first heated over melting temperature producing two single stranded DNA (ssDNA); then the two ssDNA strands act as template for DNA polymerase to selectively amplify the target DNA. This DNA sensor platform utilizes cycles of DNA hybridization to amplify target DNA. [70] So far, the majority of commercial DNA sensing instruments are built on the PCR technique, such as 454 Life Sciences and SOLid sequencing from Life Technologies. PCR is also widely incorporated into later emerging nanotechnology to develop next generation of DNA sensor. During the prevailing applications from 1980's to mid 2000's, PCR sequencing first produced human genome in 2001 and brought the cost per genome from 100 million to 10,000. [71] However, these methods require radioactive labeling, complex assay process, expensive instruments and highly skilled operators, making them expensive in biomedical applications. [72,73]

Alternative DNA detection methods to PCR have been developed, for example mechanical, electrical/electrochemical, and optical DNA sensors. [74, 75] 1) Mechanical DNA sensors are based on the mass change during DNA hybridization process, [76] which can be read/transduced onto force changes by the cantilever probe of an atomic force microscope [77] or a resonance frequency change of a quartz crystal microbalance, [78] or a surface acoustic wave on a fabricated silicon surface. [79] The mechanical DNA sensor can give real-time detection results with picomolar sensitivity and single base mismatch sequence specificity. 2) Electrical/electrochemical DNA sensors can detect DNA hybridization from electrochemical signals resulting from redox reactions by voltammetry, electrochemical impedance spectroscopy or field transistors. [80] Electrochemical DNA sensors have been applied in lab-on-a-chip platforms, such as microarrays. [81, 82] 3)Magnetic DNA sensors utilize micron-sized magnetic beads and giant magneto-resistance (GMR). [83] 4)Optical DNA sensors are categorized into reagent and reagentless (label-free). One example of reagentless sensor functions based on surface plasmon resonance (SPR), [84] where a DNA probe is immobilized on a plasmonic noble metal surface like a thin film or nanoparticles. After hybridization, the refractive index of the plasmonic surface could be readily altered leading to changes in SPR which in turn provided signal transduction for the sensor. Even though such sen-

sors did not require labeling reagents, they are affected by unspecific binding and hard to quantify. Reagent optical DNA sensors have the probe usually labeled with a fluorescent dye or a quantum dot and they can provide quantitative results through colorimetric and/or fluorimetric assays. [23, 85]A comparison of different DNA sensors can be found in Appendix 1.

1.4 DNA Sensors based on Water Soluble Conjugated Polymers

1.4.1 DNA Sensors based on Chain Conformation and Aggregation Changes

Label-free DNA sensing based on WSCPs can be accomplished by monitoring alterations in the optical properties (absorption and PL peak intensity or wavelength) of the conjugated polymer upon binding with negatively charged DNA. These DNA sensing schemes rely on changes in WSCPs chain conformation or aggregation state induced by DNA binding to the polymer leading to alterations in the extent of electronic delocalization, which in turn result in alternations of WSCPs' optical properties. In diluted solutions (lower than 1 μM polymer concentration), conjugated polymer chains can adopt flexible, coil-like conformation or stretched conformation. The later conformation exhibits an extended electronic conjugation with red shifted absorption and emission spectra and sometimes with increased PL quantum yield. [86] In concentrated solutions or in thin films, conjugated polymers experience inter-chain interactions which can lead to formation of aggregate with red shifted absorption and PL properties and at the same time severely quenched PL. [88] For example, Leclerc first reported a colorimetric (color change) and at the same time fluorimetric (intensity change) DNA assay based on a water-soluble zwitterionic polyfluorene derivative(Figure.1.8) to detect single stranded DNA (ssDNA) with high sensitivity ($10^{-11}M$) and selectivity (1 base pair mismatch). [87] As shown in Figure. 1.8, the author proposed that after forming duplex with probe ssDNA, the cationic polythiophene (PT) undergoes chain conformation change from coiled to stretched and form more self-quenched aggre-

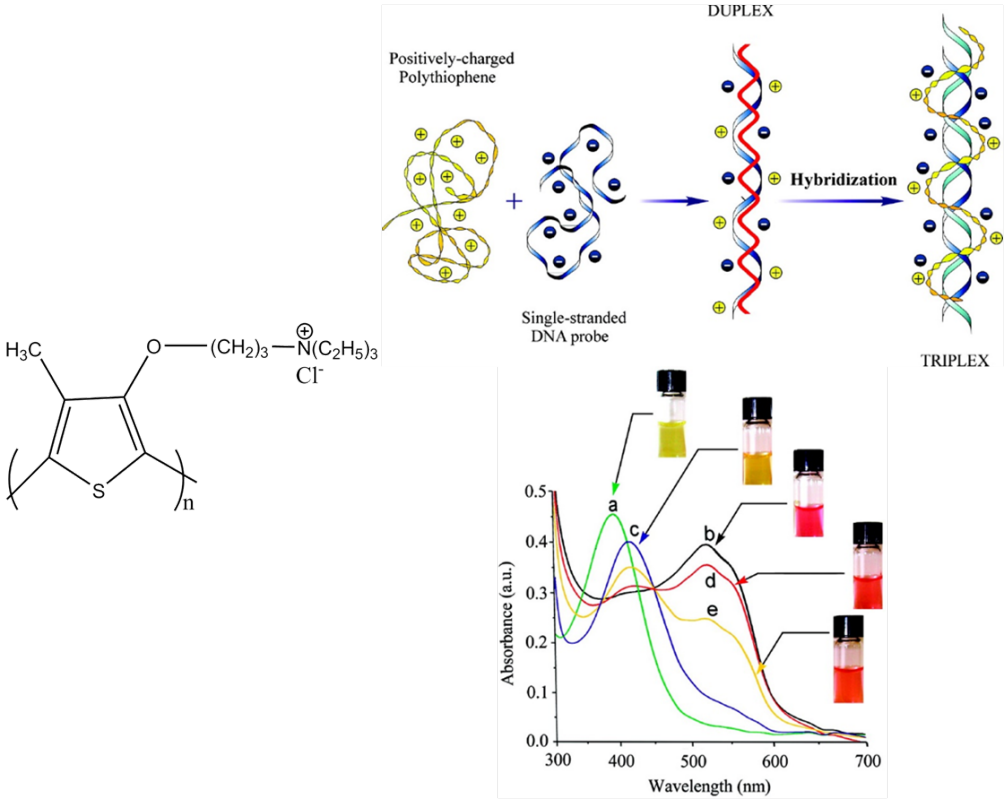

Figure 1.8. Left: chemical structure of the cationic polythiophene; Schematic description of a DNA sensor based on chain conformation/aggregation state change of a the cationic polytheiophene. Upper right: the Formation Polythiophene/Single-Stranded Nucleic Acid Duplex and Polythiophene/Hybridized Nucleic Acid Triplex. Bottom right: Uv-Vis absorption spectrum of a solution (7.9×10^{-5} M, on a monomeric unit basis) of (a) polymer 1, (b) polymer 1/X1 duplex, (c) polymer 1/X1/Y1 perfect match triplex, (d) polymer 1/X1/Y2 mixture with two mismatches, and (e) polymer 1/X1/Y3 mixture with one mismatch. Reprinted with permission from Ref [87] Copyright (2004) Wiley and Sons.

gation. The duplex of PT/probe-ssDNA was then found to show redshift in absorption and decreased PL. After addition of complementary target ssDNA,followed by hybridization, the cationic PT chain would undergo a recoiled conformation in the 'triplex' leading to blue-shift in absorption and PL spectra. At the same time, the aggregation of duplex was also broken, so the PL of the assay solution was recovered due to less self-quenched aggregates. Otherwise, if base mismatch exists in the target ssDNA, the PT chain would remain streched in 'triplex' and the self-quenched aggregates of PT/probe-ssDNA will not be broken. Then, the absorption and PL of the assay solution would not be changed, and the PL remained

quenched.

Despite the high sensitivity and selectivity of DNA sensors based on WSCPs' chain conformation/aggregation state, there is conflicting hypothesis on the mechanism of conjugated polymer/DNA interaction leading to the observed color changes and PL quenching. [89–97] A more detailed study focused on the mechanism of interaction between conjugated polymers and DNA is necessary to explain spectral behavior and to control such spectral changes towards better detection sensitivity and improved specificity in further development of DNA sensory methods.

1.4.2 DNA Sensors based on FRET

FRET is a dipole-dipole interaction between two chromophores, a donor and an acceptor, leading to non-radiative transfer of excitation energy from a photoexcited donor to an acceptor if there is spectral overlap between donor emission and acceptor absorption, and if proper orientation and distance exist [98].Figure.1.9 Due to the high sensitivity to the distance between donor and acceptor, FRET has been proposed as a 'molecular spectroscopic ruler' in many biophysical/chemical studies. [49, 57, 99] FRET based biosensing is much more sensitive and quantitative than colorimetric approaches, providing large and predictable color changes (switch from donor to acceptor emission) and ratiometric measurements (acceptor vs donor intensity changes). [100–102] In WSCP, FRET based sensors, donor WSCP and an acceptor in the form of a dye are usually brought in close proximity by electrostatic interaction induced by the target molecule. FRET rate falls off with the sixth power of donor-acceptor distance according to [103]

$$k_{FRET}(R) = \frac{1}{r^6}\kappa^2 J(\lambda) \tag{1.1}$$

with R, donor-acceptor distance, κ^2, orientation factor, J(λ), overlap integral denoting the overlap between donor emission and acceptor absorption spectra.

Owing to their large absorption cross-section (as high as $10^6 M^{-1} cm^{-1}$), conjugated polymers can serve as sensitizers/amplifiers of the PL of other dyes attached to DNA by FRET. Conjugated polymers can then enhance the sensitivity of a DNA biosensor and therefore the detection limit of DNA by FRET sensitized PL from a dye attached to a probe. FRET based DNA biosensors were first proposed by

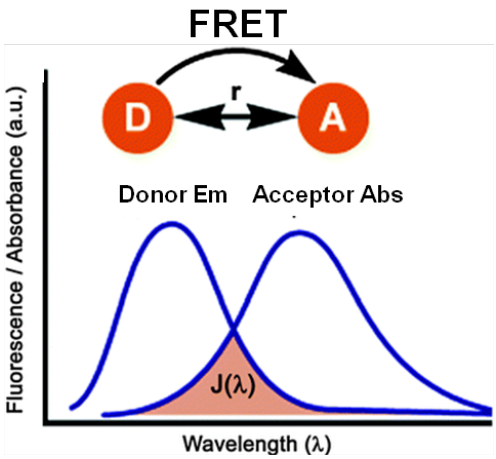

Figure 1.9. Illustration of FRET dependency on r, distance between donor and acceptor, and spectral overlap $J(\lambda)$ of donor's emission and acceptor's absorption. Reprinted with permission from Ref [98] Copyright (2012) The Royal Society of Chemistry.

Heeger and Bazan [104], and in the form of a cationic polyfluorene (PF) as donor an a FITC dye labeled on peptide nucleic acid (PNA) as acceptor. As shown in Figure.1.10, in absence of target ssDNA, the cationic PF and the dye on PNA are well separated so that the dye's PL could not be sensitized at the excitation of the cationic PF. If the target ssDNA is present, negatively charged PNA/ssDNA could form a complex by hybridization and the cationic PF could be brought by electrostatic attraction close to the dye to promote efficient FRET from the polymer to the dye upon polymer excitation. Due to the large absorption cross section of a multi-chromphoric system like the cationic PT, the signal from the acceptor dye was sensitized eight fold by FRET, and the DNA detection sensitivity was enhanced to 10^{-11} M ssDNA. Despite the enhanced sensitivity by FRET in this scheme, the proposed sensing method was expensive by PNA synthesis and dye labeling, making it cost effectiveless in practical clinic application. Meanwhile, because of the non-specific binding between PNA and non-target ssDNA, the FRET based DNA sensor lacked sequence specificity.

To further improve the sequence specificity and reduce associated costs for PNA synthesis, the same group proposed later on a DNA sensor based on a cationic polyfluorene (PF) and a two-step FRET scheme, introducing an intercalating dye, ethidium bromide (EB), and replacing the dye labeled PNA with a dye labeled ssDNA. [49] As shown in Figure.1.11, if the target ssDNA is non-complementary

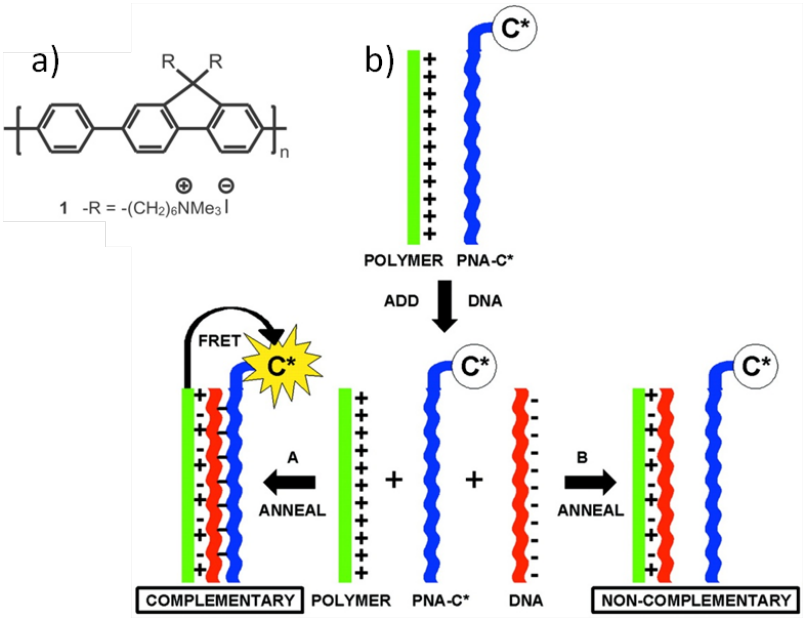

Figure 1.10. a) Chemical structure of the cationic polyfluorene. b) Scheme of DNA sensor based on FRET from the cationic polyfluorenes to a dye labled PNA (C*-PNA). Reproduced from Ref. [104] Copyright (2002) with Permission of National Academy of Sciences of the United States of America.

to the dye (C*) labeled ssDNA probe, hybridization with ssDNA probe would not occur and EB would not intercalate to become fluorescent. This way, only the first FRET step could be realized, from the cationic PF to the dye C* labeled on ssDNA probe. In the presence of complementary ssDNA, EB intercalates to become fluorescent and the dye C* labeled on ssDNA acts as an energy gate during the two-step FRET from the cationic PF to EB. Benefiting from the improved spectral overlap and closer distance between the energy gate and EB, the emission of EB could be enhanced through the two-step FRET to achieve high detection sensitivity. The sequence specificity of this DNA sensing scheme was also improved due to the introduction of the intercalating EB. Even though those proposed DNA sensing platforms achieved high sensitivity and sequence specificity, the requirement for chemical labeling of DNA probes makes it difficult for practical applications. Xu developed a DNA sensor based on FRET from a cationic PF to an intercalating dye, Picogreen, without requiring chemical labeling. [105] As shown in Figure.1.12 after hybridization of ssDNA probe and target ssDNA, the intercalating dye Picogreen was brought close proximity to the cationic PF to

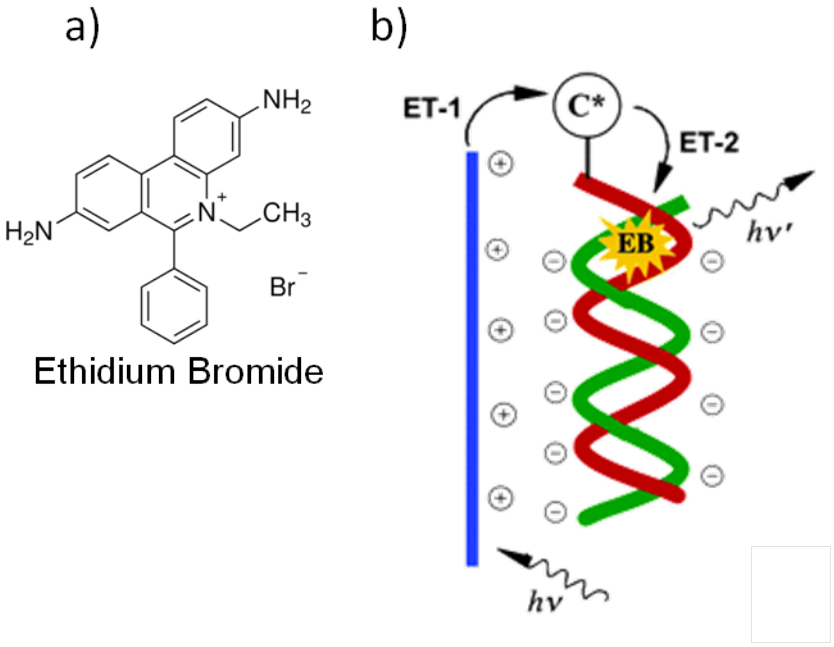

Figure 1.11. a) Chemical structure of the intercalating dye ethidium bromide (EB). b)Scheme of two-step FRET based DNA sensor based on a cationic PF, a dye labeled on ssDNA and intercalating dye ethidium bromide; Reprinted with permission from Ref. [49] Copyright (2004) American Chemical Society.

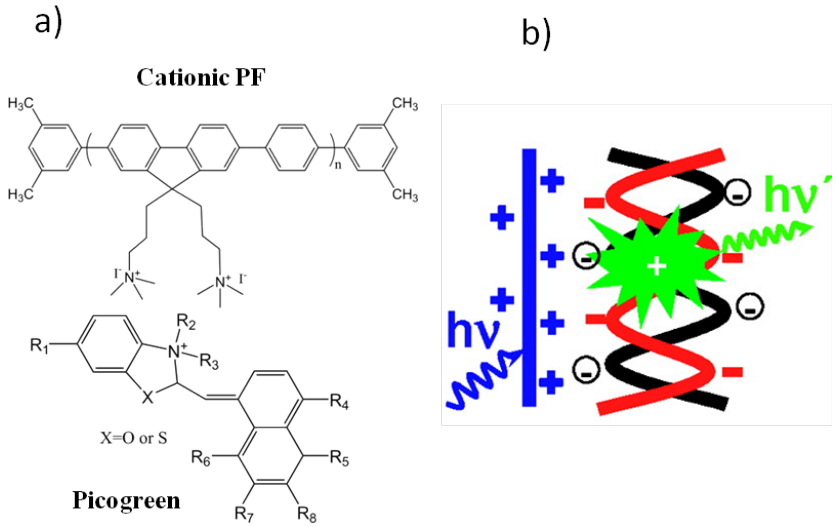

Figure 1.12. a) Chemical structures of the cationic PF and the intercalating dye Picogreen; b) Scheme of DNA sensor based on FRET from the cationic PF to intercalating picogreen dye. Reprinted with permission from Ref [105] Copyright (2008) American Chemical Society

achieve FRET sensitized emission from Picogreen. The DNA detection limit was enhanced to 10^{-9} M target concentration with a sequence specificity down to 1 base mismatch.

1.4.3 Optimization of Water Soluble Conjugated Polymers based DNA Sensor

To improve the performance of DNA sensors based on FRET, various parameters and conditions can be optimized. [106] WSCPs with various backbones and side chains have been synthesized in order to achieve improved spectral overlap with acceptor dyes. Woo varied the counterions on the side groups of the WSCP to tune the electrostatic interaction with DNA in an attempt to enhance FRET, [107] and Liu [106,108]tested how salt concentration and buffer affect sensor sensitivity. Here it should be noted that not only FRET can be possible, but also photo-induced charge transfer (PCT) can occur between WSCP and dye following WSCP excitation and this process can be detrimental to FRET by quenching the FRET sensitized PL of the dye. To enhance FRET and decrease PCT, Liu and Bazan found it is important to optimize the relative alignment of molecular energy orbitals of WSCPs and acceptors. [109] As shown in Figure 1.13 (left panel), an ideal situation for FRET is the one where the molecular energy orbitals of an acceptor dye are aligned within the bandgap of the donor ones, as this makes FRET the dominant process while PCT is inhibited. Otherwise, if the molecular energy orbitals of the acceptor are outside those of the donor as shown in Figure 1.13 (right panel), PCT becomes dominant, leading to quenching of both donor and acceptor molecules.

Since WSCPs have hydrophilic side groups and hydrophobic backbones, they tend to form micelle-like aggregates in aqueous solution. Such WSCPs aggregates usually have lower PL quantum yield, improper orientation with FRET acceptors. This results in reduced FRET sensitized signals from acceptors. To solve these problems, several groups reported breakage of aggregates formed upon target binding by using buffers with different pH, mixed-solvents and surfactants. [106, 110–114] Taking advantage of nanotechnology to enhance sensitivity and selectivity, Liu incorporated silica nanoparticles into FRET based DNA sensors. Dye

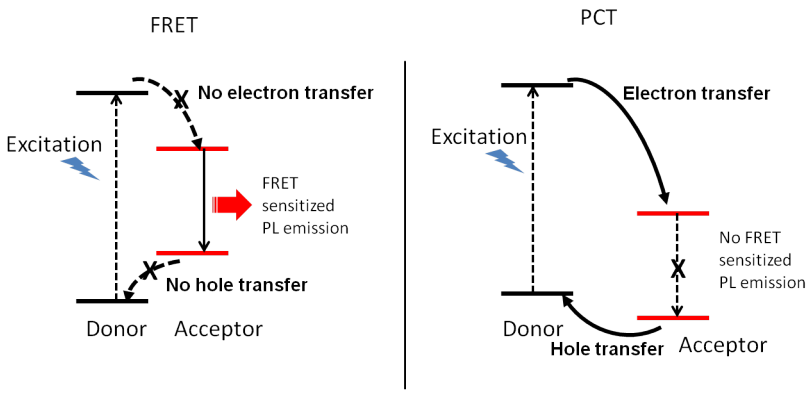

Figure 1.13. Effect of the relative alignment of molecular energy orbitals on FRET (left panel) versus PCT (right panel) preferences. Reprinted with permission from Ref [109] Copyright (2006) American Chemical Society

labeled ssDNA probes were grafted onto silica nanoparticles to minimize the self-quenching of dyes and to increase the local concentration of WSCPs-dyes donor-acceptor pairs to achieve enhanced FRET. [115] Wang demonstrated that the selectivity of the FRET based DNA sensors was enhanced by immobilization of ssDNA probe on magnetic nanoparticles. [116] FRET based DNA sensors were also transferred to substrates such as microarrays, biochips, to achieve high throughput screening and easier operation. [57, 117, 118]

1.4.4 Studies of the Mechanism of the Interaction between Water Soluble Conjugated Polymers and DNA

Understanding the interactions between WSCPs and DNA is essential for rational design of improved WSCP-based DNA sensors. Tapia and coworkers systematically studied DNA induced chain conformation/aggregation state change to a cationic polyfluorene. [119] SsDNA was found to induce larger spectral change to the polymer's absorption and PL spectra than dsDNA did, and this was rationalized in terms of different charge density, flexibility and hydrophboic interaction, which agreed with previous study. [89] The molecular weight of the cationic polyfluorene was observed to contribute to the hydrophobic interaction between the polymer backbone and DNA bases. WSCPs with higher molecular weight showed stronger π-π interaction between polymer backbone and DNA bases, lead-

ing to enhanced chain conformation/aggregation state changes at similar molar ratio of polymer and DNA. Surin reported that cationic the DNA inducued chirality to a series of cationic polythiophenes with different types of positive charged side groups. They studied the chirality as a function of DNA sequence and of temperature and found that both electrostatic and π-π interactions contributed to the DNA induced chirality onto polymer. [93] Using atomic force microscopy, Bazan and coworkers investigated the aggregation state change of a FRET-based DNA sensor combining on a cationic polyfluorene (PF) and a dye labeled ssDNA probe. [91] They monitored the growth of aggregates formed by the cationic PF, dye-labeled ssDNA probe, and target ssDNA during the DNA assay. Upon complexing with dye-labeled ssDNA probe, the cationic PF was induced to form aggregates containing self-quenched dye and weak FRET sensitized dyes emission. After addition of target ssDNA, despite the fact that larger aggregates were induced, the self-quenching of the dye was decreased and FRET sensitized dye emission was enhanced in larger aggregates. Modeling has also been applied to investigate interactions between conjugated polymers and DNA, for example, Aleman investigated hydrogen bonding and π-π stacking between DNA bases and CPs backbone units. [120, 121]

1.5 Photo-induced Charge Transfer between Conjugated Polymers and Fullerenes

Photo-induced charge (PCT) transfer plays an essential role in the performance of OPVs. Due to its high electron affinity, fullerene (C_{60}) was first introduced as an electron acceptor next to MEH-PPV as electron donor by Heeger and coworkers. [122] Time-resolved spectroscopy revealed ultrafast PCT in MEH-PPV/fullerene complexes(10^{13}/s in thin-film) [122–124]and these studies triggered enormous interest in the development of OPVs based on various CPs and fullerene derivatives [4, 125–127]

According to Marcus' theory [128], the charge transfer rate, k_{CT} follows the equation:

$$k_{CT} = \frac{2\pi}{\hbar}|H^2|(4\pi\lambda T)^{-1/2} exp(-\frac{(\Delta G^0 + \lambda)^2}{4\pi\lambda k_B T}) \tag{1.2}$$

where $H^2 \approx Cexp(-\beta r)$ is the electronic coupling between donor and acceptor, which is a function of donor-acceptor separation distance, r, and β is a preexponential factor. ΔG^0 is the Gibbs free energy change. λ is the reorganization energy; k_B is the Boltzmann constant and T is absolute temperature. A highly efficient PCT in MEH-PPV/fullerene was attributed to good HOMO LUMO overlap, good orientation from the high symmetry of fullerene, and close contact of donor-acceptor CP-fullerene pairs, [122, 129, 130] together with the large inter-facial area in disordered CPs/fullerenes nanostructures formed during the casting process. [131–134]

The ultrafast photo-induced charge transfer between CPs and fullerene have been studied by monitoring PL quenching of CPs using steady state and time-resolved PL spectroscopies, transient absorption spectroscopy and light induced electron spin resonance. [122–124]

1.6 Motivation and Outline

As detailed so far, WSCPs have been comprehensively studied for both the development of optoelectronic devices and of chemical/biological sensors. The DNA detection methods based on WSCPs have reached high sensitivity and sequence specificity, comparable to commercially available detections like PCR. Nevertheless, the requirement for chemical (dye) staining associated with costly purification of free dye and in some cases with costs associated with PNA synthesis makes current FRET based assays technologically unappealing. As such, there is increased interest in developing cost effective, conjugated polymer based DNA sensors with improved sensitivity and selectivity (sequence specificity). Furthermore, little is known about the particulars of the DNA/conjugated polymers interaction such as the contribution of electrostatic and hydrophobic components, the sequence specificity of these interactions, either or not polymers/DNA π-π stacking plays a role in defining the strength of the interaction. More questions can be asked, for example, why is the interaction between DNA and water soluble conjugated polymers different for different types of polymers (for example polythiophenes vs polyvinylenes) or from that of polyelectrolyte/polyelectrolyte interactions. Understanding this particular type of interactions may lead to improved DNA sensing schemes. In my thesis, I report in chapter 2 a fundamental study about the mechanism of interac-

tion between DNA and a WSCP, a cationic poly(p-phenylene vinylene) (C-PPV) with the observation, for the first time, of DNA sequence-dependent PL enhancement in the cationic PPV, with the PL enhanced as much as 7 fold for a particular DNA sequence. Enhancement was found to be the result of an interplay between two interactions: electrostatic attraction between C-PPV's side chains and DNA's phosphate backbone and hydrophobic interactions in the form of π-π stacking between CP backbone and DNA bases, the later imposing the sequence-specific PL enhancement. Inspired by the DNA induced PL enhancement, I developed a label-free FRET based DNA sensor with the C-PPV acting as a donor and an intercalating dye, malachite green chloride, as acceptor, and this study is presented in chapter 3. In this study I showed that by using such a small dye, hybridized DNA can be intercalated at maximum, one-to-one dye-to-base pair ratio, which in combination with FRET with C-PPV provides a wide range for base pair mismatch, from 1 up to 5 mismatches in the case of a 25 base pair DNA. Lastly, in chapter 5, to prove the concept that biomaterials like DNA could be integrated into WSCPs based optoelectronic devices, I used DNA as an optically 'inert' glue to demonstrate the ability to promote charge transfer between a water soluble cationic PPV and a cationic fullerene, a pair that usually repels each other and exhibits no charge transfer. With the assistance of ssDNA, I showed that these same charge sign donor and acceptor molecules can undergo charge transfer as efficient as that observed for oppositely charged donor and acceptor molecules with identical backbones and I investigated in detail the mechanism of quenching in the presence of DNA.

Chapter 2

DNA Sequence-Dependent Photoluminescence Enhancement in a Cationic Conjugated Polymer

2.1 Introduction

As mentioned in chapter 1 (Figure.1.2), cationic conjugated polymers have positively charged side groups rendering water solubility and the ability to bind negatively charged biomolecules like DNA and proteins. Cationic conjugated polymers have been proposed for DNA sensing owing to their chain conformation and aggregation state changes induced upon binding with DNA, changes that can produce colorimetric/fluorimetric signals that in turn can provide a transduction mechanism for DNA detection. [19, 87, 143–146] The bulk of studies involving cationic conjugated polymers and DNA have focused on the development of DNA sensing platforms, whether with increased detection sensitivity or with sequence specificity. [18–20] Recently, several studies attempted addressing the mechanism of interaction and the interplay of various intermolecular interactions between DNA and cationic CPs. [91, 93–95].

In this chapter, I describe my study on DNA sequence dependent photoluminescence (PL) enhancement for a cationic CP, poly2,5-bis [3-(N,N,N-triethylammonium)-1-oxapropyl]-1,4-phenylene vinylene -dibromide (C-PPV, MW=15 kDa)(Figure.2.1) when this is complexed with DNA, with the observation

of PL enhancement as high as seven fold. The DNA induced chain conformation/aggregation state change results from a combination of electrostatic and π-π interactions. The electrostatic interaction was found to be the prerequisite of DNA sequence dependent spectral change, and the π-π interaction between C-PPV's backbone and DNA bases was the major contribution to the sequence dependency. A non-ionic PPV (N-PPV) was also used to confirm the electrostatic interaction between C-PPV and DNA to promote sequence dependent behavior. Parts of this chapter are published in Ref [20] and [147] and reprinted with permission from Copyright (2014) The Royal Society of Chemistry and Copyright (2014) American Chemistry Society.

2.2 Materials and Methods

As shown in Figure.2.1, in each unit, C-PPV has two positively charged side groups, and the peaks of absorption and PL spectra are at 442 nm and 530 nm respectively. The cationic C-PPV was synthesized as reported in ref [148]. Five

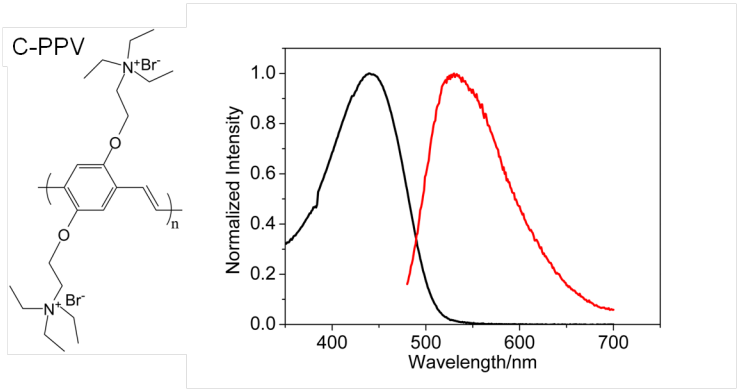

Figure 2.1. Left: chemical structure of C-PPV; Right: Uv-vis absorption (black curve) and PL (red curve) spectra. Reprinted with permission from Ref [147] Copyright (2014) The Royal Society of Chemistry

types of 25 mer ssDNA oligomers were used in the present study, homo oligomeric DNAs, ssDNAd$(A)_{25}$, ssDNAd$(C)_{25}$, ssDNAd$(G)_{25}$ and ssDNAd $(T)_{25}$, and a random sequence, ssDNA$(R)_{25}$, 5'-*ATT GTC TGT GTC TGG TGT GCG TCT G*-3'. C-PPV was mixed with each oligomer at various molar ratios in phosphate buffered saline (10 mM PBS, pH 7.4). Homo and hetero oligonucleotides were pur-

chased from Integrated DNA Technologies. Poly(vinylsulfonic acid, sodium salt) (PVSA, MW=4000-6000Da) was purchased from Sigma-Aldrich. Spectroscopic experiments were performed in 10 mM phosphate buffered saline (PBS, pH=7.2). For Uv-vis absorption and PL spectroscopy, C- PPV and N-PPV concentrations were 353 nM and experiments were performed on a Perkin Elmer Lambda 25 spectrophotometer and a Cary Eclipse fluorimetric, respectively, in the later case with 460 nm excitation. Circular dichroism (CD) spectroscopy was performed at 5μM concentration of C-PPV, N-PPV and DNA with a Jasco J-815 spectrophotometer. The pH values measured from all PPV/DNA complexes after mixing in 10 mM phosphate buffer was around 7.0, indicating a negligible pH effect on the absorption and PL of C-PPV. [148]

2.3 DNA-Induced Chain Conformational Change to C-PPV: ssDNA vs dsDNA

First, we compared the chain conformational change of C-PPV induced by ssDNA vs that of dsDNA. As shown in Figure 2.2, before binding with DNA, C-PPV alone absorbs at 442 nm and emits at 530 nm, with both Uv-vis absorption and PL spectra broad and structureless. With increasing concentration, both ssDNA and dsDNA induced chain conformation state changes to C-PPV, as indicated by isosbestic points observed in both absorption and PL spectra. Moreover, it should be noted the different spectral changes induced by ssDNA and by dsDNA to C-PPV. As shown in Figure.2.2, after binding with ssDNAd$(R)_{25}$, Uv-vis ab-

Complex	$\Delta\lambda^{abs}/nm$	$\Delta\lambda^{PL}/nm$	$QY_{COMPLEX}/QY_{C\text{-}PPV}$
C-PPV/ssDNAd$(R)_{25}$	48	30	3.87
C-PPV/dsDNAd$(R)_{25}$	33	32	2.70

Table 2.1. Spectroscopic parameters derived from Uv-vis absorption and PL data from Figure.2.2, absorption shift, $\Delta\lambda^{abs}$; PL shift,$\Delta\lambda^{PL}$; PL QY enhancement, $QY_{complex}/QY_{C-PPV}$. Reprinted with permission from Ref [147] Copyright (2014) The Royal Society of Chemistry

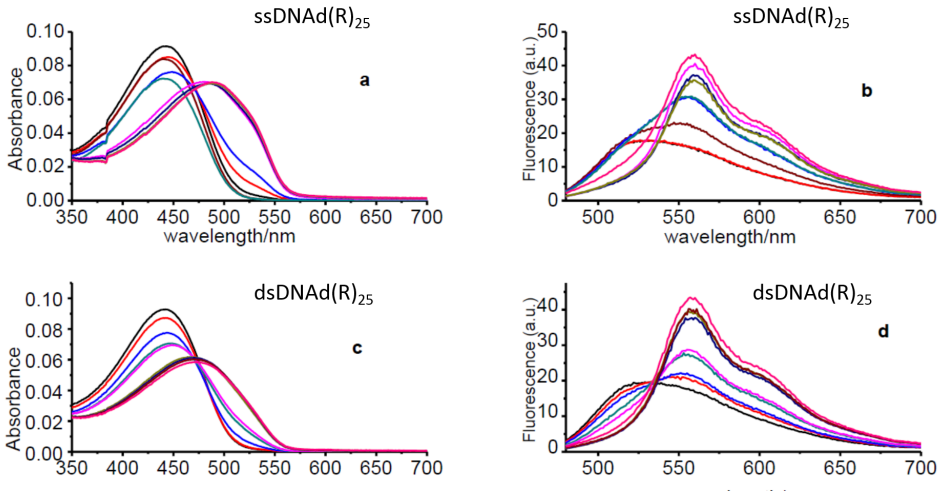

Figure 2.2. Uv-vis absorption (a,c) and PL spectra(b,d) of C-PPV with increasing concentration of dsDNA (a, b) and ssDNA (c,d) in 10 mM phosphate saline buffer, pH=7.1. C-PPV at 0.3 μM. Reprinted with permission from Ref [20, 147] Copyright (2014) The Royal Society of Chemistry and American Chemistry Society

sorption and PL spectra showed redshift, 48 nm and 30 nm, respectively, and the PL quantum yield (QY) of C-PPV enhanced 3.87 fold.(Table. 2.1) In contrast, dsDNAd$(R)_{25}$ induced 33 nm and 32 nm redshift in absorption and PL spectra, respectively and PL enhancement of 2.70 fold, (Table. 2.1) relative to C-PPV only. The different spectral changes and PL enhancements indicate stronger interactions in C-PPV/ssDNA complex compared with C-PPV/dsDNA complex, which agrees with previous studies [89]. This result can be explained as: 1) ssDNA takes a more planar secondary structure than dsDNA does, so the backbone of C-PPV gets more stretched after binding with ssDNA than dsDNA. This would lead to larger redshift, and higher PL enhancement with decreased self-quenching defects; 2) due to the hybridization, the π-π interaction between bases and C-PPV backbone in dsDNA is weaker than that in ssDNA. As to be discussed in the next sections, the chain conformational change of C-PPV induced by DNA results from a combination of electrostatic and π-π interactions, the latter being weaker in dsDNA, and leading to smaller spectral redshifts and lower PL enhancement. My results agree with previous studies about DNA sensors based on chain conformation/aggregation change. [87, 145]

2.4 Sequence Dependent ssDNA induced Chain Conformational Change to C-PPV

To study the sequence dependency of ssDNA induced chain/conformational change to C-PPV, we mixed C-PPV with five types of ssDNA.(see section.2.2) Complexation of C-PPV with DNA induced red spectral shifts in both Uv-vis absorption and PL spectra (Figure.2.3) and the PL spectrum of each complex became vibronically structured.

Table 2.2 lists the spectral shifts for Uv-vis absorption ($\Delta\lambda^{abs}$) and PL ($\Delta\lambda^{PL}$) spectra observed from C-PPV alone (black curves) to C-PPV complexed with ssDNA at equimolar concentration and for various sequences.

Complexation of C-PPV with ssDNA results in PL enhancement for all sequences, except ssDNAd$(G)_{25}$ (table 2.2, $QY_{complex}/QY_{C-PPV}$). The PL enhancement is sequence dependent, strongest for C-PPV/ssDNAd $(T)_{25}$ (7.3 fold), weakest for C-PPV/ssDNAd$(C)_{25}$. It is noteworthy that the Uv-vis absorption spectra vs added DNA feature pseudo-isosbestic points for all five complexes (Figure.2.3), suggesting a transition of the C-PPV between two states. Pseudo-isosbestic points were observed also in the PL spectra of these complexes with added DNA, except for C-PPV/ssDNAd$(G)_{25}$ where a gradual red shift occurred (Figure.2.3j). This together with the observation of vibronically structured and enhanced PL

Complex	$\Delta\lambda^{abs}/nm$	$\Delta\lambda^{PL}/nm$	$QY_{COMPLEX}/QY_{C\text{-}PPV}$
C-PPV/ssDNAd$(C)_{25}$	58	40	1.97
C-PPV/ssDNAd$(T)_{25}$	43	22	7.33
C-PPV/ssDNAd$(A)_{25}$	38	21	3.77
C-PPV/ssDNAd$(G)_{25}$	18	25	0.83
C-PPV/PVSA	10	27	0.48

Table 2.2. Spectroscopic parameters derived from Uv-vis absorption and PL data from Figure.2.3 and 2.4, absorption shift, $\Delta\lambda^{abs}$; PL shift, $\Delta\lambda^{PL}$; PL enhancement, $QY_{complex}/QY_{C-PPV}$. Reprinted with permission from Ref [147] Copyright (2014) The Royal Society of Chemistry

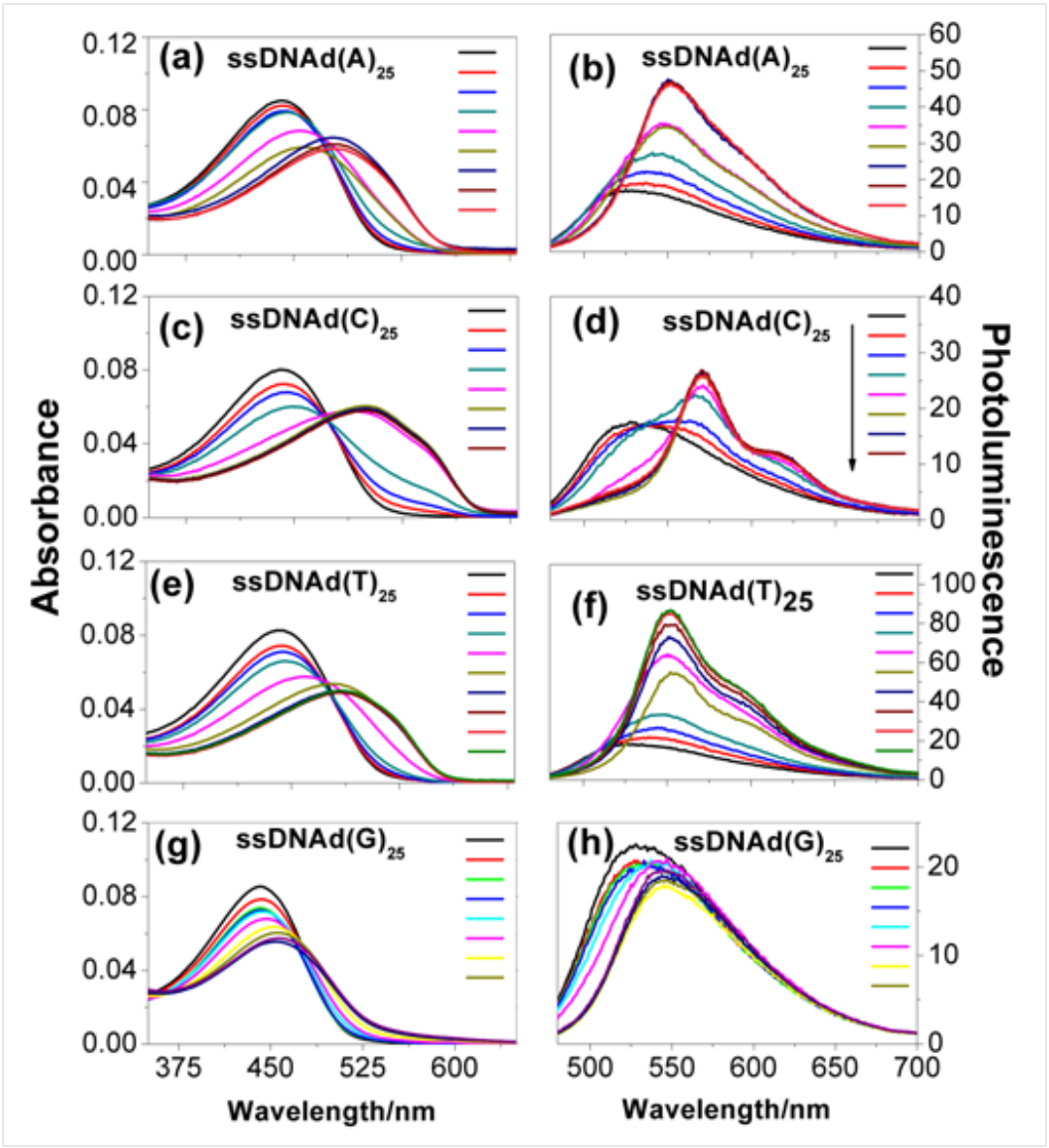

Figure 2.3. Uv-vis absorption and PL spectra in PBS buffer (pH 7.4) for C-PPV (black curves in each panel) and C-PPV complexed with ssDNAd$(A)_{25}$ (a-b), ssDNAd$(C)_{25}$, ssDNAd$(T)_{25}$, and ssDNAd$(G)_{25}$(g-h) at various C-PPV:DNA molar ratios, from 10:1 up to 1:1.2, with C-PPV at 1 μM. Arrows indicate increase in DNA concentration. Reprinted with permission from Ref [147] Copyright (2014) The Royal Society of Chemistry

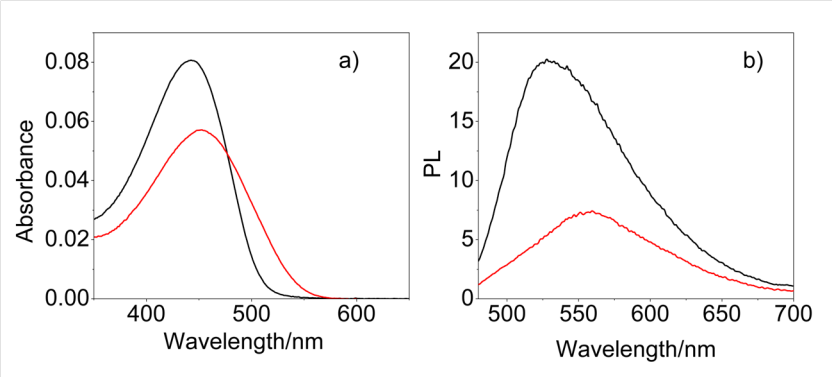

Figure 2.4. a)Uv-vis absorption and b) PL spectra of C-PPV complexed with poly(vinylsulfonic acid, sodium salt) (PVSA, MW=4000-6000Da) at 1:1 molar ratio in 10 mM PBS (red color). Also show in black are the spectra for C-PPV only. C-PPV and PVSA were at a concentration of 0.3 μM. Reprinted with permission from Ref [149] Copyright (2014) American Chemistry Society

emission from C-PPV/DNA complexes, suggest that complexation of C-PPV with DNA involves a polymer chain conformational change from a quenched state to a bright emitting state accompanied by an extended chain conformation, rather than polymer chain aggregation state changes. [90, 150] CP aggregation results usually in quenched, spectrally red shifted, and rather broad PL emission. [90] For C-PPV/ssDNAd$(G)_{25}$, PL quenching with added DNA is most probably a result of photo-induced electron transfer between C-PPV's phenylene vinylene backbone and guanine (G), with guanine known to quench organic fluorophores and water soluble CPs. [58,151] In contrast with ssDNA, as shown in Figure.2.4, C-PPV complexed with ordinary anionic polymers like poly(vinylsulphonic acid, sodium salt) (PVSA) results in formation of self-quenched aggregates with broad, structureless absorption and PL spectra and with the PL severely quenched, [20] due to the absence of π-π interactions between DNA bases and C-PPV's backbone.(Figure.2.4, section2.7)

2.5 Sequence-dependent ssDNA-induced Chirality to C-PPV

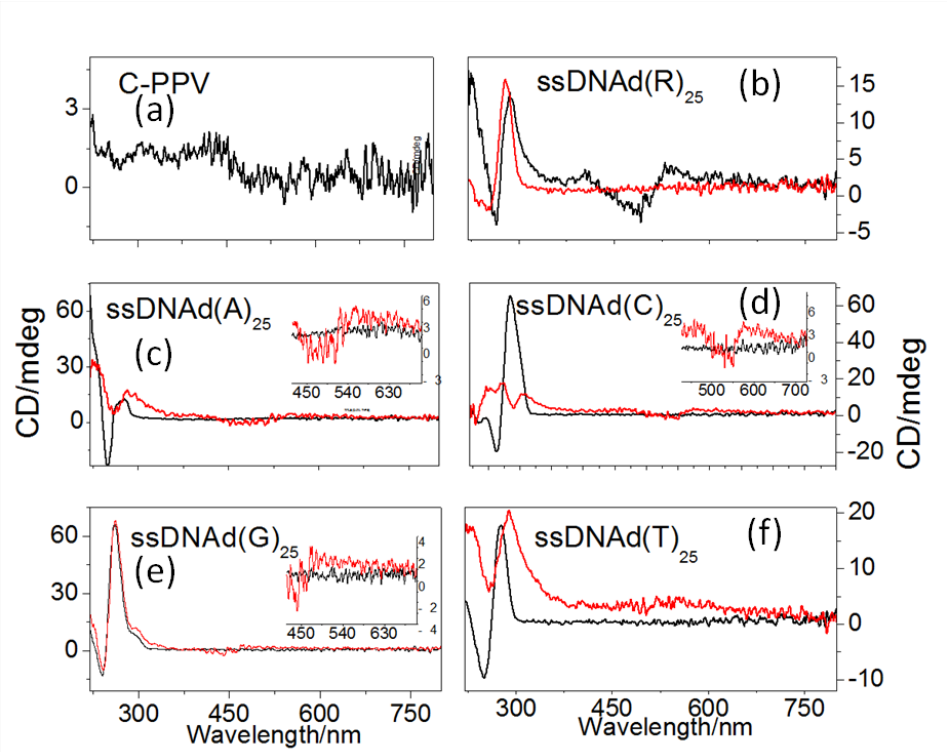

Figure 2.5. CD spectroscopy of C-PPV (a) (black color), DNA (b-f) (black color) and C-PPV/DNA complexes (b-f) (red color). C-PPV and DNA were each 5 μM in 10 mM PBS buffer. Insets in panels (c), (d) and (e) are zooms of the visible region of the CD spectra. Reprinted with permission from Ref [147] Copyright (2014) The Royal Society of Chemistry

To study the chirality of C-PPV chain induced by ssDNA,circular dichroism (CD) spectroscopy of C-PPV/ssDNA complexes was performed. Figure.2.5 shows evidence of strong interaction between the two moieties for all sequences, less for ssDNAd$(G)_{25}$. DNA alone (red curves in Figure.2.5) shows negative and positive bands in the region 200-300 nm, and they are a result of the right-hand stacking of DNA bases. C-PPV alone is achiral (Figure.2.5a), but attains chiroptical activity in the visible region (400-600 nm) upon complexation with DNA, (Fig2.5b-f, red curves), providing an excitonic system is induced in the C-PPV/DNA complex. CD spectroscopy of C-PPV/DNA complexes show strong perturbation of the bands associated with DNA (200-300 nm), less for ssDNAd$(G)_{25}$(2.5 f), that is, for all complexes exhibiting PL enhancement (Table2.2). This suggests strong interactions occurring between the hydrophobic parts of the two moieties (see below),

and disturbing the right-hand stacking of the ssDNA and its chirality. This results in weak DNA-induced chiroptical signals in the visible region for C-PPV/DNA complexes when compared to those reported for other cationic CPs complexed with DNA. [87, 93, 96]

2.6 Electrostatic Interaction between ssDNA and C-PPV

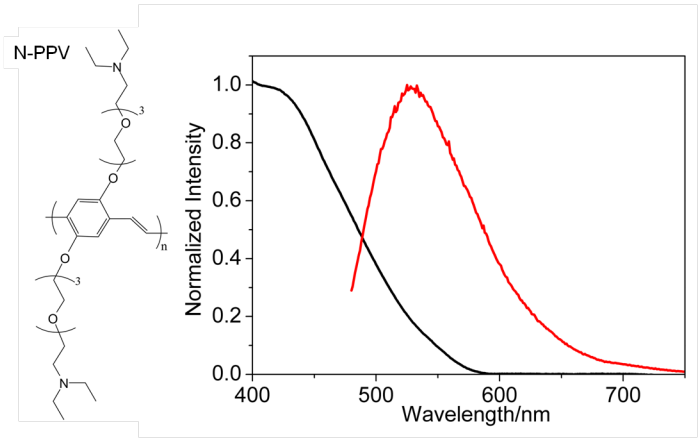

Figure 2.6. Left: chemical structure of N-PPV; Right: Uv-vis absorption (black curve) and PL (red curve) spectra. Reprinted with permission from Ref [147] Copyright (2014) The Royal Society of Chemistry

According to previous studies, the electrostatic attraction between the oppositely charged side cationic WSCPs and anionic phosphate backbone of DNA is the driving force the DNA induced chain conformation and aggregation state change of WSCPs. [91] To test this assumption, we mixed DNA with a non-ionic PPV (N-PPV)which has identical backbone as C-PPV

and non-ionic side groups,with absorption and PL maximum at 423 nm and 529 nm respectively [152].(Figure.2.6).Indeed, from Figure.2.7 after complexation with ssDNA, N-PPV showed neither spectral changes, nor shifts or broadening in absorption when mixed with ssDNAd$(C)_{25}$, ssDNAd$(T)_{25}$, ssDNAd$(R)_{25}$ and ssDNAd$(G)_{25}$. N-PPV mixed with ssDNAd$(G)_{25}$ exhibited dramatic PL quenching (50%), reconfirming the possibility of photoinduced electron transfer occurring

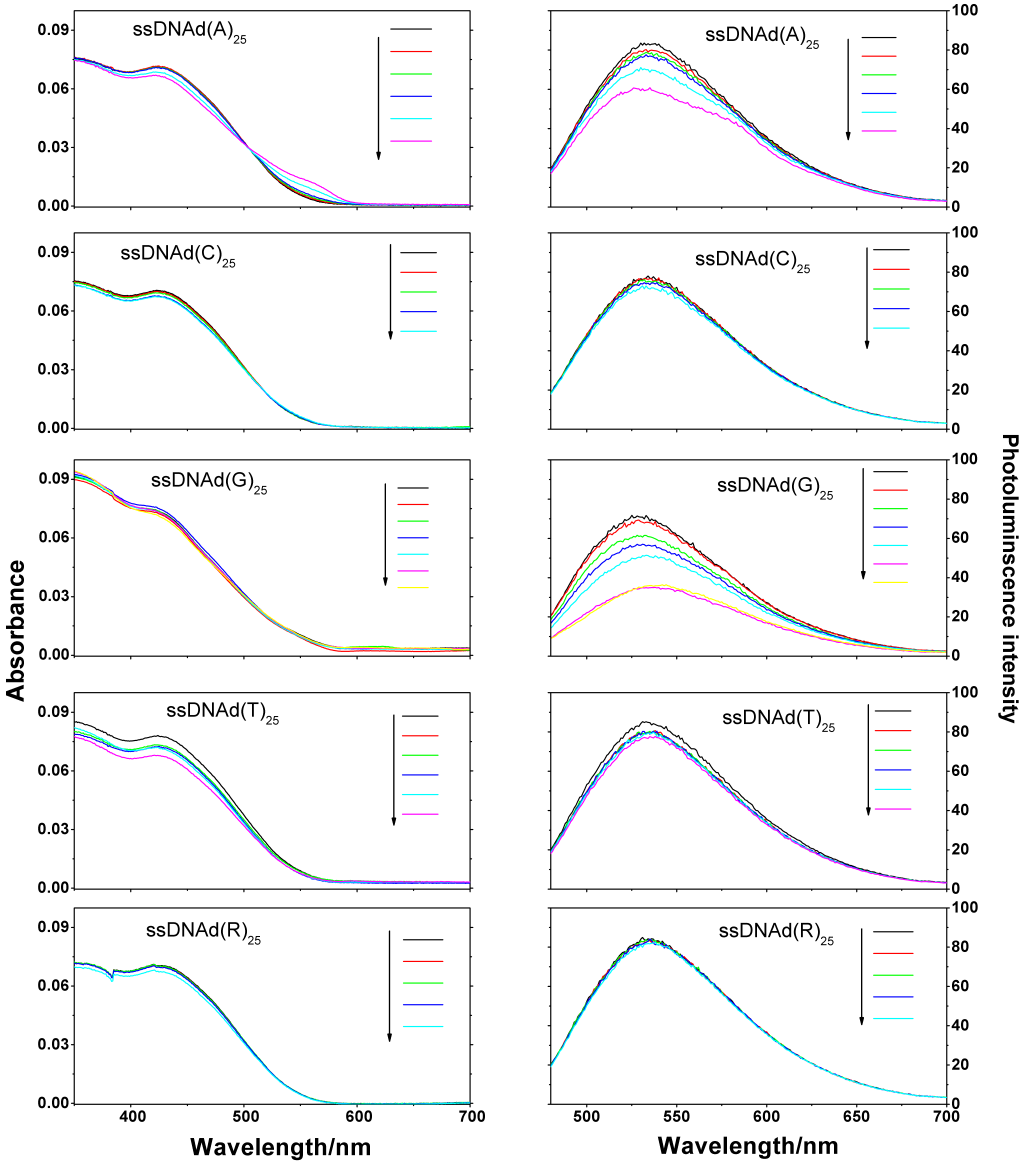

Figure 2.7. Uv-vis absorption spectra (left panels) and PL spectra (right panels) of N-PPV (black curves) and N-PPV/DNA mixtures for various DNA oligos and with varying N-PPV:DNA molar ratio, from 10:1 to 1:1.2 (arrows indicate increased DNA concentration), with N-PPV at 0.5 μM concentration. Reprinted with permission from Ref [147] Copyright (2014) The Royal Society of Chemistry

between PPV's backbone and guanine. N-PPV mixed with ssDNAd$(A)_{25}$ showed formation of self-quenched aggregates by the occurrence of a red shifted shoulder (590 nm) in the absorption spectrum (Figure.2.7) and quenched PL (table2.3).

Complex	$\Delta\lambda^{abs}/nm$	$\Delta\lambda^{PL}/nm$	$QY_{COMPLEX}/QY_{N\text{-}PPV}$
N-PPV/ ssDNAd$(A)_{25}$	132	0.0	0.81
N-PPV/ssDNAd$(C)_{25}$	0.0	0.0	0.00
N-PPV/ssDNAd$(T)_{25}$	0.0	0.0	0.00
N-PPV/ssDNAd$(G)_{25}$	0.0	0.0	0.50
N-PPV/ssDNAd$(R)_{25}$	0.0	0.0	0.00

Table 2.3. Spectroscopic parameters derived from Uv-vis absorption and PL data from Figure.2.7, absorption shift, $\Delta\lambda^{abs}$; PL shift,$\Delta\lambda^{PL}$; PL enhancement, $QY_{complex}/QY_{N-PPV}$. Reprinted with permission from Ref [147] Copyright (2014) The Royal Society of Chemistry

2.7 Hydrophobic Interaction between ssDNA and C-PPV

Next to electrostatic attraction leading to polymer chain conformation change in the case of C-PPV complexed with DNA, hydrophobic interactions also define the resulting spectroscopic properties for the complex, as suggested for other heterocyclic aromatic conjugated polymers interacting with DNA. [91,93,96] For example, [93], researchers examined DNA induced chirality to a cationic polythiophene-PT-PMe_3^+ (Figure.2.8). It was found that the chirality of DNA with different sequences was disturbed after binding to PT-PMe_3^+, while PT-PMe_3^+ chain following the DNA helix. From the chirality of PT-PMe_3^+ chain induced by different DNA, due to the large π-conjugated planes, the double ringed purine bases (A and G), exhibits stronger π-π stacking interactions with PT-PMe_3^+'s thiophene backbone than the other two single ringed pyrimidine bases (T and C).(Figure.2.8)

In the case of C-PPV/DNA complex, the complexation between C-PPV and DNA perturbs the right-hand stacking of DNA bases as shown by CD spectra (Figure.2.5), suggesting strong hydrophobic interactions between C-PPV's backbone and DNA bases. For C-PPV, hydrophobic interactions most probably occurred as π-π stacking, here between C-PPV's phenylene vinylene backbone and DNA bases. π-π stacking increases the π-conjugation system next to PPV's poly-

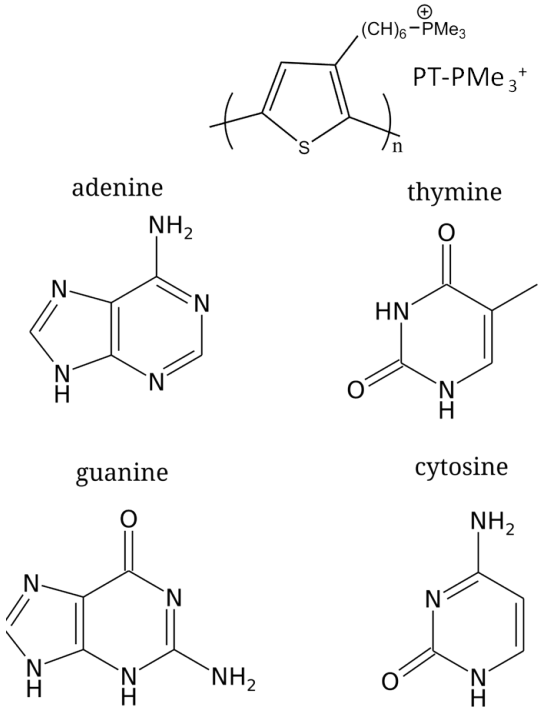

Figure 2.8. Chemical structures of PT-PMe_3^+, and four types of DNA bases: adenine (A), thymine (T), guanine (G), cytosine (C). Reprinted with permission from Ref [93] Copyright (2013) The Royal Society of Chemistry

mer chain unfolding induced by the electrostatic attraction with DNA's phosphate backbone, and both lead to a red shift of the absorption spectrum of the polymer (Figure.2.3 and $\Delta\lambda^{abs}$ in Table.2.2,).

Assuming that the electrostatic interaction between C-PPV's charged side groups and DNA's phosphate backbone is similar among different DNA sequences, and as such is the red shift resulting from the uncoiling of the C-PPV upon complexation with DNA, the overall magnitude of the red shift in absorption for a given C-PPV/DNA complex (sections. 2.3 and 2.4) quantifies the strength of the π-π stacking between C-PPV's backbone and DNA bases. The largest spectral shift in absorption, e.g. strongest π-π stacking, occurs for C-PPV/ssDNAd$(C)_{25}$ (58 nm), followed by ssDNAd$(T)_{25}$ (43 nm), ssDNAd$(A)_{25}$ (38 nm) and ssDNAd$(G)_{25}$ (18 nm). From these absorption data we conclude that C-PPV's phenylene vinylene backbone, a six member aromatic ring, interacts stronger with single ringed pyrimidines (C,T bases) than with double ringed purines (C,G bases). These

findings are opposite to those previously reported for a cationic polythiophene (PT-PMe_3^+) interacting with DNA where stronger stacking was observed with

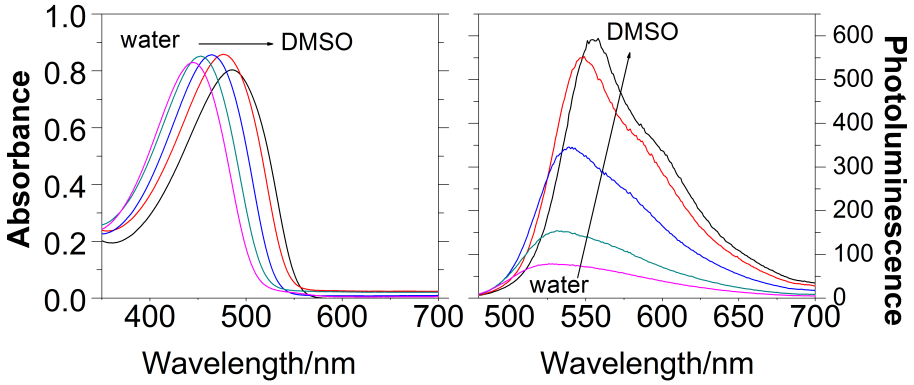

Figure 2.9. Uv-vis absorption and PL spectra of C-PPV in water/DMSO mixed solvent. Reprinted with permission from Ref [147] Copyright (2014) The Royal Society of Chemistry

Complex	$\Delta\lambda^{abs}/nm$	$\Delta\lambda^{PL}/nm$	$QY_{in\ DMSO}/\ QY_{in\ water}$
C-PPV in DMSO	44	28	6.30

Table 2.4. Spectroscopic parameters derived from Uv-vis absorption and PL data from Figure.2.9, absorption shift, $\Delta\lambda^{abs}$; PL shift, $\Delta\lambda^{PL}$; PL enhancement, $QY_{C-PPV\ in\ DMSO}/QY_{C-PPV\ in\ water}$. Reprinted with permission from Ref [147] Copyright (2014) The Royal Society of Chemistry.

purines. [94](Figure.2.8) This is not controversial because a five-member aromatic ring like thiophene might prefer stacking with a homologous ring that is present only in purines.(Figure.2.8)

C-PPV/ssDNAd$(G)_{25}$ behaves different than all other complexes, featuring small spectral shift in absorption and quenched PL. G oligonucleotides are known to form secondary structures [153] which in this case might prevent π-π stacking with C-PPV. As such, in a C-PPV/ssDNAd$(G)_{25}$ complex, interaction between C-PPV and DNA will be purely electrostatic attraction, resulting in turn in the smallest observed red shift in absorption. In conjugated polymers, conformational

disorder in the polymer backbone can exists in the form of chemical defects, backbone torsion or coiling [154, 155] and this can affect the π-system conjugation length and the resulting spectroscopic properties. For C-PPV, the hydrophobic backbone self-coils in water to reduce polymer-solvent interaction, breaking the π-system conjugation length and promoting self-quenching. [156] Spectroscopic changes similar to those observed for C-PPV complexed with DNA, including PL enhancement, could be reproduced when C-PPV was dissolved in a mixed water/dimethyl sulphoxyde (DMSO) solution, with DMSO a better solvent for C-PPV than water (see Table 2.4 and Figure.2.9). Thus, this confirms the hypothesis of a polymer chain conformation change for C-PPV when complexed with DNA.

2.8 Conclusion

In this chapter, I demonstrated DNA sequence specific PL enhancement of a cationic PPV (C-PPV) when complexed with homo and hetero oligonucleotides and discussed it as a manifestation resulting from an interplay between electrostatic and hydrophobic interactions. Electrostatic attraction between WSCP charged side groups and DNA phosphate backbone is essential in promoting hydrophobic interactions responsible for the observed sequence dependent PL enhancement, here in the form of π-π stacking between the polymer backbone and the DNA bases. Homo oligonucleotide ssDNAd$(T)_{25}$ induces the highest PL enhancement to C-PPV. With stronger hydrophobic and π-π interaction between unhybridized bases, ssDNA shows stronger ability to induce C-PPV's chain conformational change from coiled to stretched chain conformation leading to higher PL enhancement. On the other hand, dsDNA induces less chain conformational change and more aggregation, resulting in lower PL enhancement. Moreover, next to chain conformational change, DNA also induces sequence dependent chiroptical activity to C-PPV. Further engineering of such conjugated polymers might provide complexes with tunable PL and chiroptical properties that will be useful towards biosensing with sequence specific recognition.

Chapter 3

DNA Sensing based on FRET from Water Soluble Conjugated Polymer to DNA Photonic Wire

3.1 Introduction

Modern medical, biological and forensic assay require reliable DNA sensing with real-time response, high sensitivity and specificity. [40–42] DNA sensors based on cationic conjugated polymers promise as a simple, cost-effective alternative to labour intensive, cost-expensive methods like polymerase chain reaction. [43, 52, 86, 157–160] Because both single and multiple DNA base pair mismatches cause genetic disease, it is important to detect wide range of DNA base mismatch for genetic diagnosis and treatment. [161, 162]

As discussed in chapter 2, cationic conjugated polymers (CCPs) possess positively charged side groups rendering water-solubility and the ability to bind electrostatically to negatively charged DNA [43, 53, 56, 86]. The binding of a cationic CP to DNA can induce chain conformation or aggregation state changes in the former, thus altering CCP's optical properties including the emitted PL, thus providing a form of signal transduction for the detection of DNA. [55, 86, 89, 157, 163]

Inspired by the observation of chain conformation/aggregation state changes induced by DNA to the cationic PPV (C-PPV) as reported in the previous chapter, here I demonstrate a label-free, sequence specific DNA sensor based on F*ö*rster

resonance energy transfer (FRET) occurring between a cationic conjugated polymer and a small intercalating dye, malachite green chloride. The sensor combines (1) conjugated polymer chain conformation changes induced by the binding with DNA, with the conjugated polymer wrapping/twisting around the DNA helical duplex and experiencing a three-fold increase in its photoluminescence quantum yield and (2) FRET from the conjugated polymer to the dyes intercalated into dsDNA. Owing to its small size, the dye intercalates at maximal, one-to-one dye-to-base pair load, making the dye intercalated dsDNA a molecular photonic wire with dyes excitonically coupled and chiroptical active. Any sequence mismatch between probe and target ssDNA degrades the intercalated DNA photonic wire by decreasing its brightness, excitonic coupling and chiroptical properties, and this provides a signal transduction method for the DNA sensor. Coupling of dye intercalated dsDNA with the conjugated polymer via FRET provides target signal amplification and increased sensitivity towards sequence mismatch, with the FRET efficiency decreasing with added sequence mismatches.Parts of this chapter are published in Ref [20] and [147] and reprinted with permission from Copyright (2014) The Royal Society of Chemistry and Copyright (2014) American Chemistry Society.

3.2 Materials and Methods

The intercalating dye (Figure.3.1), malachite green chloride (MGC) was purchased from Sigma Aldrich.DNA oligomers were purchased from Integrated DNA Technologies. In each experiment, equimolar (1μM) target and probe ssDNA in 10 mM phosphate buffered saline were hybridized at 80 ^{o}C for 5 min, annealed at room temperature for 30 mins and subsequently incubated with MGC dye (25μM) for another 30 mins. The intercalated dsDNA/MGC complex was further incubated with an equimolar amount of PPV (1μM) for an additional 30 mins at room temperature and the resulting complex was subjected to spectroscopic investigations. Uv-vis spectra were measured with a Perkin Elmer Lambda 25 spectrophotometer, photoluminescence spectra with an ISS PC1 fluorimeter and circular dichroism (CD) spectra with a Jasco J-815 spectrophotometer. Photoluminescence decays were measured by the time-correlated single photon counting method using a Pi-

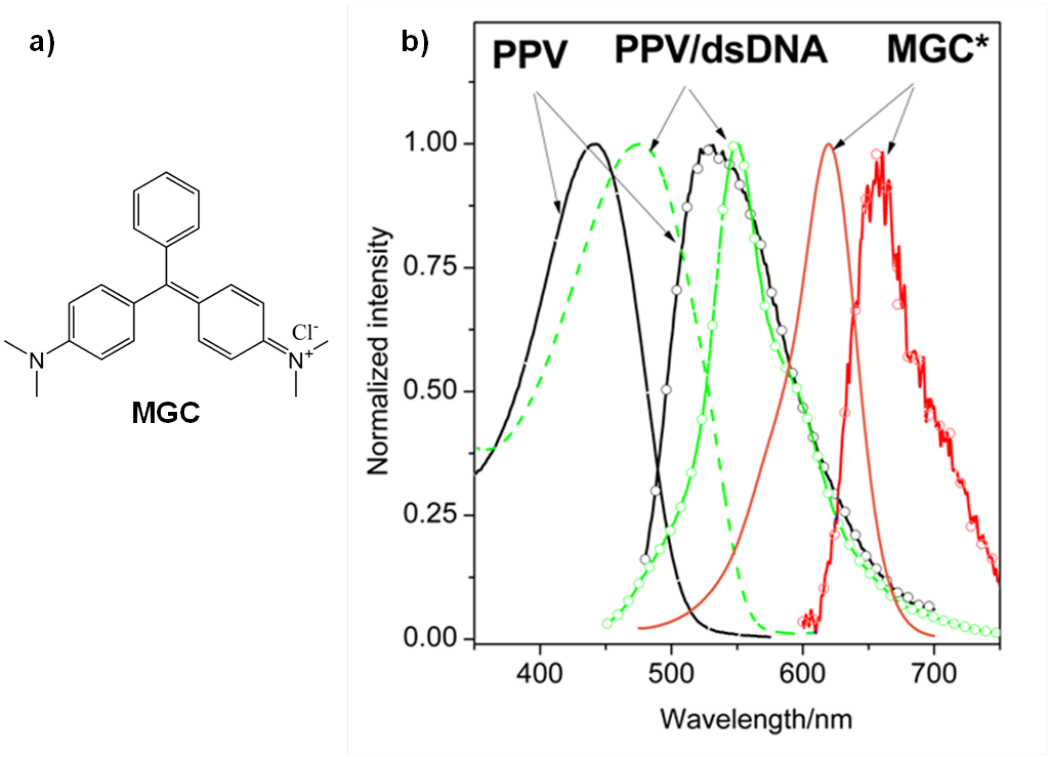

Figure 3.1. a) Chemical structure of malachite green chloride (MGC); b) Uv-vis absorption (line) and PL (line and circle) spectra for PPV (black), PPV/dsDNA (green) and intercalated dsDNA/MGC complex (red) in 10 mM phosphate buffered saline. PPV excitation 460 nm, MGC, 610 nm. Reprinted with permission from Ref [20] Copyright (2014) American Chemistry Society

coquant FluoTime 200 spectrometer combined with a solid state femtosecond laser system delivering either 460 nm or 590 nm pulses. A complete description of the system can be found in ref [164]. PL lifetimes were estimated by reconvolution of the measured PL decay with the instrumental response function and using a multiexponential function and according to

$$\tau_{ave} = (a_i \times \tau_i) / \sum (a_i \times \tau_i) \tag{3.1}$$

Both stationary and time-resolved photoluminescence experiments were performed using a front face excitation/detection configuration to avoid inner filter effects. [103]

3.3 Biosensor Concept

Figure 3.2 shows the principle of DNA sensing for complementary (a) and for mismatched (b) sequences. Probe (P) and target (T) ssDNAs were first hybridized and the dsDNA was stained by malachite green chloride (MGC). Like other intercalating dyes, MGC is non-fluorescent free in solution and becomes fluorescent upon intercalation with hybridized dsDNA (Figure.3.1). [165] As to be shown in section 3.5, this particular dye can be intercalated at 1:1 dye-bp ratio, e.g. at maximum site density, and the result is an intercalated dsDNA/MGC complex with unique chiroptical and excitonic properties, similar to a photonic wire. In the final step, C-PPV is introduced to amplify the PL signal from MGC dyes intercalated into dsDNA.(Figure.3.1). As shown in Figure. 3.1, C-PPV's PL emission

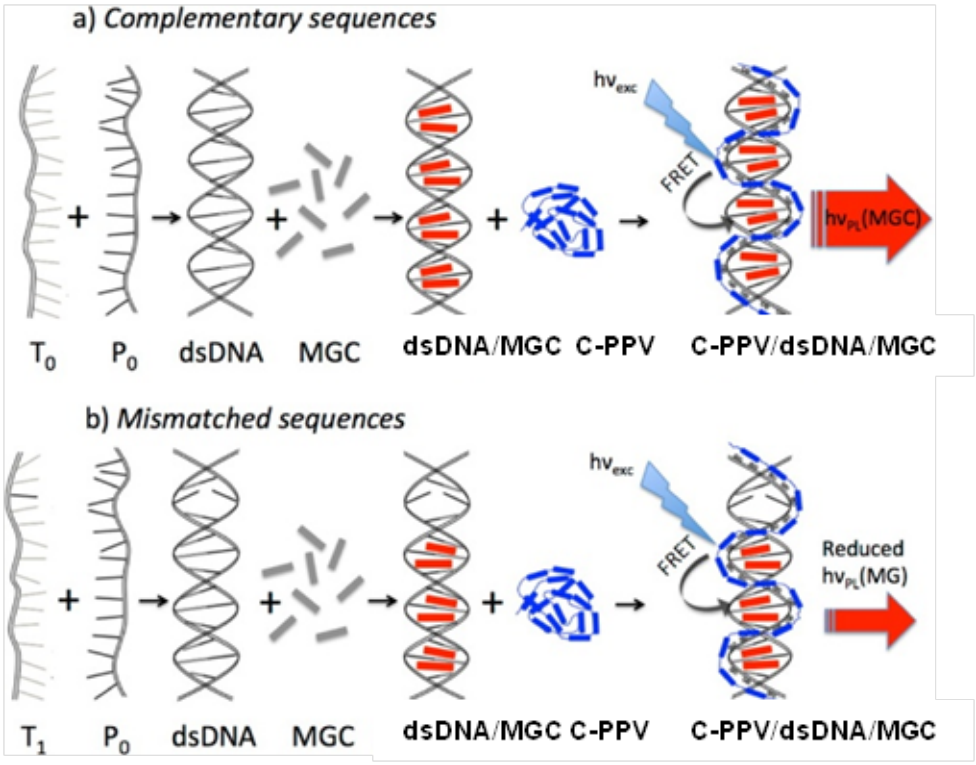

Figure 3.2. Proposed label-free, sequence-specific DNA sensing platform based on a cationic PPV and intercalating MGC dyes experiencing FRET and shown for a) complementary and b) mismatched probe and target ssDNA sequences. Reprinted with permission from Ref [20] Copyright (2014) American Chemistry Society

and MGC's absorption spectra overlap considerably (Figure.3.1) to enable FRET

between the two moieties when brought in close proximity by the dsDNA scaffold, and when exciting the conjugated polymer with blue light (e.g. 460 nm). Moreover, as discussed in Chapter 2, binding of C-PPV to dsDNA$(R)_{25}$ induces redshift in C-PPV's PL spectrum, increasing the spectral overlap of C-PPV emission and MGC's absorption (Figure.3.1) and increases C-PPV's PL quantum yield (QY), changes that are expected to improve the efficiency of FRET between C-PPV and intercalated MGC. For C-PPV/dsDNA$(R)_{25}$/MGC with dsDNA$(R)_{25}$ hybridized from complementary sequences and intercalated at 1:1 dye:bp load, the FRET sensitized PL signal from C-PPV/dsDNA$(R)_{25}$/MGC complex measured at the PL peak of intercalated MGC will be maximal since the acceptor site contains a maximum number (25) of dyes. Any mismatch between probe and target DNA results in a decrease in the number of intercalated MGC dyes constituting the acceptor site, thus decreasing the FRET sensitized PL signal of C-PPV/dsDNA/MGC complex. The FRET sensitized PL signal of the C-PPV/dsDNA$(R)_{25}$/MGC complex is expected to scale with the amount of base pair mismatch (Figure.3.2). For non-complementary sequences, since they lack the acceptor site (intercalated MGC), the FRET sensitized PL signal will be absent.

3.4 Biosensor Testing

I tested the DNA sensor scheme from Figure.3.2 using the following 25bp DNA sequences, probe (P_0)*ATT GTC TGT GTC TGG TGT GCG TCT G* , complementary target (T_0) *CAG ACG CAC ACC AGA CAC AGA CAA T* and target sequences with one- (T_1), *CAG ACG CAC ACC ATA CAC AGA CAA T*, three- (T_3), *CAG ACT CAC ACC ATA CAC TGA CAA T* and five mismatches (T_5), *CAG ACT CAC GCC ATA CAC TGA TAA T*, noticing that base mismatches are evenly spaced. In each experiment, equimolar (1μM) target and probe DNA. Biosensing experiments were performed with 460 nm excitation and the results are shown in Figure.3.3a. Control experiments of C-PPV bound with dsDNA at equimolar concentration for various base-pair mismatches showed similar PL enhancement and PL red shift as observed for complementary sequences (Figure.3.4). Control experiments with C-PPV and MGC dyes mixed at 1:25 molar ratio showed little (lower than 5%) quenching of C-PPV's PL by the free MGC dye following

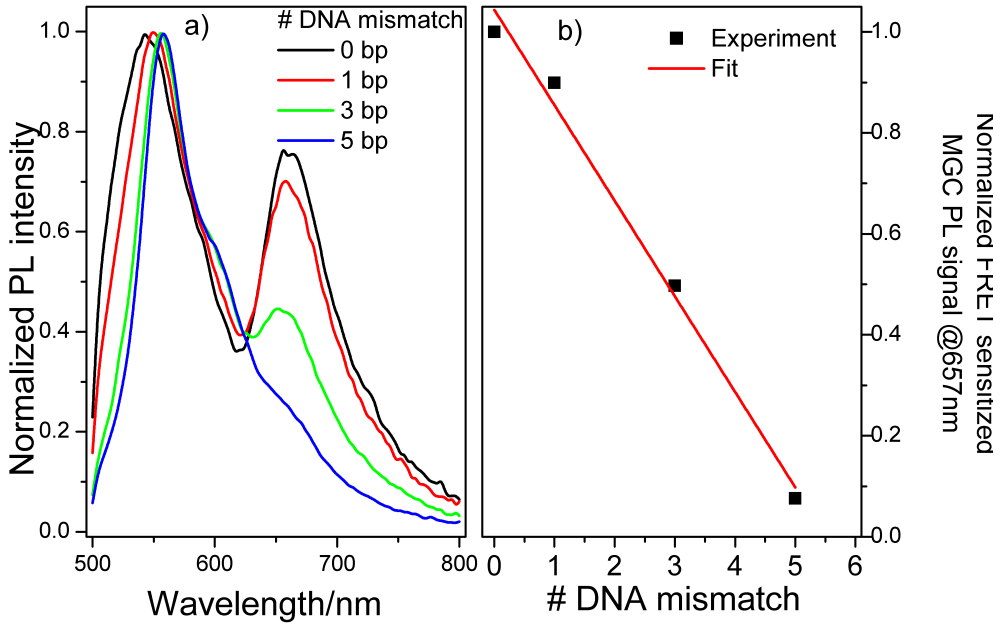

Figure 3.3. a) PL spectra (excitation @460 nm) for C-PPV/dsDNA/MGC complexes with complementary sequences (P_0, T_0), black line, sequences with 1 bp mismatch (P_0, T_1), red line, with 3bp mismatch (P_0, T_3), green line, and with 5 bp mismatch (P_0, T_3), blue line. The molar ratio in each complex was 1:1:25 C-PPV:dsDNA:MGC.b) FRET sensitized PL signal @657 nm vs bp mismatch for C-PPV/dsDNA$(R)_{25}$/MGC complexes and linear fit (dash line). Reprinted with permission from Ref [20] Copyright (2014) American Chemistry Society

460 nm excitation. Similarly, control experiments with 610 nm excitation showed no evidence for PL quenching of intercalated dsDNA/MGC by the C-PPV by an eventual charge transfer of the dye with the C-PPV as reported for other intercalators. [105, 166] As expected, the FRET sensitized PL signal measured at MGC's PL peak (660 nm) is maximal for complementary sequences, with an amplification of 2.8x compared to direct excitation (610 nm) and decreases with the increase of the number of bp mismatch (Figure.3.3a), thus demonstrating the sequence specificity of the proposed sensor. The FRET-sensitized PL signal measured at 657 nm (subtracted by the contribution from the free C-PPV polymer) scales linearly with the amount of mismatch, with a predicted measurable range up to 5 base pair mismatches for the particular DNA probe and for the concentration range employed herein (Figure.3.3b). For non-complementary sequences (P_0, P_0) there

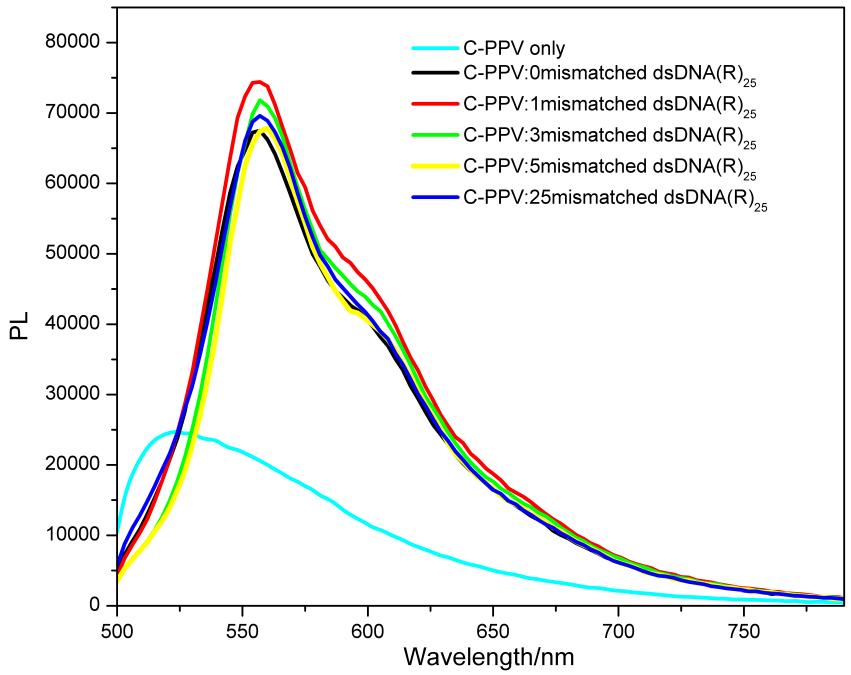

Figure 3.4. PL spectra for C-PPV/dsDNA$(R)_{25}$ vs base-pair mismatch, with C-PPV and dsDNA$(R)_{25}$ at 1 μM concentration in 10 mM phosphate buffer. Reprinted with permission from Ref [20] Copyright (2014) American Chemistry Society

was no sensitized PL at 657 nm since MGC does not intercalate to become fluorescent. Instead quenching of C-PPV's PL of about 44% was observed compared to C-PPV/dsDNA. This result came with no surprise because PPV and MGC can still bind to single stranded DNA to be in close proximity and to experience FRET because non-fluorescent/nonintercalated MGC can still absorb and therefore quench PPV's PL by energy transfer.

In the past two sections, I demonstrated a label free FRET based DNA sensor based on C-PPV and MGC combining chain conformational change. With the number of base mismatches in target ssDNA increasing from 1 to 5, the FRET sensitized PL signal decreases and thus the DNA sensor shows better sequence specificity than previous reported. [105] Due to the low cost of MGC and label free processing, this DNA sensor is more cost-effective than previous FRET based DNA sensors [49, 158] and can be potentially deployed for field detection. My DNA sensor can detect 1 to 5 DNA base mismatches out of 25 bp DNA, a wider range than previous studies, [105], which promises ability to detect genetic disease

caused by single and multiple base mismatches. In the next sections, fundamental studies are reported with the aim to understand the mechanism of FRET, excitonic coupling, DNA induced chain conformation of C-PPV, as I believe this is equally important for future design of WSCPs based biosensors.

3.5 Intercalated DNA/MGC complex

Cationic MGC absorbs at 618 nm, it is non-fluorescent in aqueous solution and it becomes fluorescent upon intercalation with hybridized dsDNA (PL peak at 657 nm). Presumably, intercalation restricts MGC's photoisomerization and restores PL emission. [167] As shown in Figure.3.5, the PL titration curves for 25 bp random dsDNA (dsDNA$(R)_{25}$) vs MGC dye loading for hybridized DNA with various base-pair (bp) mismatches: complementary (black color), 1 (blue), 3 (green) and 5 (red) base-pair mismatches. PL was monitored at 657 nm (excitation at 610 nm) and each titration performed at 1μM dsDNA$(R)_{25}$.

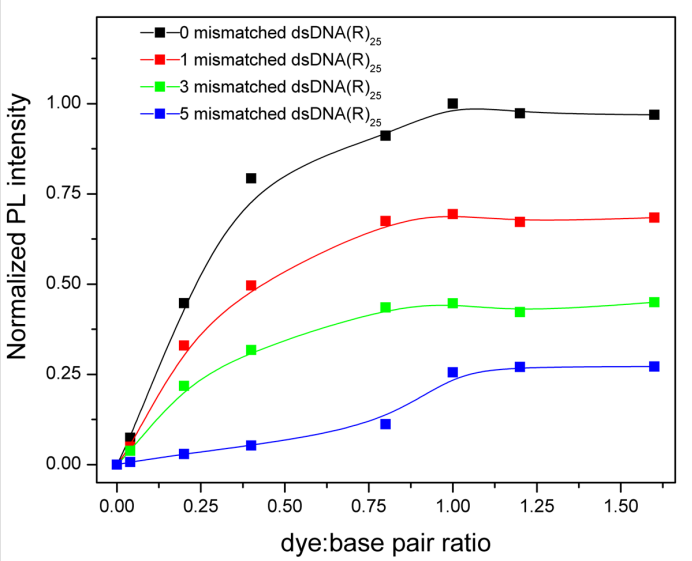

Figure 3.5. PL titration curves for 25 bp random dsDNA (dsDNA$(R)_{25}$) vs MGC dye loading for hybridized DNA with various base-pair (bp) mis-matches: complementary (black color), 1 (blue), 3 (green) and 5 (red) base-pair mismatches. PL was monitored at 657 nm (excitation at 610 nm) and each titration performed at 1μM dsDNA$(R)_{25}$. Reprinted with permission from Ref [20] Copyright (2014) American Chemistry Society

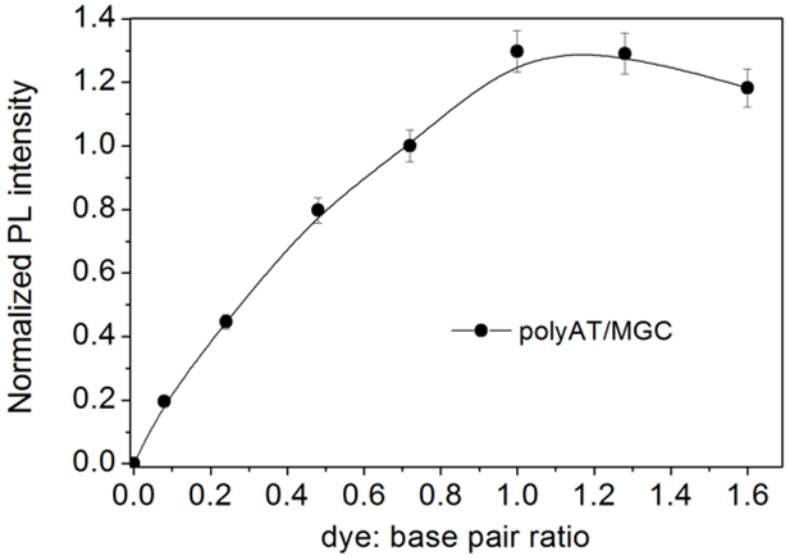

Figure 3.6. PL titration for a 25 bp polyAT vs MGC dye load performed at 1μM polyAT in 10 mM phosphate buffered saline (PBS). Reprinted with permission from Ref [20] Copyright (2014) American Chemistry Society

The PL titration curve for a 25bp random dsDNA (dsDNA$(R)_{25}$) hybridized from complementary sequences, 5'-*ATT GTC TGT GTC TGG TGT GCG TCT G*-3' (probe, P_0) and 5'-*CAG ACG CAC ACC AGA CAC AGA CAA T* (target, T_0) (black squares), (Figure.3.5, black squares and line) saturate at 1:1 dye:bp load, demonstrating the ability of MGC to intercalate hybridized DNA at maximum site occupancy. MGC is known to intercalate preferentially with A-T bp. [168, 169] Herein a 25 bp polyAT dsDNA was used as a model system in connection with 25 bp dsDNA$(R)_{25}$. PolyAT shows similar PL titration curve saturating at 1:1 dye:bp ratio (Figure.3.6).

The PL signal at maximum site density is 1.4-fold higher for polyAT/MGC than for dsDNA$(R)_{25}$/MGC, with dsDNA$(R)_{25}$ containing only 12 A-T bps (see Figure.3.6 vs Figure.3.5), thus confirming the preference of MGC towards intercalation with A-T bp where the intercalated dye presumably adopts a more rigid conformation that is less prone to photoisomerization than with C-G. This hypothesis is confirmed by the PL lifetimes measured from these complexes, 72 ps for polyAT/MGC vs 50 ps for dsDNA$(R)_{25}$/MGC, with both complexes loaded at maximum site occupancy. Circular dichroism (CD) spectroscopy of

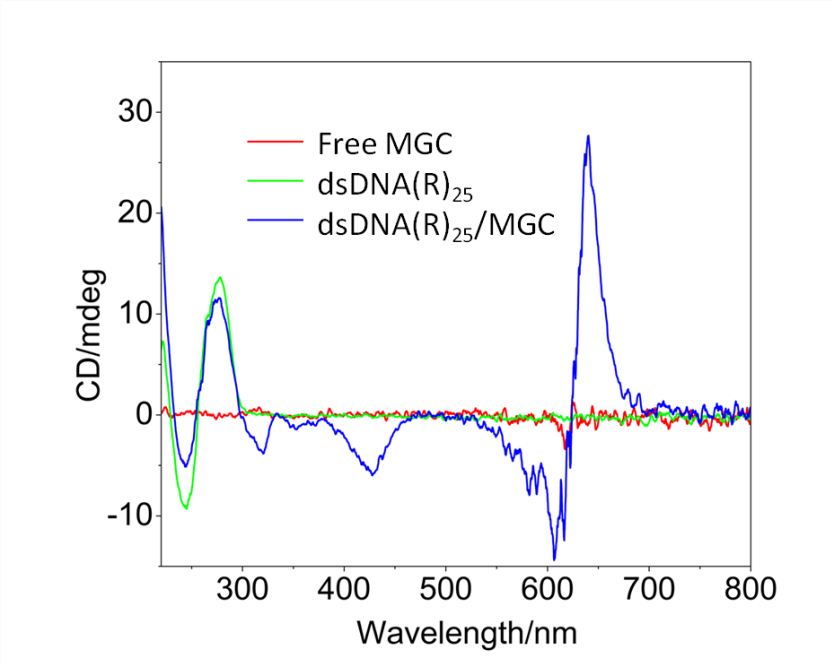

Figure 3.7. CD spectra of free MGC (62.5 μM), dsDNA$(R)_{25}$ (P_0, T_0) (black, 2.5 μM) and intercalated dsDNA$(R)_{25}$/MGC (blue, dsDNA$(R)_{25}$ 2.5μM, dye:bp ratio of 1:1). Reprinted with permission from Ref [20] Copyright (2014) American Chemistry Society

free MGC shows no chiroptical activity across the Uv-vis range. Instead, a dsDNA$(R)_{25}$/MGC complex intercalated at maximum site occupancy exhibits strong chiroptical activity in the 600-700 nm region (Figure.3.7), with a cross over at 620 nm where MGC absorbs maximally (Figure.3.5), providing the dsDNA$(R)_{25}$/MGC forms a complex. The negative band at high energy and the positive band at low energy are characteristic to dyes intercalated with dsDNA following the right-handed DNA helix, and with dyes excitonically coupled. [170–173] CD spectroscopy vs MGC dye loading for dsDNA$(R)_{25}$ reconfirms that this particular dye can be loaded at maximum site density (Figure.3.8). The CD-based titration data from show that intercalation produces small changes for the dsDNA$(R)_{25}$ bands at the 200-300 nm regions, provided that dye intercalation does not produces major disturbance to the dsDNA$(R)_{25}$ helix(Figure.3.8). The same data confirm, by the lack of change in both shape and peak position of the negative and positive CD bands of MGC with increased dye loading, that this dye does not change its binding mode from low to high site occupancy. [174] While MGC was suggested to bind both as an intercalator and as a groove

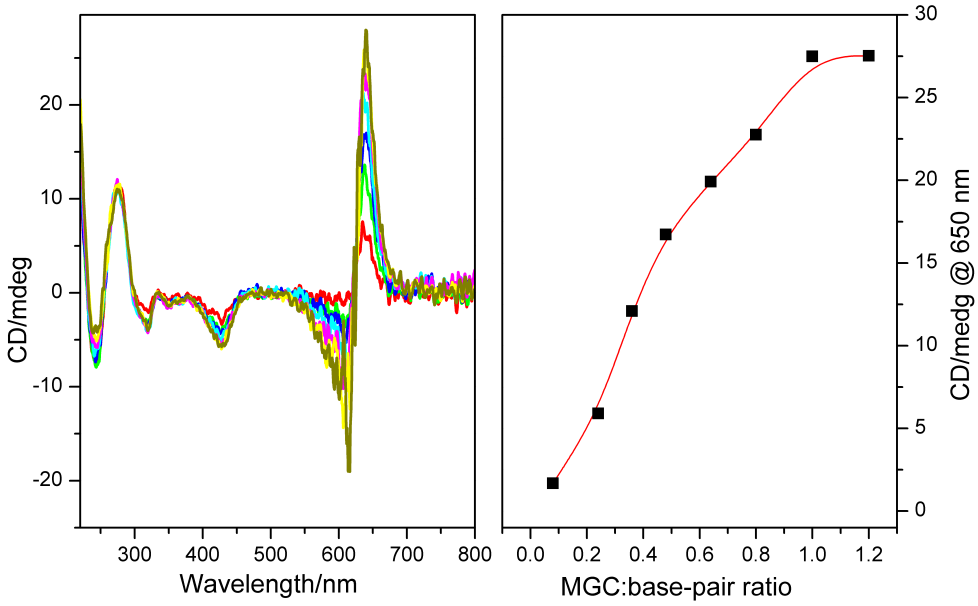

Figure 3.8. Left: CD spectra of dsDNA$(R)_{25}$ (P_0, T_0) vs MGC dye loading. Right: Titration of CD signal intensity @650 nm vs MGC dye loading.

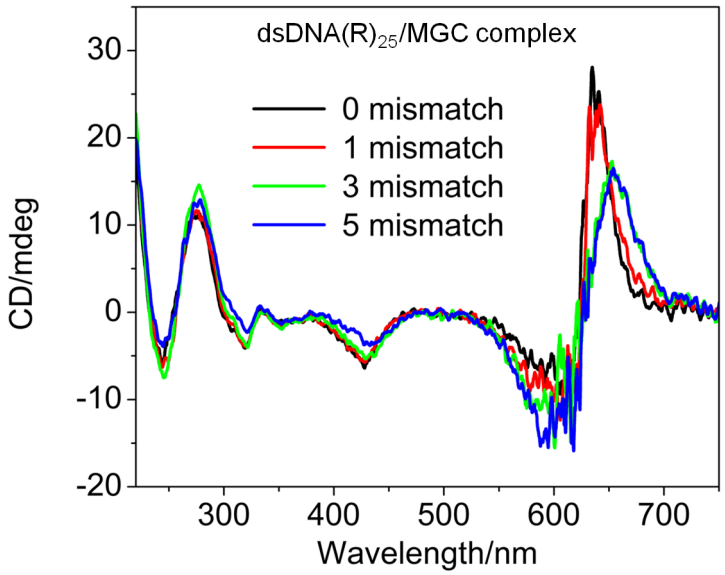

Figure 3.9. CD spectra for dsDNA$(R)_{25}$/MGC complex (1:1 dye:bp load) vs bp mismatch (dsDNA$(R)_{25}$ 2.5μM). Reprinted with permission from Ref [20] Copyright (2014) American Chemistry Society

binder, the CD data from Figure.3.8 suggests that intercalation is more likely the binding mechanism. For polyAT, a better chiral template than dsDNA$(R)_{25}$,

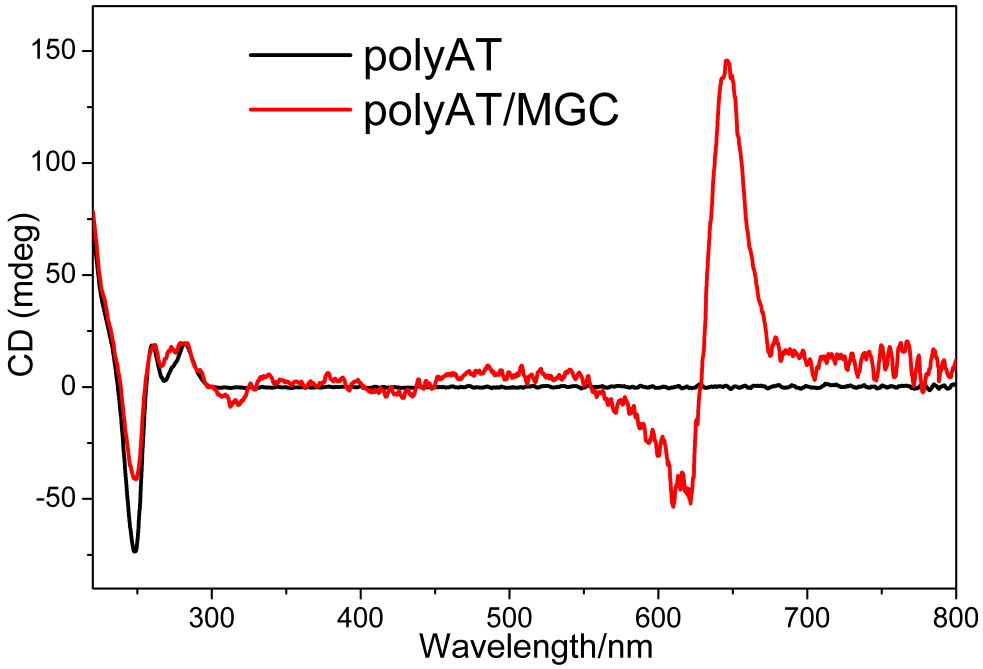

Figure 3.10. CD spectra of polyAT (black) and polyAT/MGC (red, 1:1 dye:bp ratio), each at a concentration of 5 μM polyAT in 10 mM PBS. Reprinted with permission from Ref [20] Copyright (2014) American Chemistry Society

the chiral signal at 600-700 nm becomes much stronger (Figure.3.10), providing that polyAT is a better template for MGC than dsDNA$(R)_{25}$ when imposing its chirality. The absorption spectra of dsDNA$(R)_{25}$/MGC and free MGC are identical, both in shape and peak position (Figure.3.11). Even polyAT/MGC absorption has similar shape like the free dye, and a slightly red shifted (2 nm) peak (Figure.3.11). Intercalators such as YOYO-1, TO-PRO1 and some other cyanine dyes where found to exhibit strong excitonic coupling in the form of H-type or J-type aggregates with characteristic blue or red shifted spectral bands next to the absorption of the free dye. [170, 171, 175, 176] In contrast, MGC seems to exhibit a weak excitonic coupling when complexed with dsDNA$(R)_{25}$, even at maximum site occupancy, most probably because of unfavorable dye-dye (dipole) orientation, and this topic is addressed later in this work. PL lifetimes vs site

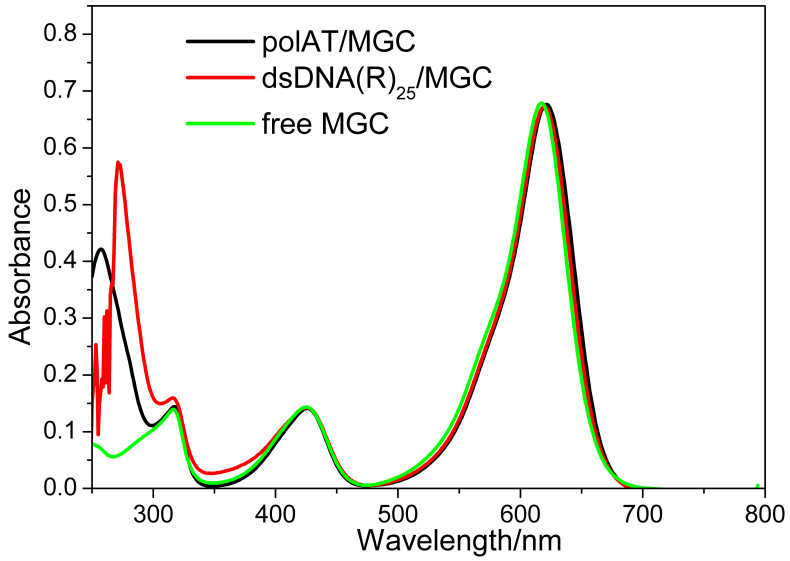

Figure 3.11. Uv-vis absorption spectra of free MGC (green color), dsDNA$(R)_{25}$/MGC complex (red color, 1:1 dye:bp load) and polyAT/MGC complex (black color, 1:1 dye:bp ratio), all in 10 mM PBS. dsDNA$(R)_{25}$ and polyAT were at a concentration of 1 μM, MGC at 25 μM, all in 10 mM PBS. Reprinted with permission from Ref [20] Copyright (2014) American Chemistry Society

density further confirm a weak excitonic coupling for intercalated MGC. For example, when the site density changes from 0.08:1 to 1:1 dye:bp, polyAT/MGC shows no change in PL lifetime (72 ps), while dsDNA$(R)_{25}$/MGC complex shows an 8% decrease in PL lifetime (from 72 ps to 50 ps), this later change reflecting the preference of MGC to bind first A-T bps. The dsDNA$(R)_{25}$/MGC complex with dyes loaded at maximum site density can be considered a molecular photonic wire with dyes excitonically coupled and exhibiting chiroptical activity. If any mismatch is present between probe and target ssDNA$(R)_{25}$, the number of dyes intercalated per hybridized dsDNA$(R)_{25}$ will decrease with the amount of base pair mismatch, and so will decrease the PL signal of the intercalated dsDNA$(R)_{25}$ (Figure.3.5) and the chiroptical signal at 600-700 nm (Figure.3.9) In other words, an increase in the number of bp mismatched degrades the quality of the intercalated dsDNA$(R)_{25}$ photonic wire. The dependency MGC's PL intensity vs base-pair mismatch provides sequence specificity for the proposed sensor.

3.6 C-PPV/DNA Complex

As discussed in section 2.2, this C-PPV has broad and structureless Uv-vis absorption and PL spectra (peaks at 440 nm and 527 nm, respectively), a molar extinction of $7 \times 10^5 M^{-1} cm^{-1}$ and a PL quantum yield (QY) of 15% in water. [148] Upon binding with the 25 bp dsDNA$(R)_{25}$ (T_0, P_0), as also shown in Figure.2.2 both the absorption and PL spectra of C-PPV red shift to 473 nm and 559 nm, respectively, (Figure.3.12ab), the PL spectrum gains vibronic structure and becomes strongly enhanced, with the PL QY increasing to 270% (Figure.3.12 c). These

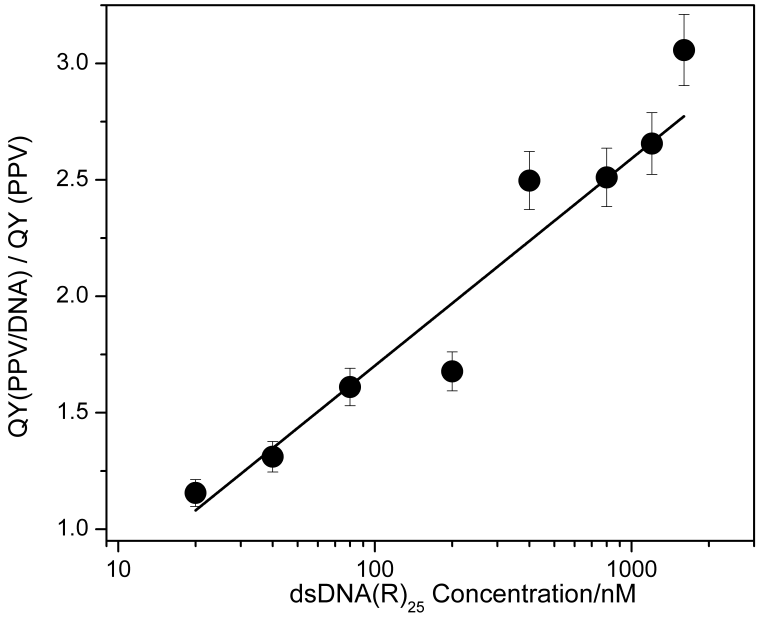

Figure 3.12. Relative PL quantum yield increase for C-PPV (1μM) binding to dsDNA$(R)_{25}$ (complementary P_0, T_0) as a function of dsDNA$(R)_{25}$ concentration. Reprinted with permission from Ref [20] Copyright (2014) American Chemistry Society

spectroscopic changes result from a polymer chain conformation change induced by the binding of C-PPV with DNA, with the polymer unfolding from a coiled state (C-PPV only) prone to inter/intra-molecular quenching (PL QY 15%), to an unfolded, stretch and less quenched state (C-PPV/DNA complex, PL QY 40%). PL lifetimes measured from C-PPV (0.14 ns) and C-PPV/dsDNA$(R)_{25}$ complex (0.40 ns) also support the assumption of a polymer conformation change in C-PPV when binding with dsDNA$(R)_{25}$. CD spectroscopy of C-PPV only (Figure.3.13)

shows no indication of chiroptical activity, instead a C-PPV/dsDNA$(R)_{25}$ equimolar complex (5 μM) displays chiroptical activity in the 350-550 nm region where C-PPV absorbs, with negative (high energy) and positive (low energy) bands crossing over at around the absorption peak of C-PPV/DNA complex. These bands

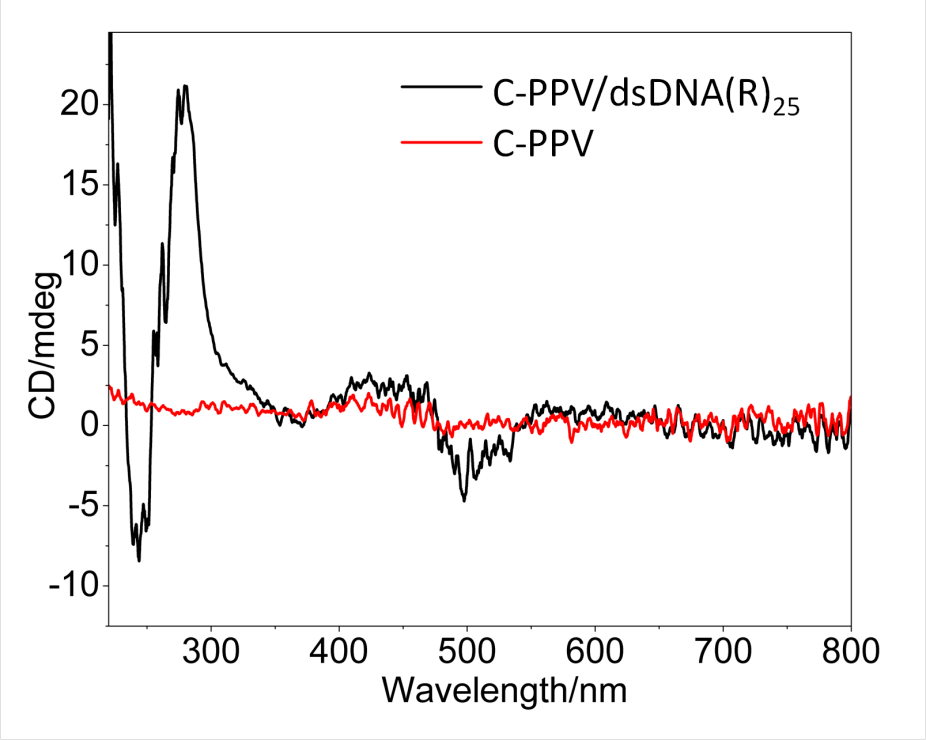

Figure 3.13. (a) CD spectra of C-PPV (red) and C-PPV/dsDNA$(R)_{25}$ complex (black). C-PPV and dsDNA$(R)_{25}$ concentrations were 2.5μM. Reprinted with permission from Ref [20] Copyright (2014) American Chemistry Society

and the crossover are much more clear for C-PPV/polyAT complex (Figure.3.14). Similar DNA-induced chiroptical activity has been reported for other cationic conjugated polymers. [93, 157] To attain such chirality, C-PPV binds electrostatically along the dsDNA$(R)_{25}$ phosphate backbone to uncoil and twist around the DNA duplex, following its helical structure (Figure.3.2). DsDNA$(R)_{25}$ imposed chirality on C-PPV is further supported by the observation of enhanced chirality for the case of polyAT (Figure.3.14), a better chiral template than dsDNA$(R)_{25}$. The proposed binding mechanism also agrees with the spectroscopic changes shown in Figure. 3.12 for C-PPV binding to complementary dsDNA$(R)_{25}$. Whether or not C-PPV's binding to dsDNA$(R)_{25}$ results in some disturbance of the dsDNA$(R)_{25}$

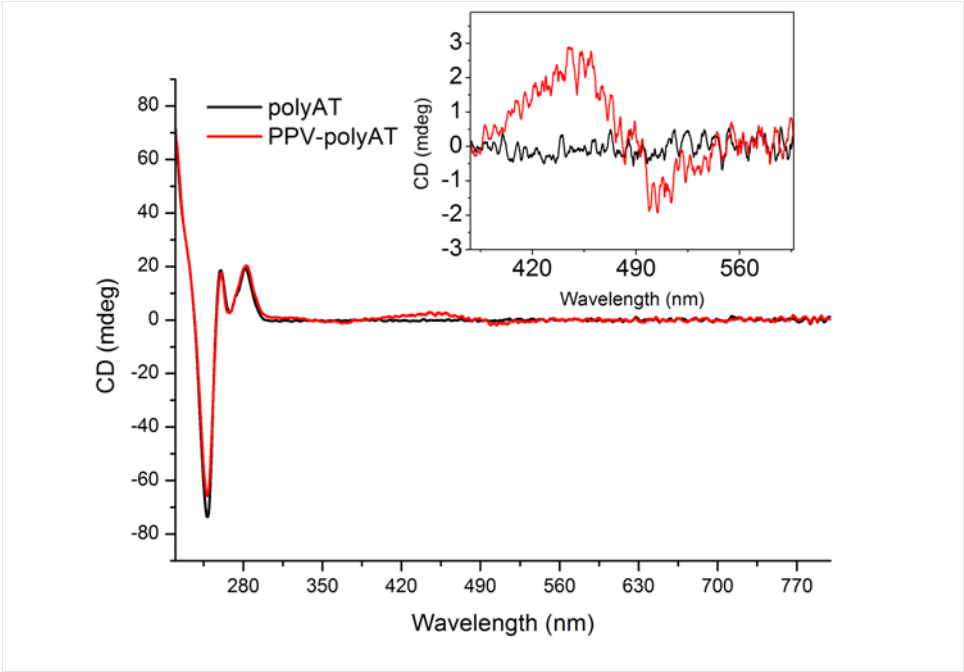

Figure 3.14. CD spectra of polyAT and C-PPV/polyAT complex. Each at a concentration of 5μM in 10mM phosphate buffer. Reprinted with permission from Ref [20] Copyright (2014) American Chemistry Society

helix is hard to assess based on the data from Figure.3.13 because C-PPV absorbs in the region of dsDNA$(R)_{25}$ and this might frustrate the CD signal from the C-PPV/dsDNA$(R)_{25}$ complex. The rather weak contribution of the positive band at around 600 nm in the CD spectrum of C-PPV (Figure.3.13), compared to two oppositely chiral peaks observed for intercalated MGC (Figure.3.7) is an indication that π-π stacking of C-PPV with dsDNA$(R)_{25}$ is weak and binding occurs mainly by electrostatic interaction.

3.7 C-PPV/DNA/MGC Complex

CD spectroscopy for the C-PPV/dsDNA$(R)_{25}$/MGC complex (Figure.3.15) shows that DNA induced chiroptical activity is preserved for both C-PPV and MGC when part of the complex and even at maximum, 1:1 dye:bp load. It is noticed from the comparison of the signals associated with DNA (200-300 nm) in the case of C-PPV/dsDNA$(R)_{25}$ (Figure.3.13) and C-PPV/dsDNA$(R)_{25}$/MGC that

there is a two-fold reduction in the intensity of the positive peak, which suggests alteration of the DNA helical structure when the intercalating dye is present. This opens the question if the C-PPV/dsDNA$(R)_{25}$/MGC complex is or is not partially bound. For C-PPV (Figure.2.1), each monomer bears two positively charged groups placed oppositely on the polymer backbone, but only one group will bind electrostatically with the phosphate backbone due to the sterical hindrance imposed by the C-PPV backbone. MGC (Figure.3.1) will also be stabilized by a single negative charge from the DNA phosphate backbone. Given that C-PPV (15 kDa) and dsDNA (25bp) are similar in length when fully extended, it can be deduced that the overall charge in the C-PPV/dsDNA$(R)_{25}$/MGC complex is balanced.

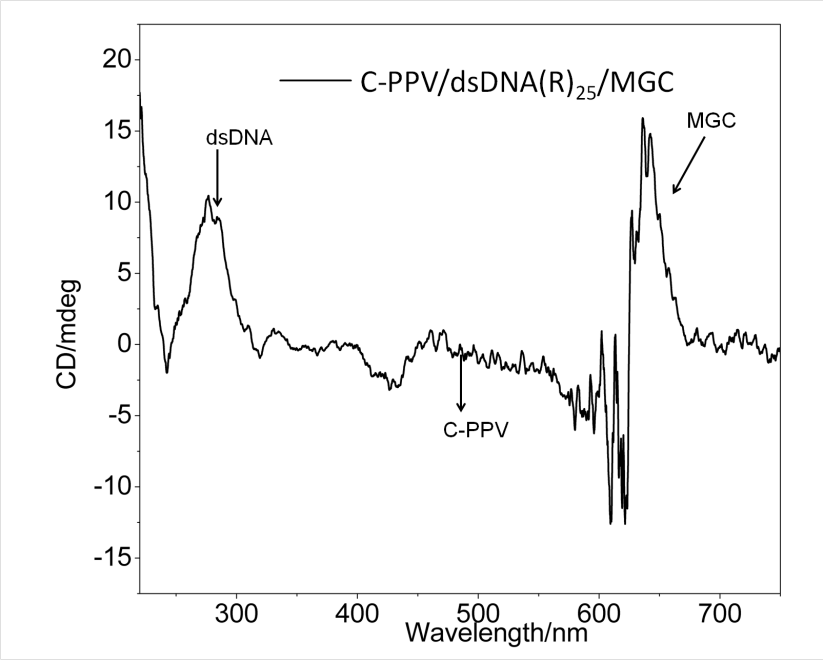

Figure 3.15. CD spectrum of C-PPV/dsDNA$(R)_{25}$/MGC complex with the MGC dye intercalated at 1:1 dye:bp ratio. C-PPV and DNA concentrations were 2.5μM. Reprinted with permission from Ref [20] Copyright (2014) American Chemistry Society

3.8 FRET in C-PPV/DNA/MGC Complex

I also studied the two FRET processes in the C-PPV/dsDNAR_{25}/MGC complex. One is homo FRET between intercalated MGC dyes and this occurs as a

manifestation of their excitonic coupling and as a result of the overlap existent between MGC's absorption and PL spectra. [177, 178] The second is hetero FRET from C-PPV to intercalated MGC dyes following C-PPV photoexcitation. Both processes are discussed below in relation to the unique binding of MGC and C-PPV imposed by the DNA scaffold.

3.8.1 Homo FRET between intercalated MGC dyes

Homo FRET induces depolarization of the PL emitted by the intercalated MGC dyes in a DNA/MGC complex and can be quantified by the steady-state PL anisotropy, A, which is defined as:

$$A = \frac{I_{\parallel} - I_{\perp}}{I_{\parallel} + 2I_{\perp}} \tag{3.2}$$

$I_{\parallel}$ is PL intensity measured parallel to the polarization of excitation light, while $I_{\perp}$ is PL intensity measured perpendicular to the polarization of excitation light. [103] The efficiency of homo FRET can be estimated by

$$E_{homo} = 1 - (A_{FRET}/A_0) \tag{3.3}$$

where A_{FRET} and A_0 are PL anisotropies in the presence and absence of homo FRET, respectively. Specific to our case, A_{FRET} and A_0 are the photoluminescence anisotropies measured from the intercalated DNA at maximum site density (1:1 dye:bp load) and at minimum site density (1 dye per dsDNA$(R)_{25}$, e.g. 1:25 dye:bp load) and equivalent to a population of randomly oriented dyes, that is A_0=0.4. In this assumption, eq.3.3 estimates a homo FRET efficiency of 65% for dsDNA$(R)_{25}$ (P_0, T_0), indicating a weak coupling between intercalated dyes in the dsDNA$(R)_{25}$/MGC complex.

For polyAT/MGC the measured PL anisotropy is 0.02 and this estimates a homo FRET efficiency of 95% according to eq.3.3, a value reflecting the increased excitonic coupling in polyAT compared to dsDNA$(R)_{25}$, as previously confirmed by CD spectroscopy (Figure.3.11). Weakly coupled excitonic interactions leading to homo FRET can be treated in the Förster formalism, where the FRET efficiency

[103] is

$$E = 1/[1 + (r/R_0)^6] \tag{3.4}$$

with R_0 Förster radius for energy transfer (donor-acceptor distance at which E becomes 50%). Let us assume dsDNA$(R)_{25}$ is of B-DNA type, with 10 bps per turn, and a 3.4 nm length per turn. Intercalation of dyes like YOYO-1 with DNA was found to extend DNA's persistence length with as much as 50% [176] that is, 5.1 nm per turn. Assuming the limiting case where the DNA helix is unperturbed, that is, a separation distance between adjacent intercalated MGC dyes of 0.34, eq.3.4 delivers a F*ö*rster radius of 0.36 nm for homo FRET for dsDNA$(R)_{25}$/MGC and of 0.49 nm for polyAT/MGC, when both complexes are intercalated at maximum site density. The F*ö*rster radius is,

$${R_0}^6 = (8.8 \times 10^{-5} \times \phi_D \times \kappa^2/n^4) \times J(\lambda) \tag{3.5}$$

with ϕ the PL QY of the unquenched donor, κ^2 the orientation factor, n the refractive index of the medium between donor and acceptor moieties and

$$J(\lambda) = F_D(\lambda)\epsilon_A(\lambda)\lambda^4 d\lambda \tag{3.6}$$

the overlap integral defining the spectral overlap between donor's PL and acceptor's absorption. For a limiting $R_0 = 0.36$ nm, and using the spectral data from Figure.3.1, and equation 3.5,3.6 estimate an orientation factor κ^2 less than 10^{-4} for dsDNA$(R)_{25}$/MGC using a molar extinction coefficient of $10^5 M^{-1}L^{-1}cm^{-1}$ and a PL QY of 2% for intercalated MGC, and a refractive index n=1.7 (DNA). This suggest an unfavorable orientation between adjacent dyes in the DNA scaffold, thus supporting the hypothesis of a weak excitonic coupling, as pointed out previously by the similarity between the absorption spectra of the intercalated and the free MGC dyes (Figure.3.11). A previous report on the binding of leuco malachite green (LMG), the reduced form of MGC, with DNA [169] suggested strong complexation with the phenyl group intercalated with the hydrophobic base pockets while the hydrophilic dimethylaminophenyl groups bind to the DNA's phosphate backbone. For MGC, the two dimethylaminophenyl groups are not equivalent, only one group is positively charged while the second retains a hydrophobic character. Since the

optical transition involved in both homo and hetero FRET (618 nm band) has a dipole polarized along the two dimethylaminophenyl groups, binding of a single such group to the phosphate backbone for MGC might result in an awkward conformation of the chromophore with a transition dipole moment oriented largely off the base pairs plane. At the same time, such binding might provide sufficient space to fill the DNA with this particular dye at maximum site density. In support of a more twisted intercalated MGC chromophore compared to intercalated LGM is the blue shifted main absorption peak of the former (618 nm for MGC compared to 640 nm for LGM). [173]

3.8.2 Hetero FRET from PPV to intercalated MGC

The hetero FRET efficiency E_{hetero} vs bp mismatch for C-PPV/dsDNA$(R)_{25}$ /MGC is shown in Figure.3.16 (square and line) and it was estimated from the PL quenching of the donor (C-PPV/DNA) by acceptor MGC intercalated into dsDNA (C-PPV/dsDNA/MGC complex).

$$E_{hetero} = 1 - (PL_{C-PPV/dsDNA/MGC}/PL_{C-PPV/DNA}) \tag{3.7}$$

Hetero FRET from C-PPV to intercalated DNA has the highest efficiency (93%) for complementary sequences (Figure.3.16). We now recall that CD spectroscopy indicated that MGC intercalates to follow the right-handed DNA helix (Figure.3.7,3.8,3.9) and C-PPV binds along DNA's phosphate backbone (Figure.3.13) and that MGC's and C-PPV's chirality are preserved in the C-PPV/dsDNA$(R)_{25}$/MGC complex (Figure.3.15). To estimate a Förster radius using eq.3.4 is unlikely in this case, as it is hard to precisely calculate the separation distance between C-PPV's backbone and the intercalated dyes. Nevertheless, the high value of E is due in part to the large spectral overlap between donor and acceptor moieties (Figure.3.1) and the high PL QY of the donor (C-PPV) attained upon binding with DNA. For C-PPV/polyAT/MGC complex, FRET proceeds with 99% providing that the quality of the intercalated DNA photonic wire is essential in attaining a highly efficient hetero FRET. Indeed, for sequences with mismatch, deterioration of the DNA scaffold due to mismatch results in a reduction of the acceptor dyes involved in FRET with C-PPV, but also in a

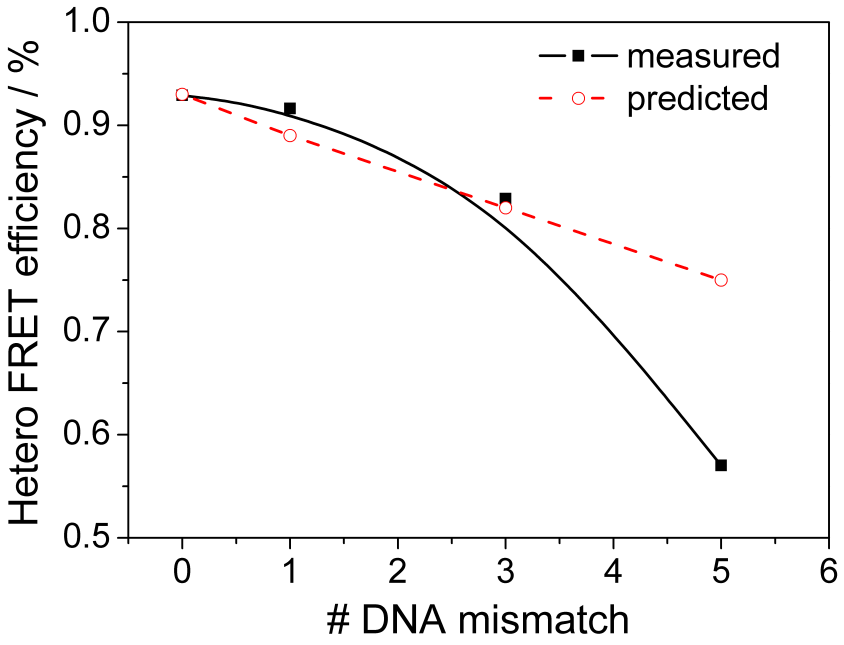

Figure 3.16. FRET efficiency vs bp mismatch for C-PPV/dsDNA$(R)_{25}$/MGC complex (see text for details on calculations). Reprinted with permission from Ref [20] Copyright (2014) American Chemistry Society

decreased donor-acceptor coupling and reduced FRET efficiency as shown by the non-linear dependency FRET efficiency vs mismatch from Figure.3.16 (square and line). Assuming each bp mismatch would result in the loss of one intercalated dye for the acceptor site, the expected FRET efficiency vs bp mismatch should be a linear dependency (Figure.3.16). It is indicated that any added mismatch perturbs the intercalated dyes, at least those in the adjacent base pairs, inducing more conformation flexibility for the in-tercalated dyes, that in turn enhances non-radiative channels against their emitted PL and degrades their excitonic coupling. In support of this hypothesis is the observation of a broadening and blue shift of the absorption spectrum of intercalated dsDNA$(R)_{25}$/MGC complex with added bp mismatch (Figure.3.9). While an increase in bp mismatch degrades the quality of the intercalated dsDNA$(R)_{25}$/MGC photonic wire, this in turn increases the sequence sensitivity at higher number of bp mismatches.

Several DNA sensors have been proposed with blue absorbing/emitting CPs combined with intercalators [105, 175, 179, 180], the majority reporting improved

target detection sensitivity by FRET. In ref [105] the rather unfavorable orientation for FRET between CP and intercalator (ethidium bromide), was compensated by the use of a dye labeled DNA with the dye acting as FRET mediator between the CP and intercalator. To overcome dye labeling of the probe DNA, in reference [105] ethidium bromide was replaced with a commercial intercalator, picogreen, a cyanine dye, to achieve increased sensitivity and sequence specificity up to 3 bp mismatch. For our sensor, DNA induced polymer chain conformation change combined with the particular binding and intercalation of MGC provides orientation favorable for a high FRET and higher sequence specificity. Meanwhile, our assay is more cost-effective by the use of an inexpensive intercalator compared to cyanine intercalators like picogreen.

3.9 Conclusion

In this chapter, I demonstrated a label free DNA sensing method that uses FRET between a cationic conjugated polymer and an intercalating dye, malachite green chloride, and I demonstrated detection of target DNA with sequence specificity down to single base pair mismatch and with a clear dependency of the FRET sensitized signal on the number of base-pair mismatches between probe and target sequences. The intercalated DNA/dye complex has a photonic wire behavior, with dyes excitonically coupled and chiroptically active, undergoing homo FRET. Any mismatch between probe and target sequences degrades the quality of the photonic wire, altering the emitted PL and chiroptical properties. The PL intensity vs bp mismatch provides the transduction mechanism for attaining sequence specificity for the proposed sensor. Coupling of the intercalated DNA photonic wire with a conjugated polymer in a hetero FRET scheme provides target signal amplification and increased sensitivity toward base pair mismatch. A gain in FRET efficiency is achieved through a polymer chain conformation resulting from the binding of the conjugated polymer with DNA and leading to an increase in PL quantum yield and red shift of the PL spectrum now better overlapping with acceptor's absorption. Polymer conformation proceeds from a coiled, self-quenched state to an uncoiled (stretched), unquenched state where the conjugated polymer twists around the DNA helix to achieve optical chirality. Despite the rather unfavorable orientation

for the intercalated dyes in the DNA scaffold leading to weak homo FRET, hetero FRET from the conjugated polymer to the intercalated dyes proceeds with rather high efficiency due to the unique binding of both moieties with DNA, providing short donor-acceptor separation distances and improved donor-acceptor spectral overlap.

Chapter 4

DNA-assisted Photoinduced Charge Transfer between Cationic Polyphenylene Vinylene and Cationic Fullerene

4.1 Introduction

Complexation of conjugated polymers like poly(phenylene vinylene) (PPV) with fullerene (C_{60}) for photo-induced charge transfer has attracted intense interest due to the potential utilization of nanomaterials like these in organic solar photovoltaic and sensory devices. [181–183] The underlying mechanism for these charge transfer complexes exhibits a photophysics dominated by the electronic structure of donor (conjugated polymers) and acceptor (fullerene), with an efficiency for charge transfer affected by the donor-acceptor energy band alignment and related interfacial separation. Depending on the solvent used for casting, nanomaterials like PPV and C_{60} can have different solubility and this can lead to poor donor and acceptor miscibility and/or aggregate formation, leaving interaction as the only driving force that is able to bring together the donor and acceptor molecules. [131] Water-soluble, oppositely charged conjugated polymers and fullerene are an alternative, featuring highly efficient charge transfer due to the electrostatic interaction that can bring the two moieties in close proximity as

showed by others [37, 131, 184] and herein. However, water soluble, same charge type (sign) PPV and fullerene exhibit poor or negligible charge transfer as the repulsion between same-sign charged species repel the donor and acceptor molecules. For such molecules one alternative to promote charge transfer is to use an optically inactive glue, such as oppositely charged DNA to bring same charged donor and acceptor molecules in close proximity. DNA has structural features that can facilitate interaction with such conjugated polymers like no other polyelectrolytes can, providing future possibility of constructing charge transfer nanoassemblies or acting as injection layer in conjugated polymer light emitting diodes. [185, 186]

In this chapter we show that DNA-assisted charge transfer between donor cationic PPV and acceptor cationic fullerene molecules can approach an efficiency as high as that observed for oppositely charged, cationic PPV and anionic fullerene and that charge transfer efficiency between such same sign molecules can be tuned just by switching ssDNA with dsDNA. As shown in Figure.4.1, DNA first induces chain conformational change to the cationic PPV (C-PPV), resulting in photoluminescence (PL) redshift and PL enhancement, as previously demonstrated in chapter 2. As also shown from sample solution in cuvette in Figure.4.1, the solution turned into bright yellow from dim green. After addition of cationic fullerene (C-C_{60}), DNA promotes the charge transfer between C-PPV and C-C_{60} by electrostatic attraction in C-PPV/DNA/C-C_{60} complex aggregates, with the PL of C-PPV/DNA complex solution severely quenched.(Figure.4.1) By combining steady state and time-resolved PL spectroscopic experiments with dynamic light scattering and zeta potential measurements, I unraveled the mechanism of PL quenching by charge transfer for DNA-assisted donor-acceptor complexes. While oppositely charge donor and acceptor molecules feature charge transfer in the form of static quenching, for DNA-assisted charge transfer complexes, the charge transfer proceeds as a combination of static and dynamic quenching for ssDNA and purely dynamic for dsDNA.

4.2 Materials and Methods

Cationic fullerene (C-C_{60})(Figure.4.2) and anionic fullerene (A-C_{60})(Figure.4.2) were synthesized according to ref. [186].Uv-vis spectra were measured with a Perkin

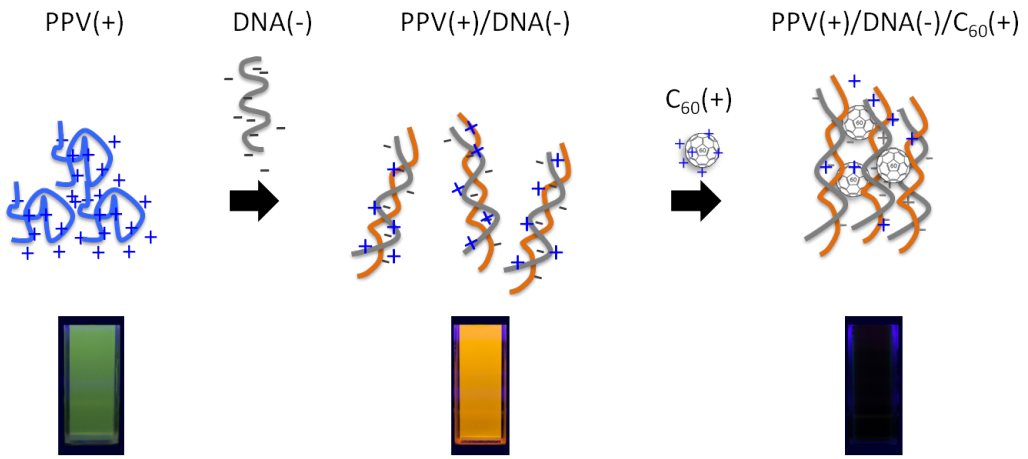

Figure 4.1. Scheme of DNA assisted charge transfer between cationic PPV (C-PPV) and cationic C_{60} (C-C_{60}).

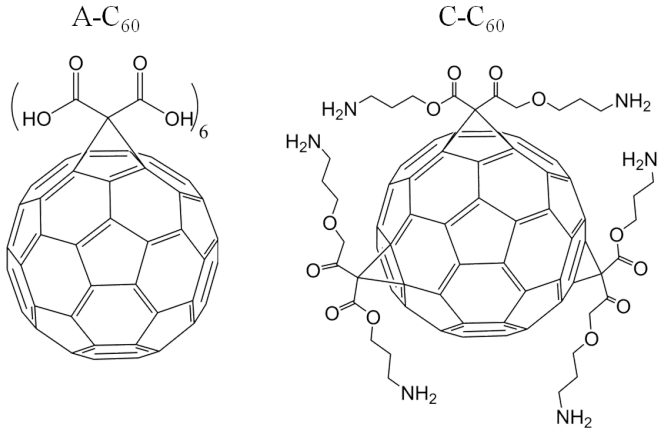

Figure 4.2. Chemical structures of anionic fullerene (A-C_{60}) and cationic fullerene (C-C_{60}) fullerene.

Elmer Lambda 25 spectrophotometer, photoluminescence spectra with a Varian Cary Eclipse fluorimeter. Dynamic Light Scattering (DLS): measurements were carried on a Malvern Zetasizer ZS instrument, equipped with a 633 nm laser source. Photoluminescence decays were measured and analyzed as discussed in chapter 3, section 3.2.

4.3 Charge transfer between oppositely charged PPV and Fullerene

An oppositely charged donor acceptor complex was made using the water soluble, cationic PPV (C-PPV, donor, Figure.2.1) and an anionic fullerene (A-C_{60}, acceptor, Figure.4.2). As shown in Figure.4.3, the electronic energy levels of PPV and C_{60} favor photo-induced electron transfer from photoexcited PPV to C_{60}, with PPV's lowest unoccupied (LUMO) and highest occupied (HOMO) molecular orbitals positioned at -3.7 eV and -6.2 eV, respectively and C_{60}'s LUMO and HOMO positioned at -4.7 eV and -6.8 eV, respectively. [148, 186] As already discussed in

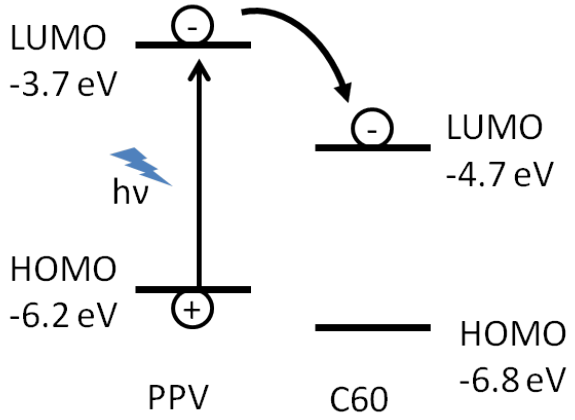

Figure 4.3. Scheme of photo-induced charge transfer from PPV to C_{60}

chapter 2, (Figure.2.1) C-PPV, [187] when dissolved in water (pH 5.5-6) absorbs at 430 nm and emits at 525 nm with an average PL lifetime of 0.19 ns. Addition of A-C_{60} to an aqueous solution of donor C-PPV (0.3 μM) dramatically quenches the PL of the conjugated polymer (see Figure.4.4a). A Stern-Volmer (SV) PL quenching plot PL(D)/PL(DA) vs [A-C_{60}] is shown in Figure.4.5 (black square and line), with PL(D) and PL(DA) being the PL intensities measured at the emission peak for donor only (C-PPV) and donor:acceptor (C-PPV:A-C_{60}) complex, respectively, and derived from the PL spectra from Figure.4.4a. The SV curve exhibits an upward curvature, with the highest quenching efficiency E=92%

$$E = 1 - PL(DA)/(PL(D) \tag{4.1}$$

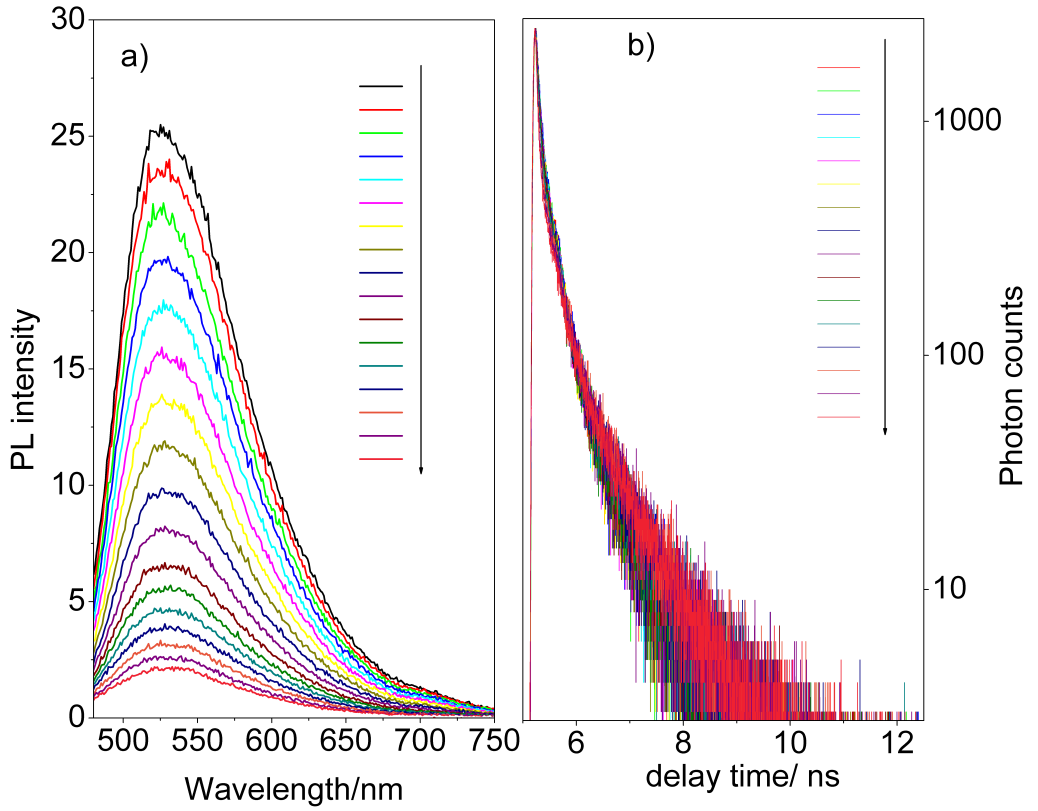

Figure 4.4. Charge transfer in C-PPV:A-C_{60} complex. (a) PL spectra and (b) PL decays for the C-PPV:A-C_{60} complex for various donor:acceptor molar ratios, from 10:1 to 1:3. C-PPV concentration at 0.3 μM. The arrows indicate the increasing concentration of A-C_{60}.

observed for a C-PPV:A-C_{60} molar ratio of 1:3. PL decays from C-PPV:A-C_{60} complexes at various donor:acceptor molar ratios are shown in Figure.4.4b and the PL lifetime dependency τ_D/τ_{DA} is shown in Figure.4.4 (red square and line) is flat, i.e., there is no change in PL lifetime value of C-PPV with added A-C_{60}. Such manifestation is known as static quenching [103, 188, 189] and in this case donor (C-PPV) and acceptor (A-C_{60}) pre-associate in the ground state to form a stable complex (C-PPV:A-C_{60}) where the acceptor completely quenches the donor's PL. As such, the true efficiency for charge transfer in the case of oppositely charged, pre-complexed C-PPV and A-C_{60} molecules can be considered E=100%. Static quenching can be described by a Stern-Volmer (SV) equation of the type [189]

$$PL(D)/PL(DA) = 1 + k_s[A] \tag{4.2}$$

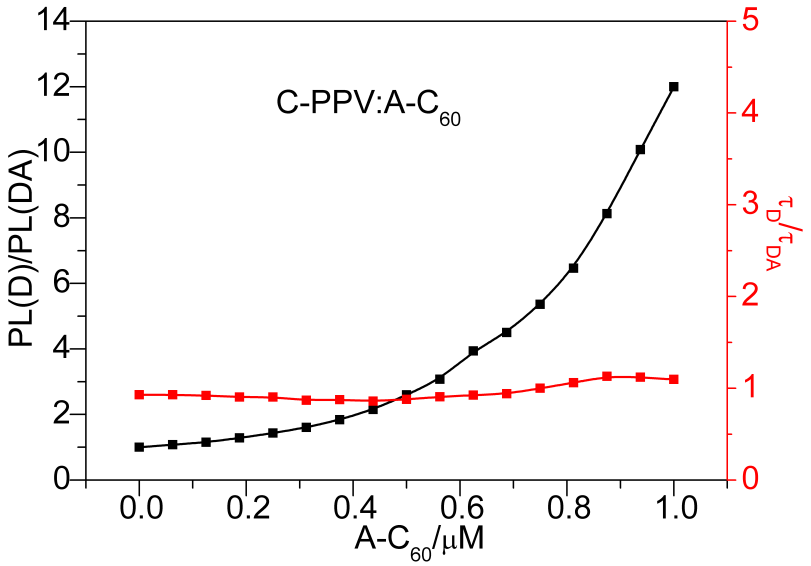

Figure 4.5. Stern-Volmer quenching curve PL(D)/PL(DA) intensity vs [A-C_{60}], black squares and line, and lifetime τ_D/τ_{DA} vs [A-C_{60}], red squares and line. C-PPV concentration 0.3 μM.

with k_s association constant for the donor-acceptor complex. A fit of the linear part of the Stern-Volmer curve from Figure.4.5 with eq.4.2 yields k_s=2.2 $(\mu M)^{-1}$. When same-sign charge, cationic C-PPV and cationic C-C_{60}, were mixed at various molar ratios, no PL quenching was observed, neither in intensity nor in lifetime (see Figure.4.6,), confirming that same-sign charge, cationic donor and acceptor molecules repel each other at distances cancelling the charge transfer (E=0%).

Another oppositely charged donor-acceptor complex, anionic PPV (A-PPV) (Figure.4.7) [152]and cationic C_{60} (C-C_{60}) (Figure.4.2) was also studied. After addition of C-C_{60}, the PL of A-PPV is also severely quenched, as shown in Figure.4.8. The SV plot calculated from PL spectra also shows an upward curvature, and the quenching efficiency E=1-$PL(DA)/PL(D)$= 93%, similar to that of C-PPV/A-C_{60} complex. However, the dependency of PL(DA)/PL(D) shows a nonlinear decrease with increasing [C-C_{60}]concentration which behaves differently from that formed in C-PPV:A-C_{60}(Figure.4.5), with the PL lifetime dependency τ_D/τ_{DA} in A-PPV/A-C_{60} complex increasing at high acceptor concentration (0.7μM-1.0μM). Such lifetime changes indicate that dynamic (collisional) quenching occurs at high [C-C_{60}] concentration. As found by DLS measurements (Figure.4.10), complexation of A-PPV with [C-C_{60}], [A-PPV] results in aggregates,(size increases from

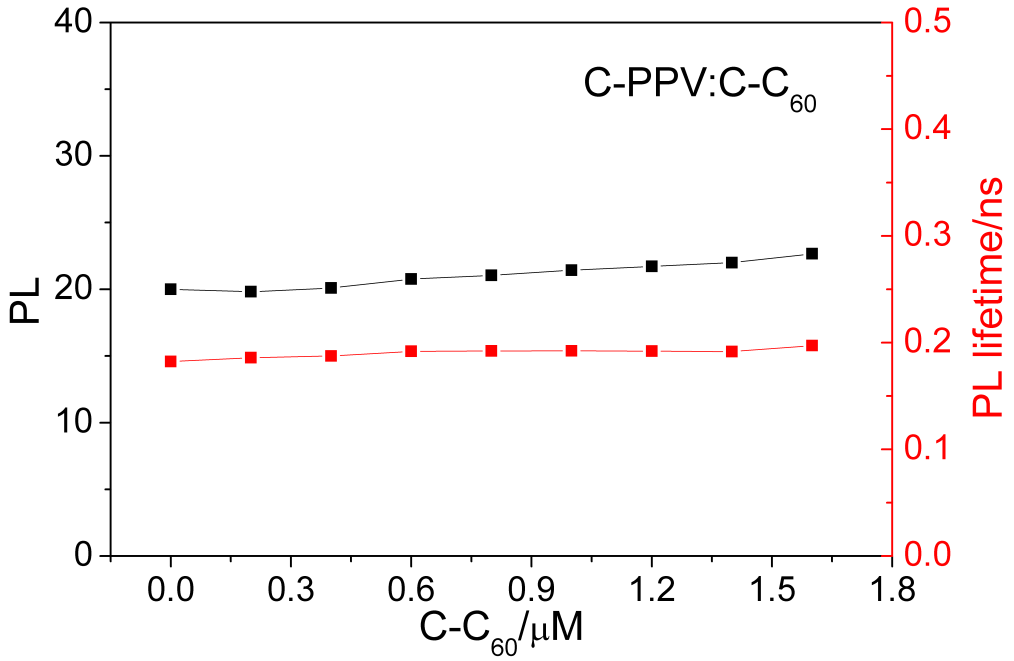

Figure 4.6. PL intensity (black) and lifetime (red) vs [C-C_{60}]. C-PPV concentration 0.3 μM.

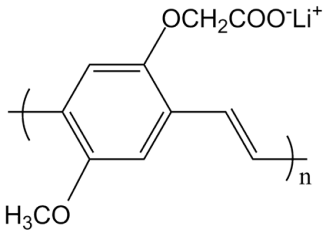

Figure 4.7. Chemical structure of A-PPV.

11 nm to 47 nm.) This suggest formation of aggregates leading to collisional quenching. In contrast, [A-C_{60}] breaks [C-PPV] aggregates from 470 nm to 70 nm (Figure.4.10), which indicates good miscibility of two species facilitating purely static quenching.(Figure.4.4,4.5). From zeta potential measurements, the surface charge of C-PPV in water is +37.2 mV, and C-PPV/A-C_{60} complex decreases a little to +29.7 mV, compared with their oppositely charged counterparts -47.3 mV (A-PPV) and -12.3 mV(A-PPV:C-C_{60}), respectively. The smaller decrease of surface charge from C-PPV to C-PPV/A-C_{60} complex can be attributed to the breaking of C-PPV aggregates; the larger decrease of the oppositely charged coun-

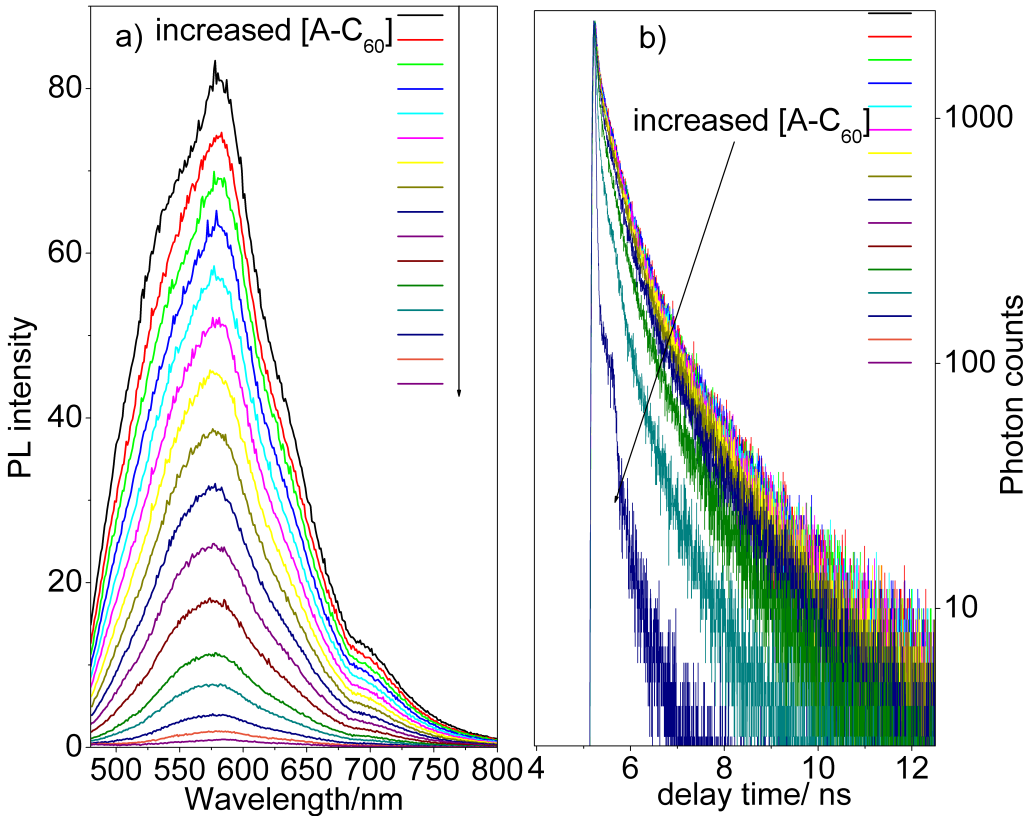

Figure 4.8. Charge transfer in A-PPV:C-C_{60} complex. (a) PL spectra and (b) PL decays for the C-PPV:A-C_{60} complex for various donor:acceptor molar ratios, from 10:1 to 1:3. A-PPV concentration 0.3 μM. The arrows indicate increased concentration of A-C_{60}.

terparts (A-PPV:C-C_{60}) should be a result of fromation of large aggregates as surface charges were neutralized during the electrostatic assembly.

4.4 SsDNA-assisted charge transfer between cationic PPV and cationic Fullerene

When negatively charged ssDNA was introduced as an optically inactive glue, efficient PL quenching by charge transfer was observed (Figure.4.11 and 4.12). A DNA-assisted, C-PPV:ssDNA:C-C_{60} charge transfer hybrid was assembled in two steps. First, C-PPV was mixed with a random 25mer ssDNA sequence in water (pH 5.5). The resulting C-PPV:ssDNA complex features spectrally red shifted

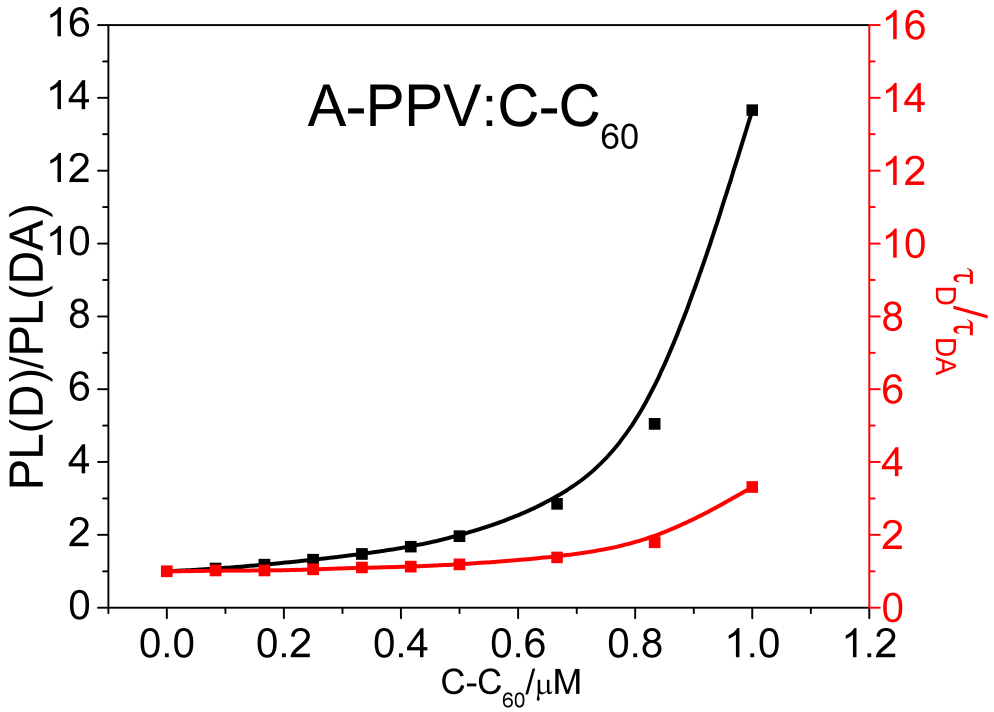

Figure 4.9. Stern-Volmer quenching curve of A-PPV:C-C_{60}, PL intensity PL(D)/PL(DA) vs [C-C_{60}], black squares and line, and lifetime τ_D/τ_{DA} vs [C-C_{60}], red squares and line. A-PPV concentration 0.3 μM.

absorp-tion and PL spectra, an almost four fold increase in PL quantum yield and an increased PL lifetime (0.47 ns in water) compare to 0.19 ns for pure C-PPV in water. We reported these observations recently in [190] and associated them with a chain conformation change of C-PPV when binding to ssDNA. DNA possesses a rich negatively charged phosphate backbone, and as such, the resulting C-PPV:DNA complex, as examined by zeta potential measurements, has an a net negative charge (Table 4.1, zeta potential -20.1 mV), therefore still being able to bind positively charged molecules/species. In a second step, to the aqueous solution of precomplexed C-PPV:DNA, we added the acceptor, cationic C-C_{60}, to observe dramatic PL quenching from the resulting C-PPV:ssDNA:C-C_{60} hybrid, both in intensity and lifetime (see Figure.4.11,4.12), with a maximum quenching efficiency of 90.7% observed at a donor:acceptor molar ratio of 1:6. A Stern-Volmer quenching plot, PL(D)/PL(DA) vs [C-C_{60}], could be derived from the PL spectra from Figure.4.11a and Figure.4.12, black square and line). The SV quenching curve shows a complex behavior, with an upward curvature at low-to-intermediate accep-

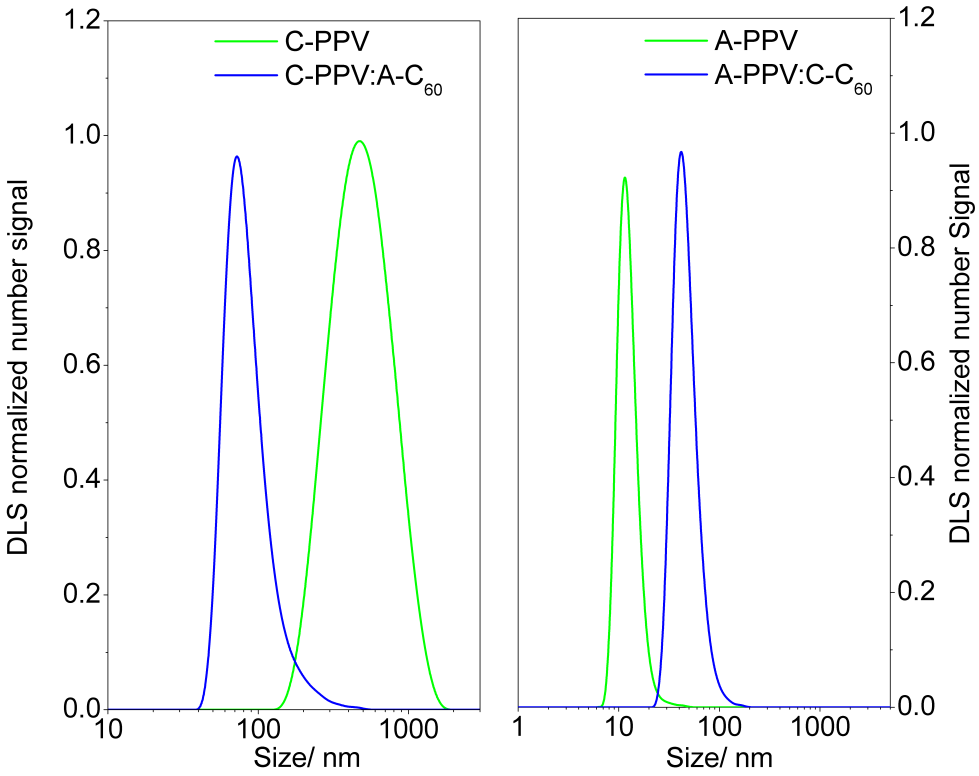

Figure 4.10. Left: dynamic light scattering measurements of C-PPV(green), C-PPV:A-C_{60} (blue); Right: dynamic light scattering measurements of A-PPV (green line), A-PPV:C-C_{60}(blue). Both PPV was dissolved in water at concentration 0.3 μM. PPV:C_{60} ratio is 1:3.

tor concentration (Figure.4.12, 0-0.8μM [C-C_{60}], followed by a downward curvature at high acceptor concentration (Figure.4.12, 0.8-1.6μM), with a point of inflexion at 0.8μM estimated from the 2nd derivative of PL(D)/PL(DA) vs [C-C_{60}] curve from Figure.4.12 (see Figure.4.13,). PL decays from the C-PPV:ssDNA:C-C_{60} hybrid are displayed in Figure.4.11b, and they feature a reduction in PL lifetime with added acceptor, up to 52 ps at a donor:acceptor molar ratio of 1:5. The quenching efficiency calculated from PL lifetimes at this molar ratio is $E = 1 - \tau_{DA}/\tau_D = 89\%$, close to that calculated from the PL intensity. The trend in PL lifetimes with added acceptor is shown by the τ_D/τ_{DA} vs [C-C_{60}] dependency from Figure.4.12c (red square and line). Changes in PL intensity accompanied by changes in PL lifetime may be indicative that both static and dynamic (collisional) quenching

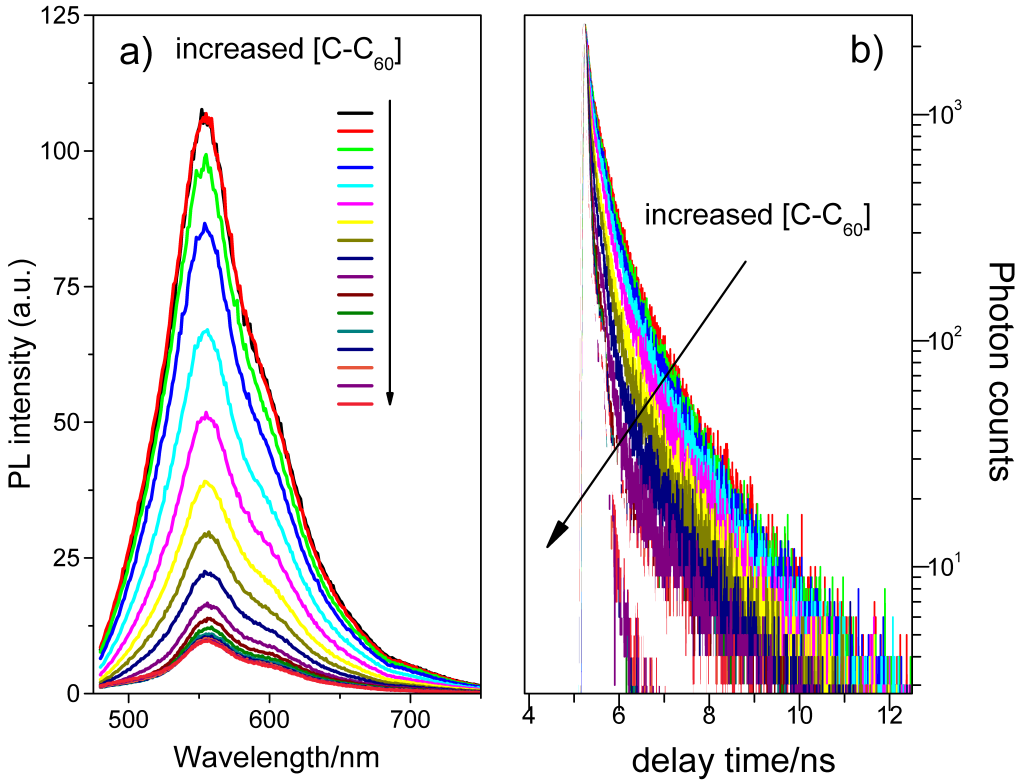

Figure 4.11. Charge transfer in C-PPV:ssDNA:C-C_{60} hybrid. (a) PL spectra, (b) PL decays. C-PPV:DNA molar ratio was 1:3 (0.3 μM C-PPV),the arrows indicate the increasing concentration of C-C_{60}.

are present. [189] When PL(D)/PL(DA) vs [A] exhibits a linear dependency,

$$\tau_D/\tau_{DA} = 1 + k_D[A] \tag{4.3}$$

with k_D dynamic quenching constant, the SV quenching curve can be modeled by a combined static/dynamic quenching model featuring a quadratic dependency, [189, 191]

$$PL(D)/PL(DA) = (1 + k_s[A])(1 + k_D[A]) \tag{4.4}$$

For nonlinear SV curves like that exhibited by C-PPV:ssDNA:C-C_{60} hybrid and shown in Figure.4.12 and accompanied by nonlinear PL(D)/PL(DA) vs [A] dependencies (Figure.4.12, red square and line), the quenching sphere of action is a more appropriate model. [103,190–192] This model assumes no static quenching to be present, instead an apparent static quenching component is attributed to the

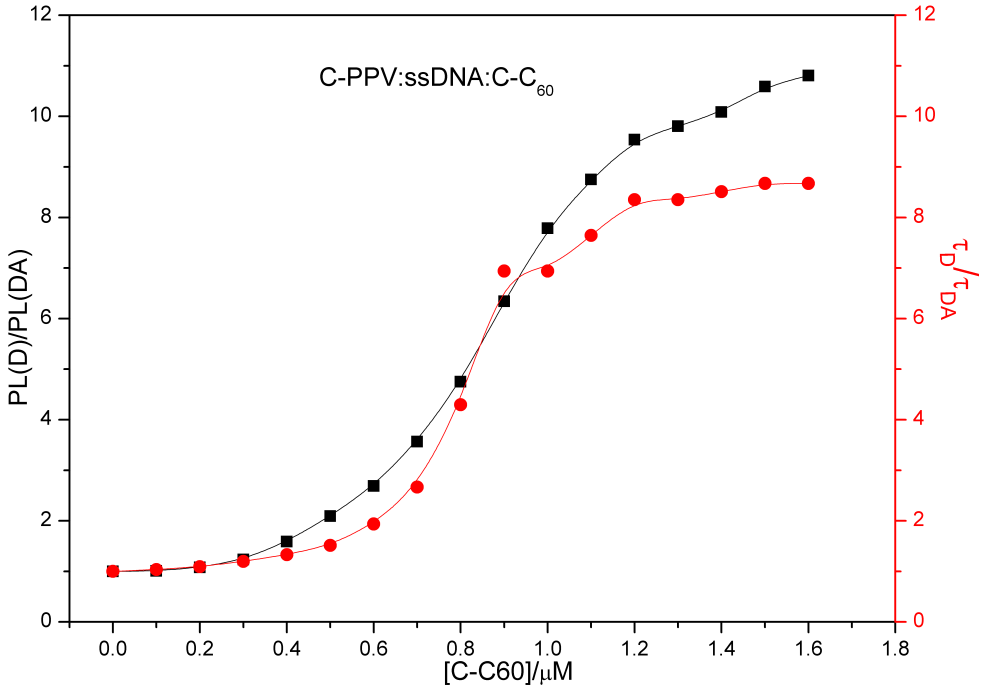

Figure 4.12. Stern-Volmer quenching curve, PL(D)/PL(DA) vs [C-C_{60}], black squares and line, and τ_D/τ_{DA} vs [C-C_{60}], red squares and line. C-PPV:DNA molar ratio was 1:3 (0.3 μM C-PPV).

Complex	Zeta potential/mV
C-PPV(in water)	+37.2
C-PPV (1mM PBS)	+11.0
C-PPV: A-C_{60} (water)	+29.7
C-PPV:ssDNA (in water)	-20.1
C-PPV:ssDNA:C-C_{60} (in water)	-5.19
C-PPV:dsDNA (1mM PBS)	-33.7
C-PPV:dsDNA:C-C_{60}(1mM PBS)	-16.56

Table 4.1. Surface zeta potential measurements. C-PPV was 0.3 μM. Molar ratio of C-PPV:A-C_{60} was 1:3, C-PPV:ssDNA:C-C_{60}=1:3:5; C-PPV:dsDNA:C-C_{60}=1:3:15.

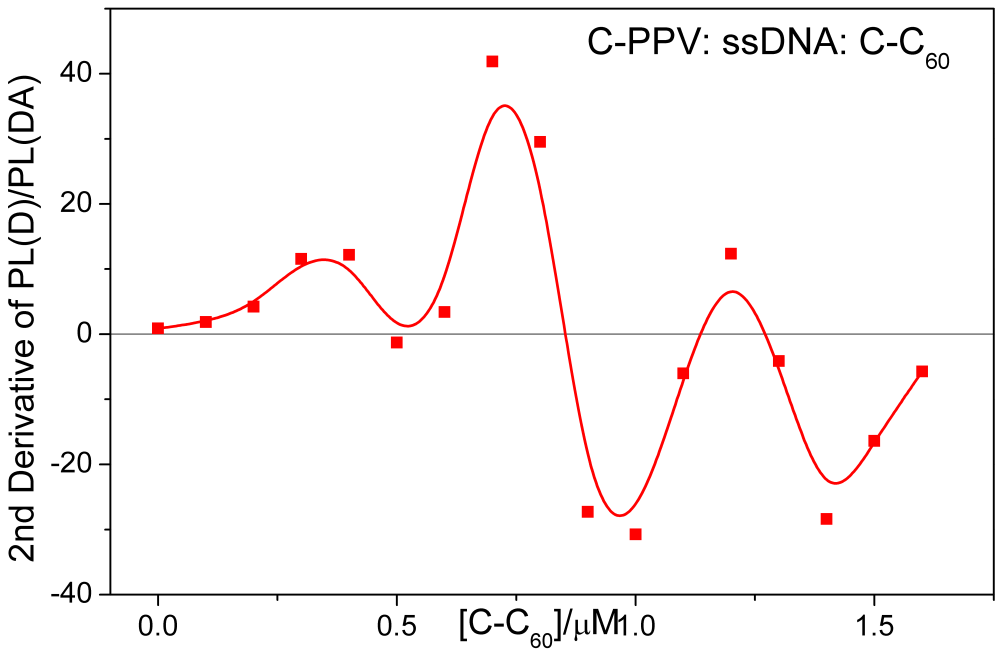

Figure 4.13. 2nd derivative of PL(D)/PL(DA) vs [C-C_{60}] dependency from Figure.4.12, with an inflexion point at a C-C_{60} concentration of about 0.8 μM.

presence of the quencher near the emitter in a volume (sphere of action) where the probability of quenching following optical excitation is unity. [20, 189, 192] A general equation can be written for this model as follows: according to ref [192], the fractional accessibility, or the percentage of emitters available for quenching can be defined as:

$$f_a = \frac{I_0^a}{I_0^a + I_0^b} I_0 = I_0^a + I_0^b \tag{4.5}$$

with

$$I_0 = I_0^a + I_0^b \tag{4.6}$$

the total PL intensity in the absence of the quencher, composed of I_a^0 as the PL intensity from emitters available (accessible) for quenching, and I_b^0 as the PL intensity from emitters inaccessible for quenching. According to the quenching sphere of action model, the PL intensity in the presence of a acceptor A can be written:

$$I = \frac{I_0^a}{(1 + k_{SV})[A] exp(V[A])} + I_0^b \tag{4.7}$$

Combining equations 4.5-4.7 we obtain

$$PL(DA)/PL(D) = (1 - f_a) + \frac{f_a}{(1 + k_D)exp(V[A])} \tag{4.8}$$

Thus,

$$PL(D)/PL(DA) = ((1 - f_a) + \frac{f_a}{(1 + k_D)exp(V[A])})^{-1} \tag{4.9}$$

with f_a=$PL^a(D)/[PL^a(D) + PL^b(D)]$ representing the fraction of emitters available for quenching and V, the sphere of action volume. For a SV curve exhibiting upward curvature, $f_a = 1$ (all emitters are available to be quenched) and eq. 4.9 becomes the classic formula describing the sphere of action model [20, 103]

$$PL(D)/PL(DA) = (1 + k_D)exp(V[A]) \tag{4.10}$$

The complex SV curve from Figure.4.12 could be analyzed by splitting it according to the acceptor concentration range in low (0-0.4μM) and intermediate (2) (0.5-0.8μM) concentration regimes exhibiting upward curvature and a high concentration regime (3) (0.9-1.6μM) with downward curvature (see Figure.4.13). Distinction between low (1) and intermediate (2) regimes was done based on the PL(D)/PL(DA) vs [A] dependency, that is, linear vs nonlinear, respectively. For the first two regimes, we assume f_a=1 (all emitters available for quenching), and use eq. 4.10 to retrieve $k_D(1)$=$3.3 \times 10^{-5}(\mu M)^{-1}$ and V(1)=$1.05(\mu M)^{-1}$ and $k_D(2)$=$3.3 \times 10^{-5}(\mu M)^{-1}$and V(2)=$1.49(\mu M)^{-1}$, suggesting radii for the sphere of action of r(1)=75 nm and r(2)=84 nm, and very little or even absent dynamic quenching. Since the size of the C-PPV:ssDNA complex is around 50 nm (see Figure.4.16), we hypothesize that the radius of gyration for the C-PPV:ssDNA donor and the sphere of action radius at low and intermediate concentration are similar in value, provided that the acceptor concentration is sufficiently high so that there are always quenchers within the charge-transfer range of a C-PPV:ssDNA complex. [192] C-C_{60} is prone to aggregate at high concentration and it induces aggregation of C-PPV:ssDNA when part of the donor:acceptor hybrid (see Figure.4.16, 44-255 nm size range for C-C_{60} and 295 nm size for the C-PPV:ssDNA:C-C_{60} hybrid (Figure.4.16). At high concentration, the SV curve bends downwards (Figure.4.12), which according to equation4.9 would imply

C-C_{60} concentration/μM	0 – 0.4	0.5 – 0.8	0.9 – 1.6
f_a	1	1	0.9
V/(μM)$^{-1}$	1.05	1.46	2.07
k_D/(μM)$^{-1}$	3.3x10^{-5}	3.3x10^{-5}	0.46
r/nm	75	84	94

Table 4.2. Parameters derived from fitting Stern-Volmer quenching curve of C-PPV:ssDNA:C-C_{60} complex with modified "sphere of action" model. f_a, the percentage of emitters available for quenching; V, the sphere of action volume; k_D, dynamic quenching constant; r, radius of "sphere of action".

the number of emitters available to be quenched decreases. In fact, due to the aggregation of C-C_{60} at high acceptor concentration, it is the number of acceptors that are available to quench the emitters that change due to their grouping onto large sized aggregates. A fit of the SV curve for the high concentration range (region (3)) with eq. 4.9 provides $f_a(3)$=0.9, (high concentration regime) $k_D(3)$=0.46 μM^{-1} and V(3)=2.07 μM^{-1} which in turn provides a sphere of action radius of 94 nm, values which suggest that at high acceptor concentration charge transfer is mostly dynamic in nature. The net charge for the C-PPV-ssDNA:C-C_{60} hybrid at saturation (1:3:6 molar ratio) is -5.1 mV, From a molecular point of view, at low acceptor concentration the acceptor can still bind electrostatically to the C-PPV:ssDNA to be in the radius of quenching sphere of action since the C-PPV:ssDNA has a net negative charge. At high concentration, most of the charges in a C-PPV:ssDNA:C-C_{60} hybrid are balanced (zeta potential of hybrid at 1:3:6 molar ratio is -5.1 mV), leaving collisional quenching as the only option for the large aggregates of C-C_{60} acceptors when interacting by charge transfer with donor. Formation of aggregates of the acceptor molecules at high acceptor concentration leads to an apparent increase in the quenching sphere of action volume.

4.5 DsDNA-assisted charge transfer between cationic PPV and cationic Fullerene

C-PPV was also mixed with a random 25 base-pair dsDNA, with the DNA

hybridized in 1.0 mM phosphate buffered saline (PBS buffer) and the resulting C-PPV:dsDNA complex (1:3 molar ratio) also featured spectrally red shifted absorption and PL spectra, and increase in PL quantum yield (almost three fold)21, and an average PL lifetime of 0.32 ns. Addition of C-C_{60} to the C-PPV:dsDNA complex quenched both the PL intensity and PL lifetime as shown in Figure.4.14. We observed a maximum quenching efficiency of $E = 1 - PL(DA)(PL(D) = 92.3\%$ at saturation, where the donor (C-PPV:dsDNA)-acceptor (C-C_{60}) molar ratio was 1:3:15 (Figure.4.15). The efficiency calculated from the PL lifetimes for the same

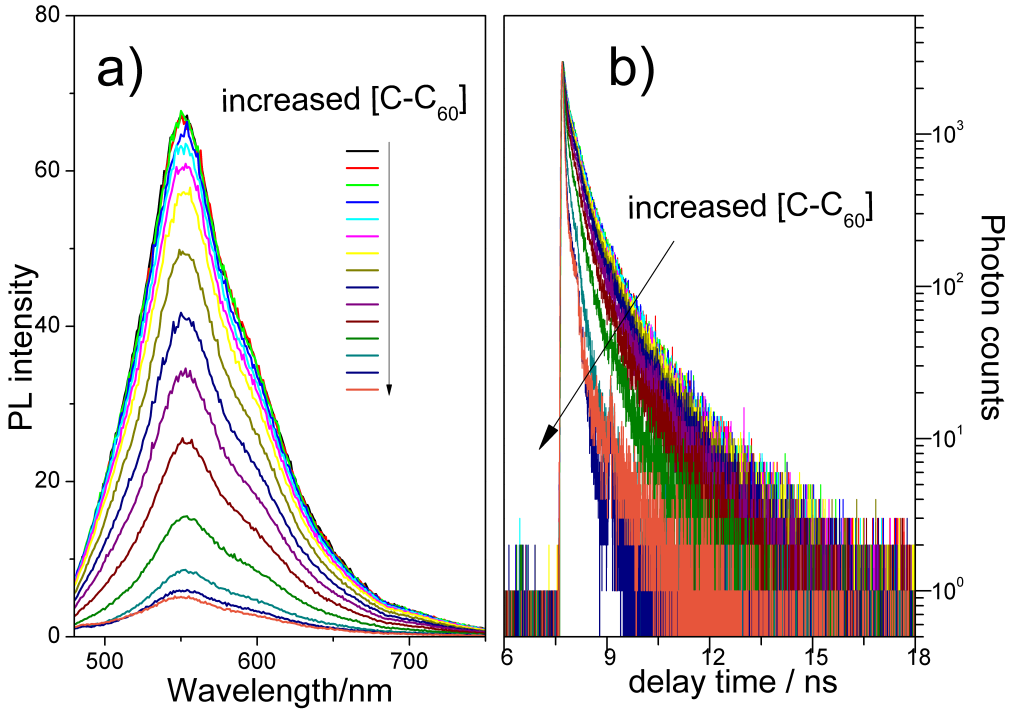

Figure 4.14. Charge transfer in C-PPV:dsDNA:C-C_{60} hybrid. (a) PL spectra, (b) PL decays. C-PPV:dsDNA molar ratio was 1:3(0.3 μM C-PPV), the arrow indicates the increasing concentration of C-C_{60}.

molar ratio was 84%. The Stern-Volmer quenching plot, PL(D)/PL(DA) vs [C-C_{60}], derived from the PL data from Figure.4.14a is shown in Figure.4.15 (black square and line), together with the PL(D)/PL(DA) vs [C-C_{60}] dependency (red square and line). Similar to the case of ssDNA (Figure.4.12), the SV curve for C-PPV:dsDNA:C-C_{60} hybrid also exhibits upward curvature at low acceptor concentration followed by downward curvature at high acceptor concentration, with an inflection point in the 3-4 μM [C-C_{60}] range. At low acceptor concentration,

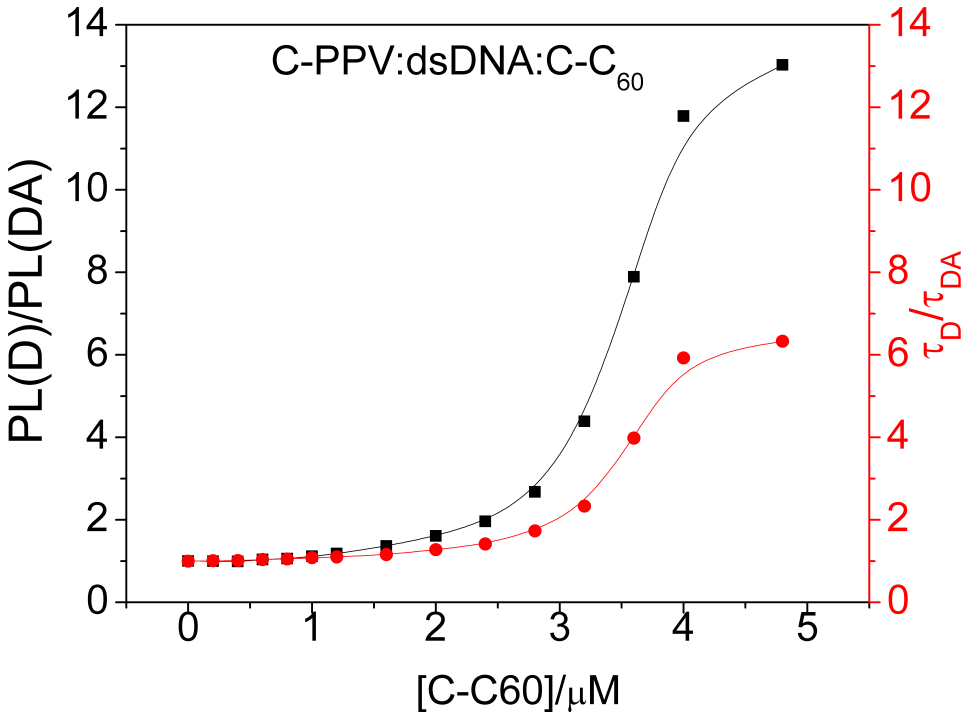

Figure 4.15. Stern-Volmer quenching curve, PL(D)/PL(DA) vs [C-C_{60}], black squares and line, and τ_D/τ_{DA} vs [C-C_{60}], red squares and line. C-PPV:dsDNA molar ratio was 1:3 (0.3 μM C-PPV).

both the SV curve and normalized PL lifetime vs [C-C_{60}] overlap and follow a linear dependency, suggesting that dsDNA assisted charge transfer is pure dynamic in this case. A fit with eq.4.3 for the PL(D)/PL(DA) vs [C-C_{60}] retrieves a $k_D = 5.6 \times 10^{-2} \mu M^{-1}$. The quenching behavior at high concentration is rather complex and hard to be modeled. DLS data point to extremely large charge transfer aggregates (1.9μm, see Figure.4.16), where molecular models like the quenching sphere of action fail. Figure.4.15 indicates that quenching in PL intensity is larger than in PL lifetimes, a fact also indicated by the difference between the Pl efficiencies estimated from intensity (92.3%) and lifetime (84%). Most probably, static quenching will play a role next to the dynamic quenching at high acceptor concentrations (higher than 1μM) where the two curves in Figure.4.15 deviate from each other. There is a significant difference between the dynamic range and the mechanism of PL quenching between ssDNA- and dsDNA-assisted charge transfer for the same donor:acceptor pair (C-PPV, C-C_{60}). For example, a maximum PL quenching of 92% observed for ssDNA-assisted CT is achieved at a donor:acceptor molar

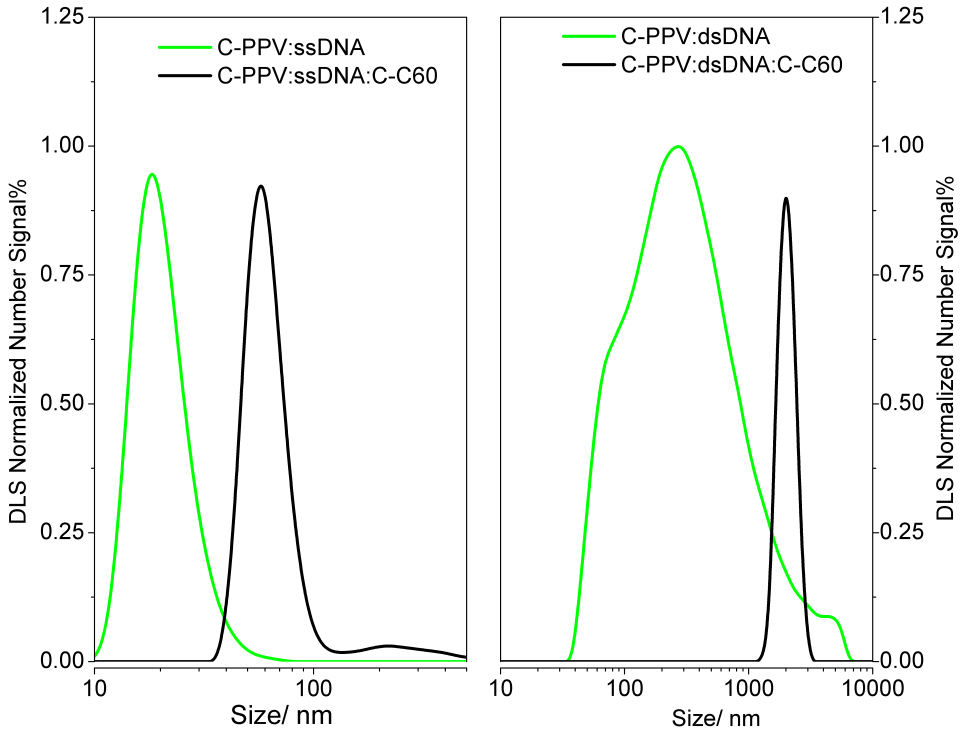

Figure 4.16. Dynamic light scattering measurements of (left) C-PPV:ssDNA (green line, water), C-PPV:ssDNA:C-C_{60} (black line, water) (right) C-PPV:dsDNA (green line, 1 mM PBS), C-PPV:dsDNA:C-C_{60} (black line, 1 mM PBS). Molar ratios for C-PPV:ssDNA, C-PPV:ssDNA:C-C_{60}, C-PPV:dsDNA and C-PPV:dsDNA:C-C_{60} were 1:3, 1:3:6, 1:3, 1:3:15, respectively. C-PPV concentration was 0.3 μM.

ratio of 1:6, while for the same donor-acceptor molar ratio, dsDNA provides only a 28% efficiency. We believe this difference in quenching efficiency is related in part to the difference in solubility of the acceptor in water vs PBS as well to differences in mutual interaction/binding between C-C_{60} and C-PPV promoted by ssDNA vs dsDNA. The zeta potential values measured for C-C_{60} in water and 1mM PBS are +44 mV and +20 mV, respectively. As such, more C-C_{60} acceptor will be needed to realize a C-PPV:dsDNA:C-C_{60} hybrid in PBS with similar quenching efficiency when compared to a C-PPV:ssDNA:C-C_{60} hybrid in water with similar efficiency. From previous studies we know that C-PPV and ssDNA bind strongly through a combination of electrostatic and hydrophobic interactions involving charged side groups, C-PPV's backbone and ssDNA bases. [190] While electrostatic interactions

ensures binding of C-C_{60} to the C-PPV:ssDNA complex, hydrophobic interactions between C-C_{60} and ssDNA bases may be responsible for bringing the donor and acceptor in close proximity for efficient CT. For C-PPV and dsDNA, hydrophobic interactions are much weaker since bases from complementary DNA sequences are now hybridized and not accessible by C-PPV, leaving only the electrostatic binding for the polymer, as a result, C-PPV was found to wrap/twist around the DNA's double helix. [20] Consequently, C-C_{60} will interact mainly electrostatically with dsDNA, and this will result in an increased separation donor-acceptor distance and as such a decreased efficiency for CT.

4.6 Conclusion

Water-soluble, same charge sign, cationic conjugated poly(phenylene vinylene) (PPV) and cationic fullerene were complexed with negatively charged ssDNA and dsDNA via electrostatic interaction and their charge transfer behavior was studied and compared to that of oppositely charged cationic PPV and anionic C_{60}, anionic PPV and cationic C_{60}. It was found that in both cases charge transfer proceeds with high efficiency but obeys different quenching mechanisms, combined static and dynamic for ssDNA and pure dynamic for dsDNA as opposed to a pure static quenching observed for opositely charge molecules. Replacing ssDNA with dsDNA provides a simple way to tune the efficiency for charge transfer, here by as much as four fold.

Chapter 5

Summary

Water-soluble conjugated polymers (WSCPs) have received intense interest in potential utilization in biosensing, including DNA sensing and in the development of optoelectronic devices. This thesis deals with the investigation of the mechanism of interaction between WSCP of the type of cationic poly(phenylene vinylene) (C-PPV) and DNA and the application of such polymers in label-free DNA sensing. Using steady-state and time-resolved PL spectroscopic methods in combination with structural characterization by dynamic light scattering and circular dichroism, a wealth of knowledge was acquired in terms of microscopic picture of the interaction between C-PPV and DNA and water-soluble electron acceptor molecules like fullerene.

Chapter 1 presents a brief survey of literature related to the utilization of WSCP in chemical/biological sensing and optoelectronic applications, highlighting works from other groups in connection to the research presented herein by myself.

Chapter 2 describes a series of spectroscopic and structural studies that helped me unravel the mechanism of interaction between a cationic poly(phenylene vinylene) (C-PPV) and DNA. Here I report the first DNA induced sequence-dependent photoluminescence enhancement ever reported for a cationic conjugated polymer, with the C-PPV's photoluminescence enhanced as high as seven fold. This manifestation is explained as resulting from an interplay between two interactions, (i) electrostatic attraction between C-PPV's positively charged side chains and DNA's negatively rich phosphate backbone and (i) hydrophobic π-π stacking between C-PPV's backbone and DNA bases imposing. I show that electrostatic interaction

is primordial in promoting hydrophobic interactions while the latter accounts for sequence-specificity of the photoluminescence enhancement.

Chapter 3 describes a label-free, sequence-specific DNA sensor based on F*ö*rster resonant energy transfer (FRET) occurring from the cationic PPV to a small intercalated dye, malachite green chloride. This sensor combines (i) conjugated polymer chain conformation change induced by the binding with DNA, and producing a wrapping/twisting of the polymer around the DNA helix and a three-fold increase in photoluminescence and (ii) FRET from conjugated C-PPV to the intercalated DNA. Because of its small size, the dye can be intercalated at maximal base pair loading, making the intercalated DNA a photonic wire with dyes excitonically coupled and chiroptically active through DNA-induced optical chirality. Base-pair mismatches between probe and target DNA decrease the amount of dye intercalated into DNA, alters the excitonic coupling of the photonic wire and decreases the photoluminescence output of the intercalated DNA, which in turn provides sequence specificity to the sensor. When coupled with the cationic PPV, FRET produces a 2.8x target signal amplification and an increased sensitivity towards base pair mismatch. In looking in detail at the mechanism of interaction between the components of the DNA sensor, I found that the DNA scaffold provides a unique structure for both polymer and intercalated dye in promoting efficient energy transfer, both directional (PPV to dye) and hopping (beteeen intercalated dyes), and this is because of the short separation distance between components of the sensor.

Chapter 4 describes the use of DNA in promoting highly efficient charge transfer between water soluble, same charge sign, donor and acceptor molecules which usually repel each other. DNA brings same charge type cationic PPV and cationic fullerene to realize a photoinduced charge transfer with efficiencies as high as those observed for oppositely charged water soluble donor and acceptor molecules with identical backbone. I then propose a simple way to tune charge transfer efficiency in such same charge sign donor and acceptor compounds by replacing ssDNA with dsDNA to observe a four-fold decrease efficiency in the latter case. Using stationary and time-resolved photoluminescence spectroscopy I investigated thoroughly the mechanism of quenching by charge transfer in DNA assisted charge transfer complexes to observe a combination of dynamic and static, different than the purely

static quenching observed for oppositely charged donor and acceptor molecules with identical backbones.

Appendix A

Comparison of DNA Sensors

Maxam-Gilbert DNA Sensor:

Technique	Chemical modification, gel electrophoresis
Reagent	Radioactive labeling
Read length/bp	>100
Sensitivity/M	10^{-9}
Sequence specificity/bp mismatch	Single (with PCR)
Advantages	Without requirement for further cloning
Disadvantages	Radioactive labeling and technical complexity

PCR based DNA Sensor:

Technique	PCR, gel electrophoresis
Reagent	Radioactive and fluorescent labeling
Read length/bp	>50
Sensitivity/M	10^{-9}
Sequence specificity/bp mismatch	Single
Advantages	Bring the cost per genome down from $100million to $10k, commercially available, widely incorporated with other methods
Disadvantages	Fluorescent and radioactive labeling, more expensive for large sequencing projects, low sequence specificity for short DNA (<50 bp), difficult to deploy in field detection

Mechanical DNA Sensor:

Technique	Atomic force microscopy, quartz crystal microbalance, photolithography, surface acoustic wave
Reagent	Cantilever, piezoelectric quartz crystal, electrode arrays
Read length/bp	15~240
Sensitivity/M	10^{-12}
Sequence specificity/bp mismatch	Single
Advantages	Real time detection
Disadvantages	High cost for silicon based photolithography

Electrical/electrochemical DNA Sensor:

Technique	Voltammetry, electrochemical impedance spectroscopy, Field-effect transistor
Reagent	Electrode, redox reagents, carboon nanotube
Read length/bp	20~300
Sensitivity/M	10^{-14}
Sequence specificity/bp mismatch	Single
Advantages	Achievable lab-on-a-chip; decreased electrochemical reaction time
Disadvantages	Electrochemically active interferences, low stability; electron-transfer pathways, high cost for miniaturization and integration of devices

Magnetic DNA Sensor:

Technique	Magnetic field
Reagent	micron-sized magnetic bead (microbead) and giant magnetoresistance (GMR) sensor arrays
Read length/bp	20~600
Sensitivity/M	10^{-14}
Sequence specificity/bp mismatch	Single
Advantages	Large surface area for DNA attachment, easy removal of nonspecific binding
Disadvantages	Inaccurate sensing results when using large microparticles; surface functionalization

Bibliography

[1] K. M. Coakley and M. D. McGehee, "Conjugated polymer photovoltaic cells," *Chemistry of Materials*, vol. 16, no. 23, pp. 4533–4542, 2004. [Online]. Available: http://dx.doi.org/10.1021/cm049654n

[2] J.-L. Brdas, D. Beljonne, V. Coropceanu, and J. Cornil, "Charge-transfer and energy-transfer processes in -conjugated oligomers and polymers: a molecular picture," *Chemical Reviews*, vol. 104, no. 11, pp. 4971–5004, 2004, pMID: 15535639. [Online]. Available: http://dx.doi.org/10.1021/cr040084k

[3] R. E. GAINS, "Outlook brightens for plastic solar cells."

[4] Z. He, C. Zhong, S. Su, M. Xu, H. Wu, and Y. Cao, "Enhanced power-conversion efficiency in polymer solar cells using an inverted device structure," *Nature Photonics*, vol. 6, no. 9, pp. 591–595, 2012.

[5] A. K. K. Kyaw, D. H. Wang, D. Wynands, J. Zhang, T.-Q. Nguyen, G. C. Bazan, and A. J. Heeger, "Improved light harvesting and improved efficiency by insertion of an optical spacer (zno) in solution-processed small-molecule solar cells," *Nano letters*, vol. 13, no. 8, pp. 3796–3801, 2013.

[6] U. Mitschke and P. Bauerle, "The electroluminescence of organic materials," *J. Mater. Chem.*, vol. 10, pp. 1471–1507, 2000. [Online]. Available: http://dx.doi.org/10.1039/A908713C

[7] S. R. Forrest and M. E. Thompson, "Introduction: organic electronics and optoelectronics," *Chemical Reviews*, vol. 107, no. 4, pp. 923–925, 2007.

[8] Y.-J. Cheng, S.-H. Yang, and C.-S. Hsu, "Synthesis of conjugated polymers for organic solar cell applications," *Chemical Reviews*, vol. 109, no. 11, pp. 5868–5923, 2009, pMID: 19785455. [Online]. Available: http://dx.doi.org/10.1021/cr900182s

[9] P. Xu, X. Han, B. Zhang, Y. Du, and H.-L. Wang, "Multifunctional polymer-metal nanocomposites via direct chemical reduction by conjugated polymers," *Chem. Soc. Rev.*, vol. 43, pp. 1349–1360, 2014. [Online]. Available: http://dx.doi.org/10.1039/C3CS60380F

[10] A. J. Heeger, "25th anniversary article: Bulk heterojunction solar cells: Understanding the mechanism of operation," *Advanced Materials*, vol. 26, no. 1, pp. 10–28, 2014.

[11] V. Coropceanu, J. Cornil, D. A. da Silva Filho, Y. Olivier, R. Silbey, and J.-L. Brdas, "Charge transport in organic semiconductors," *Chemical Reviews*, vol. 107, no. 4, pp. 926–952, 2007, pMID: 17378615. [Online]. Available: http://dx.doi.org/10.1021/cr050140x

[12] J. Roncali, "Synthetic principles for bandgap control in linear -conjugated systems," *Chemical Reviews*, vol. 97, no. 1, pp. 173–206, 1997, pMID: 11848868. [Online]. Available: http://dx.doi.org/10.1021/cr950257t

[13] P. A. Dalgarno, C. A. Traina, J. C. Penedo, G. C. Bazan, and I. D. W. Samuel, "Solution-based single molecule imaging of surface-immobilized conjugated polymers," *Journal of the American Chemical Society*, vol. 135, no. 19, pp. 7187–7193, 2013, pMID: 23590294. [Online]. Available: http://dx.doi.org/10.1021/ja311874f

[14] D. Hu, J. Yu, and P. F. Barbara, "Single-molecule spectroscopy of the conjugated polymer meh-ppv," *Journal of the American Chemical Society*, vol. 121, no. 29, pp. 6936–6937, 1999.

[15] P. F. Barbara, A. J. Gesquiere, S.-J. Park, and Y. J. Lee, "Single-molecule spectroscopy of conjugated polymers," *Accounts of chemical research*, vol. 38, no. 7, pp. 602–610, 2005.

[16] T. Huser, M. Yan, and L. J. Rothberg, "Single chain spectroscopy of conformational dependence of conjugated polymer photophysics," *Proceedings of the National Academy of Sciences*, vol. 97, no. 21, pp. 11 187–11 191, 2000.

[17] T. E. D. A, "Photophysics of conjugated polymers," Ph.D. dissertation, National University of Singapore, 2008.

[18] B. Liu and G. C. Bazan, "Homogeneous fluorescence-based dna detection with water-soluble conjugated polymers," *Chemistry of materials*, vol. 16, no. 23, pp. 4467–4476, 2004.

[19] H.-A. Ho, M. Bra-Abrem, and M. Leclerc, "Optical sensors based on hybrid dna/conjugated polymer complexes," *Chemistry A European Journal*, vol. 11, no. 6, pp. 1718–1724, 2005. [Online]. Available: http://dx.doi.org/10.1002/chem.200400537

[20] Z. Liu, H.-L. Wang, and M. Cotlet, "Energy transfer from a cationic conjugated polyelectrolyte to a dna photonic wire: Toward label-free, sequence-specific dna sensing," *Chemistry of Materials*, vol. 26, no. 9, pp. 2900–2906, 2014.

[21] K. Lee, L. K. Povlich, and J. Kim, "Recent advances in fluorescent and colorimetric conjugated polymer-based biosensors," *Analyst*, vol. 135, no. 9, pp. 2179–2189, 2010.

[22] X. Feng, F. Lv, L. Liu, H. Tang, C. Xing, Q. Yang, and S. Wang, "Conjugated polymer nanoparticles for drug delivery and imaging," *ACS applied materials & interfaces*, vol. 2, no. 8, pp. 2429–2435, 2010.

[23] K. Li and B. Liu, "Polymer-encapsulated organic nanoparticles for fluorescence and photoacoustic imaging," *Chemical Society reviews*, 2014.

[24] J. Pecher and S. Mecking, "Nanoparticles of conjugated polymers," *Chemical reviews*, vol. 110, no. 10, pp. 6260–6279, 2010.

[25] A. Kaeser and A. P. Schenning, "Fluorescent nanoparticles based on self-assembled π-conjugated systems," *Advanced Materials*, vol. 22, no. 28, pp. 2985–2997, 2010.

[26] D. Tuncel and H. V. Demir, "Conjugated polymer nanoparticles," *Nanoscale*, vol. 2, no. 4, pp. 484–494, 2010.

[27] C. Zhu, L. Liu, Q. Yang, F. Lv, and S. Wang, "Water-soluble conjugated polymers for imaging, diagnosis, and therapy," *Chemical Reviews*, vol. 112, no. 8, pp. 4687–4735, 2012, pMID: 22670807. [Online]. Available: http://dx.doi.org/10.1021/cr200263w

[28] R. Zhan, "Water-soluble pi-conjugated polymer for biosensor applications," Ph.D. dissertation, National University of Singapore, 2012.

[29] M. Stork, B. S. Gaylord, A. J. Heeger, and G. C. Bazan, "Energy transfer in mixtures of water-soluble oligomers: Effect of charge, aggregation, and surfactant complexation," *Advanced Materials*, vol. 14, no. 5, pp. 361–366, 2002.

[30] C. Fan, K. W. Plaxco, and A. J. Heeger, "High-efficiency fluorescence quenching of conjugated polymers by proteins," *Journal of the American Chemical Society*, vol. 124, no. 20, pp. 5642–5643, 2002.

[31] L. Chen, D. W. McBranch, H.-L. Wang, R. Helgeson, F. Wudl, and D. G. Whitten, "Highly sensitive biological and chemical sensors based on reversible fluorescence quenching in a conjugated polymer," *Proceedings of the National Academy of Sciences*, vol. 96, no. 22, pp. 12 287–12 292, 1999.

[32] C. Zhu, L. Liu, Q. Yang, F. Lv, and S. Wang, "Water-soluble conjugated polymers for imaging, diagnosis, and therapy," *Chemical reviews*, vol. 112, no. 8, pp. 4687–4735, 2012.

[33] K. Pu, "Application of conjugated polyelectrolyte in biosensor," Ph.D. dissertation, National University of Singapore, 2010.

[34] F. Huang, H. Wu, and Y. Cao, "Water/alcohol soluble conjugated polymers as highly efficient electron transporting/injection layer in optoelectronic devices," *Chemical Society Reviews*, vol. 39, no. 7, pp. 2500–2521, 2010.

[35] C. Duan, K. Zhang, C. Zhong, F. Huang, and Y. Cao, "Recent advances in water/alcohol-soluble [small pi]-conjugated materials: new materials and growing applications in solar cells," *Chem. Soc. Rev.*, vol. 42, pp. 9071–9104, 2013. [Online]. Available: http://dx.doi.org/10.1039/C3CS60200A

[36] C. Zhong, C. Duan, F. Huang, H. Wu, and Y. Cao, "Materials and devices toward fully solution processable organic light-emitting diodes," *Chemistry of Materials*, vol. 23, no. 3, pp. 326–340, 2010.

[37] J. K. Mwaura, M. R. Pinto, D. Witker, N. Ananthakrishnan, K. S. Schanze, and J. R. Reynolds, "Photovoltaic cells based on sequentially adsorbed multilayers of conjugated poly(p-phenylene ethynylene)s and a water-soluble fullerene derivative," *Langmuir*, vol. 21, no. 22, pp. 10 119–10 126, 2005, pMID: 16229535. [Online]. Available: http://dx.doi.org/10.1021/la050599m

[38] N. Talik, K. Yeoh, C. Ng, B. Yap, and K. Woon, "Efficient green phosphorescent tandem organic light emitting diodes with solution processable mixed hosts charge generating layer," *Journal of Luminescence*, vol. 154, no. 0, pp. 345 – 349, 2014. [Online]. Available: http://www.sciencedirect.com/science/article/pii/S002223131400266X

[39] C. Zhong, C. Duan, F. Huang, H. Wu, and Y. Cao, "Materials and devices toward fully solution processable organic light-emitting diodes," *Chemistry of Materials*, vol. 23, no. 3, pp. 326–340, 2011. [Online]. Available: http://dx.doi.org/10.1021/cm101937p

[40] S. SHOKRALLA, J. L. SPALL, J. F. GIBSON, and M. HAJIBABAEI, "Next-generation sequencing technologies for environmental dna research," *Molecular Ecology*, vol. 21, no. 8, pp. 1794–1805, 2012. [Online]. Available: http://dx.doi.org/10.1111/j.1365-294X.2012.05538.x

[41] A. Liu, K. Wang, S. Weng, Y. Lei, L. Lin, W. Chen, X. Lin, and Y. Chen, "Development of electrochemical {DNA} biosensors," *TrAC Trends in Analytical Chemistry*, vol. 37, no. 0, pp. 101 – 111, 2012. [Online]. Available: http://www.sciencedirect.com/science/article/pii/S016599361200146X

[42] A. Sassolas, B. D. Leca-Bouvier, and L. J. Blum, "Dna biosensors and microarrays," *Chemical Reviews*, vol. 108, no. 1, pp. 109–139, 2008, pMID: 18095717. [Online]. Available: http://dx.doi.org/10.1021/cr0684467

[43] B. Liu and G. C. Bazan, "Homogeneous fluorescence-based dna detection with water-soluble conjugated polymers," *Chemistry of Materials*, vol. 16, no. 23, pp. 4467–4476, 2004. [Online]. Available: http://dx.doi.org/10.1021/cm049587x

[44] S. W. Thomas, G. D. Joly, and T. M. Swager, "Chemical sensors based on amplifying fluorescent conjugated polymers," *Chemical Reviews*, vol. 107, no. 4, pp. 1339–1386, 2007.

[45] F. He, Y. Tang, S. Wang, Y. Li, and D. Zhu, "Fluorescent amplifying recognition for dna g-quadruplex folding with a cationic conjugated polymer: a platform for homogeneous potassium detection," *Journal of the American Chemical Society*, vol. 127, no. 35, pp. 12 343–12 346, 2005, pMID: 16131213. [Online]. Available: http://dx.doi.org/10.1021/ja051507i

[46] D. Wang, J. Wang, D. Moses, G. C. Bazan, and A. J. Heeger, "Photoluminescence quenching of conjugated macromolecules by bipyridinium derivatives in aqueous media: charge dependence," *Langmuir*, vol. 17, no. 4, pp. 1262–1266, 2001.

[47] C. Tan, E. Atas, J. G. Mller, M. R. Pinto, V. D. Kleiman, and K. S. Schanze, "Amplified quenching of a conjugated polyelectrolyte by cyanine dyes," *Journal of the American Chemical Society*, vol. 126, no. 42, pp. 13 685–13 694, 2004, pMID: 15493926. [Online]. Available: http://dx.doi.org/10.1021/ja046856b

[48] K.-Y. Pu and B. Liu, "Fluorescence turn-on responses of anionic and cationic conjugated polymers toward proteins: Effect of electrostatic and hydrophobic interactions," *The Journal of Physical Chemistry B*, vol. 114, no. 9, pp. 3077–3084, 2010, pMID: 20199117. [Online]. Available: http://dx.doi.org/10.1021/jp906433u

[49] S. Wang, B. S. Gaylord, and G. C. Bazan, "Fluorescein provides a resonance gate for fret from conjugated polymers to dna intercalated dyes," *Journal of the American Chemical Society*, vol. 126, no. 17, pp. 5446–5451, 2004, pMID: 15113216. [Online]. Available: http://dx.doi.org/10.1021/ja035550m

[50] C. Fan, K. W. Plaxco, and A. J. Heeger, "High-efficiency fluorescence quenching of conjugated polymers by proteins," *Journal of the American Chemical Society*, vol. 124, no. 20, pp. 5642–5643, 2002, pMID: 12010029. [Online]. Available: http://dx.doi.org/10.1021/ja025899u

[51] I.-B. Kim, J. N. Wilson, and U. H. F. Bunz, "Mannose-substituted ppes detect lectins: A model for ricin sensing," *Chem. Commun.*, pp. 1273–1275, 2005. [Online]. Available: http://dx.doi.org/10.1039/B416587J

[52] M. J. O'Connell, C. K. Chan, W. Li, R. K. Hicks, S. K. Doorn, and H.-L. Wang, "Polyelectrolyte platform for sensitive detection of biological analytes via reversible fluorescence quenching," *Polymer*, vol. 48, no. 26, pp. 7582 – 7589, 2007. [Online]. Available: http://www.sciencedirect.com/science/article/pii/S0032386107010130

[53] S. Kumaraswamy, T. Bergstedt, X. Shi, F. Rininsland, S. Kushon, W. Xia, K. Ley, K. Achyuthan, D. McBranch, and D. Whitten, "Fluorescent-conjugated polymer superquenching facilitates highly sensitive detection of proteases," *Proceedings of the National Academy of Sciences of the United States of America*, vol. 101, no. 20, pp. 7511–7515, 2004. [Online]. Available: http://www.pnas.org/content/101/20/7511.abstract

[54] C. J. Yang, M. Pinto, K. Schanze, and W. Tan, "Direct synthesis of an oligonucleotidepoly(phenylene ethynylene) conjugate with a precise one-to-one molecular ratio," *Angewandte Chemie International Edition*, vol. 44, no. 17, pp. 2572–2576, 2005. [Online]. Available: http://dx.doi.org/10.1002/anie.200462431

[55] J. Sun, Y. Lu, L. Wang, D. Cheng, Y. Sun, and X. Zeng, "Fluorescence turn-on detection of dna based on the aggregation-induced emission of conjugated poly(pyridinium salt)s," *Polym. Chem.*, vol. 4, pp. 4045–4051, 2013. [Online]. Available: http://dx.doi.org/10.1039/C3PY00350G

[56] K. Li and B. Liu, "Water-soluble conjugated polymers as the platform for protein sensors," *Polym. Chem.*, vol. 1, pp. 252–259, 2010. [Online]. Available: http://dx.doi.org/10.1039/B9PY00283A

[57] K. Lee, J.-M. Rouillard, T. Pham, E. Gulari, and J. Kim, "Signal-amplifying conjugated polymerdna hybrid chips," *Angewandte Chemie International Edition*, vol. 46, no. 25, pp. 4667–4670, 2007. [Online]. Available: http://dx.doi.org/10.1002/anie.200700419

[58] S. Kurata, T. Kanagawa, K. Yamada, M. Torimura, T. Yokomaku, Y. Kamagata, and R. Kurane, "Fluorescent quenching-based quantitative detection of specific dna/rna using a bodipy® fl-labeled probe or primer," *Nucleic acids research*, vol. 29, no. 6, pp. e34–e34, 2001.

[59] X. Zhao, Y. Liu, and K. S. Schanze, "A conjugated polyelectrolyte-based fluorescence sensor for pyrophosphate," *Chem. Commun.*, pp. 2914–2916, 2007. [Online]. Available: http://dx.doi.org/10.1039/B706629E

[60] L. Chen, D. W. McBranch, H.-L. Wang, R. Helgeson, F. Wudl, and D. G. Whitten, "Highly sensitive biological and chemical sensors based on reversible fluorescence quenching in a conjugated polymer," *Proceedings of*

the National Academy of Sciences, vol. 96, no. 22, pp. 12 287–12 292, 1999. [Online]. Available: http://www.pnas.org/content/96/22/12287.abstract

[61] K.-Y. Pu and B. Liu, "Conjugated polyelectrolytes as light-up macromolecular probes for heparin sensing," *Advanced Functional Materials*, vol. 19, no. 2, pp. 277–284, 2009. [Online]. Available: http://dx.doi.org/10.1002/adfm.200800960

[62] D. Yu, Y. Zhang, and B. Liu, "Interpolyelectrolyte complexes of anionic water-soluble conjugated polymers and proteins as platforms for multicolor protein sensing and quantification," *Macromolecules*, vol. 41, no. 11, pp. 4003–4011, 2008. [Online]. Available: http://dx.doi.org/10.1021/ma800082k

[63] H.-A. Ho and M. Leclerc, "Optical sensors based on hybrid aptamer/conjugated polymer complexes," *Journal of the American Chemical Society*, vol. 126, no. 5, pp. 1384–1387, 2004, pMID: 14759196. [Online]. Available: http://dx.doi.org/10.1021/ja037289f

[64] F. He, Y. Tang, M. Yu, F. Feng, L. An, H. Sun, S. Wang, Y. Li, D. Zhu, and G. C. Bazan, "Quadruplex-to-duplex transition of g-rich oligonucleotides probed by cationic water-soluble conjugated polyelectrolytes," *Journal of the American Chemical Society*, vol. 128, no. 21, pp. 6764–6765, 2006, pMID: 16719437. [Online]. Available: http://dx.doi.org/10.1021/ja058075w

[65] F. Feng, Y. Tang, F. He, M. Yu, X. Duan, S. Wang, Y. Li, and D. Zhu, "Cationic conjugated polymer/dna complexes for amplified fluorescence assays of nucleases and methyltransferases," *Advanced Materials*, vol. 19, no. 21, pp. 3490–3495, 2007. [Online]. Available: http://dx.doi.org/10.1002/adma.200700165

[66] J. H. Wosnick, C. M. Mello, and T. M. Swager, "Synthesis and application of poly(phenylene ethynylene)s for bioconjugation: a conjugated polymer-based fluorogenic probe for proteases," *Journal of the American Chemical Society*, vol. 127, no. 10, pp. 3400–3405, 2005, pMID: 15755158. [Online]. Available: http://dx.doi.org/10.1021/ja043134b

[67] A. M. Maxam and W. Gilbert, "A new method for sequencing dna," *Proceedings of the National Academy of Sciences*, vol. 74, no. 2, pp. 560–564, 1977.

[68] F. Sanger, S. Nicklen, and A. R. Coulson, "Dna sequencing with chain-terminating inhibitors," *Proceedings of the National Academy of Sciences*, vol. 74, no. 12, pp. 5463–5467, 1977.

[69] R. K. Saiki, S. Scharf, F. Faloona, K. B. Mullis, G. T. Horn, H. A. Erlich, and N. Arnheim, "Enzymatic amplification of beta-globin genomic sequences and restriction site analysis for diagnosis of sickle cell anemia," *Science*, vol. 230, no. 4732, pp. 1350–1354, 1985.

[70] W. Rychlik, W. Spencer, and R. Rhoads, "Optimization of the annealing temperature for dna amplification in vitro," *Nucleic acids research*, vol. 18, no. 21, pp. 6409–6412, 1990.

[71] E. T. Lagally, C. A. Emrich, and R. A. Mathies, "Fully integrated pcr-capillary electrophoresis microsystem for dna analysis," *Lab on a Chip*, vol. 1, no. 2, pp. 102–107, 2001.

[72] W. J. Ansorge, "Next-generation dna sequencing techniques," *New biotechnology*, vol. 25, no. 4, pp. 195–203, 2009.

[73] M. Strömberg, J. Göransson, K. Gunnarsson, M. Nilsson, P. Svedlindh, and M. Strømme, "Sensitive molecular diagnostics using volume-amplified magnetic nanobeads," *Nano letters*, vol. 8, no. 3, pp. 816–821, 2008.

[74] J. Shendure and H. Ji, "Next-generation dna sequencing," *Nature biotechnology*, vol. 26, no. 10, pp. 1135–1145, 2008.

[75] F. Teles and L. Fonseca, "Trends in dna biosensors," *Talanta*, vol. 77, no. 2, pp. 606–623, 2008.

[76] N. Campbell, J. A. Evans, and N. Fawcett, "Detection of poly (u) hybridization using azido modified poly (a) coated piezoelectric crystals," *Biochemical and biophysical research communications*, vol. 196, no. 2, pp. 858–863, 1993.

[77] K. M. Hansen and T. Thundat, "Microcantilever biosensors," *Methods*, vol. 37, no. 1, pp. 57–64, 2005.

[78] F. Caruso, E. Rodda, D. N. Furlong, K. Niikura, and Y. Okahata, "Quartz crystal microbalance study of dna immobilization and hybridization for nucleic acid sensor development," *Analytical Chemistry*, vol. 69, no. 11, pp. 2043–2049, 1997.

[79] J. Sakong, H. Roh, and Y. Roh, "Surface acoustic wave dna sensor with micro-fluidic channels," *Japanese Journal of Applied Physics*, vol. 46, no. 7S, p. 4729, 2007.

[80] C. Jiang, T. Yang, K. Jiao, and H. Gao, "A dna electrochemical sensor with poly-l-lysine/single-walled carbon nanotubes films and its application for the highly sensitive eis detection of pat gene fragment and pcr amplification of nos gene," *Electrochimica Acta*, vol. 53, no. 6, pp. 2917–2924, 2008.

[81] C. F. Edman, D. E. Raymond, D. J. Wu, E. Tu, R. G. Sosnowski, W. F. Butler, M. Nerenberg, and M. J. Heller, "Electric field directed nucleic acid hybridization on microchips," *Nucleic Acids Research*, vol. 25, no. 24, pp. 4907–4914, 1997.

[82] P. Fortina, S. Surrey, and L. J. Kricka, "Molecular diagnostics: hurdles for clinical implementation," *Trends in Molecular Medicine*, vol. 8, no. 6, pp. 264–266, 2002.

[83] S. Mulvaney, C. Cole, M. Kniller, M. Malito, C. Tamanaha, J. Rife, M. Stanton, and L. Whitman, "Rapid, femtomolar bioassays in complex matrices combining microfluidics and magnetoelectronics," *Biosensors and Bioelectronics*, vol. 23, no. 2, pp. 191–200, 2007.

[84] S. Kwakye and A. Baeumner, "A microfluidic biosensor based on nucleic acid sequence recognition," *Analytical and bioanalytical chemistry*, vol. 376, no. 7, pp. 1062–1068, 2003.

[85] I. L. Medintz, H. T. Uyeda, E. R. Goldman, and H. Mattoussi, "Quantum dot bioconjugates for imaging, labelling and sensing," *Nature materials*, vol. 4, no. 6, pp. 435–446, 2005.

[86] H.-A. Ho, M. Bra-Abrem, and M. Leclerc, "Optical sensors based on hybrid dna/conjugated polymer complexes," *Chemistry A European Journal*, vol. 11, no. 6, pp. 1718–1724, 2005. [Online]. Available: http://dx.doi.org/10.1002/chem.200400537

[87] H.-A. Ho, M. Boissinot, M. G. Bergeron, G. Corbeil, K. Dor, D. Boudreau, and M. Leclerc, "Colorimetric and fluorometric detection of nucleic acids using cationic polythiophene derivatives," *Angewandte Chemie International Edition*, vol. 41, no. 9, pp. 1548–1551, 2002. [Online]. Available: http://dx.doi.org/10.1002/1521-3773(20020503)41:9¡1548::AID-ANIE1548¿3.0.CO;2-I

[88] P. Wang, C. Collison, and L. Rothberg, "Origins of aggregation quenching in luminescent phenylenevinylene polymers," *Journal of Photochemistry and Photobiology A: Chemistry*, vol. 144, no. 1, pp. 63 – 68, 2001, light-Emitting Polymers. [Online]. Available: http://www.sciencedirect.com/science/article/pii/S1010603001005184

[89] K. P. R. Nilsson and O. Inganäs, "Chip and solution detection of dna hybridization using a luminescent zwitterionic polythiophene derivative," *Nature materials*, vol. 2, no. 6, pp. 419–424, 2003.

[90] J. Hong, W. Hemme, G. Keller, M. Rinke, and G. Bazan, "Conjugated-polymer/dna interpolyelectrolyte complexes for accurate dna concentration determination," *Advanced Materials*, vol. 18, no. 7, pp. 878–882, 2006. [Online]. Available: http://dx.doi.org/10.1002/adma.200501605

[91] C. Chi, A. Chworos, J. Zhang, A. Mikhailovsky, and G. C. Bazan, "Anatomy and growth characteristics of conjugated polyelectrolyte/dna aggregates," *Advanced Functional Materials*, vol. 18, no. 22, pp. 3606–3612, 2008.

[92] J. Rubio-Magnieto, A. Thomas, S. Richeter, A. Mehdi, P. Dubois, R. Lazzaroni, S. Clement, and M. Surin, "Chirality in dna-[small pi]-conjugated polymer supramolecular structures: insights into the self-assembly," *Chem. Commun.*, vol. 49, pp. 5483–5485, 2013. [Online]. Available: http://dx.doi.org/10.1039/C3CC42108B

[93] J. Rubio-Magnieto, A. Thomas, S. Richeter, A. Mehdi, P. Dubois, R. Lazzaroni, S. Clément, and M. Surin, "Chirality in dna–π-conjugated polymer supramolecular structures: insights into the self-assembly," *Chemical Communications*, vol. 49, no. 48, pp. 5483–5485, 2013.

[94] M. Surin, P. G. Janssen, R. Lazzaroni, P. Leclère, E. Meijer, and A. P. Schenning, "Supramolecular organization of ssdna-templated π-conjugated oligomers via hydrogen bonding," *Advanced Materials*, vol. 21, no. 10-11, pp. 1126–1130, 2009.

[95] F. Brustolin, M. Surin, V. Lemaur, G. Romanazzi, Q. Sun, J. Cornil, R. Lazzaroni, N. A. J. M. Sommerdijk, P. Leclère, and E. W. Meijer, "The self-assembly of amphiphilic oligothiophenes: Hydrogen bonding and poly(glutamate) complexation," *Bulletin of the Chemical Society of Japan*, vol. 80, no. 9, pp. 1703–1715, 2007.

[96] M. Surin, P. G. Janssen, R. Lazzaroni, P. Leclère, E. Meijer, and A. P. Schenning, "Supramolecular organization of ssdna-templated π-conjugated oligomers via hydrogen bonding," *Advanced Materials*, vol. 21, no. 10-11, pp. 1126–1130, 2009.

[97] J. Rubio-Magnieto, A. Thomas, S. Richeter, A. Mehdi, P. Dubois, R. Lazzaroni, S. Clement, and M. Surin, "Chirality in dna-[small pi]-conjugated polymer supramolecular structures: insights into the self-assembly," *Chem. Commun.*, vol. 49, pp. 5483–5485, 2013. [Online]. Available: http://dx.doi.org/10.1039/C3CC42108B

[98] R. Freeman and I. Willner, "Optical molecular sensing with semiconductor quantum dots (qds)," *Chemical Society Reviews*, vol. 41, no. 10, pp. 4067–4085, 2012.

[99] M. Kang, O. K. Nag, R. R. Nayak, S. Hwang, H. Suh, and H. Y. Woo, "Signal amplification by changing counterions in conjugated polyelectrolyte-based fret dna detection," *Macromolecules*, vol. 42, no. 7, pp. 2708–2714, 2009. [Online]. Available: http://dx.doi.org/10.1021/ma802647u

[100] Y. Jin, R. Yang, H. Suh, and H. Y. Woo, "Cationic and anionic conjugated polyelectrolytes: Aggregation-mediated fluorescence energy transfer to dye-labeled dna," *Macromolecular Rapid Communications*, vol. 29, no. 16, pp. 1398–1402, 2008. [Online]. Available: http://dx.doi.org/10.1002/marc.200800215

[101] J. Zhang, B. Xing, J. Song, F. Zhang, C. Nie, L. Jiao, L. Liu, F. Lv, and S. Wang, "Associated analysis of dna methylation for cancer detection using ccp-based fret technique," *Analytical Chemistry*, vol. 86, no. 1, pp. 346–350, 2014, pMID: 24320047. [Online]. Available: http://dx.doi.org/10.1021/ac402720g

[102] F. Feng, L. Liu, and S. Wang, "Fluorescent conjugated polymer-based fret technique for detection of dna methylation of cancer cells," *Nature protocols*, vol. 5, no. 7, pp. 1255–1264, 2010.

[103] J. R. Lakowicz, *Principles of Fluorescence Spectroscopy*, 2nd ed. Kluwer Academic/Plenum Publishers, 1999.

[104] B. S. Gaylord, A. J. Heeger, and G. C. Bazan, "Dna detection using water-soluble conjugated polymers and peptide nucleic acid probes," *Proceedings of the National Academy of Sciences*, vol. 99, no. 17, pp. 10 954–10 957, 2002.

[105] X. Ren and Q.-H. Xu, "Label-free dna sequence detection with enhanced sensitivity and selectivity using cationic conjugated polymers and picogreen," *Langmuir*, vol. 25, no. 1, pp. 43–47, 2008.

[106] K.-Y. Pu and B. Liu, "Optimizing the cationic conjugated polymer-sensitized fluorescent signal of dye labeled oligonucleotide for biosensor applications," *Biosensors and Bioelectronics*, vol. 24, no. 5, pp. 1067–1073, 2009.

[107] O. K. Nag, M. Kang, S. Hwang, H. Suh, and H. Y. Woo, "Counterion effects on fluorescence energy transfer in conjugated polyelectrolyte-based dna detection," *The Journal of Physical Chemistry B*, vol. 113, no. 17, pp. 5788–5793, 2009. [Online]. Available: http://dx.doi.org/10.1021/jp8107733

[108] K.-Y. Pu, S. Y.-H. Pan, and B. Liu, "Optimization of interactions between a cationic conjugated polymer and chromophore-labeled dna for optical amplification of fluorescent sensors," *The Journal of Physical Chemistry B*, vol. 112, no. 31, pp. 9295–9300, 2008.

[109] B. Liu and G. C. Bazan, "Optimization of the molecular orbital energies of conjugated polymers for optical amplification of fluorescent sensors," *Journal of the American Chemical Society*, vol. 128, no. 4, pp. 1188–1196, 2006, pMID: 16433535. [Online]. Available: http://dx.doi.org/10.1021/ja055382t

[110] M. Kang, O. K. Nag, S. Hwang, I. Kim, H. Yang, K. Kyhm, and H. Y. Woo, "Solvent-assisted optical modulation of fret-induced fluorescence for efficient conjugated polymer-based dna detection," *Phys. Chem. Chem. Phys.*, vol. 12, pp. 15 482–15 489, 2010. [Online]. Available: http://dx.doi.org/10.1039/C0CP01025A

[111] M. Kang, O. K. Nag, R. R. Nayak, S. Hwang, H. Suh, and H. Y. Woo, "Signal amplification by changing counterions in conjugated polyelectrolyte-based fret dna detection," *Macromolecules*, vol. 42, no. 7, pp. 2708–2714, 2009. [Online]. Available: http://dx.doi.org/10.1021/ma802647u

[112] B. Liu, B. S. Gaylord, S. Wang, and G. C. Bazan, "Effect of chromophore-charge distance on the energy transfer properties of water-soluble conjugated oligomers," *Journal of the American Chemical Society*, vol. 125, no. 22, pp. 6705–6714, 2003, pMID: 12769580. [Online]. Available: http://dx.doi.org/10.1021/ja028961w

[113] H. A. Al Attar and A. P. Monkman, "Effect of surfactant on water-soluble conjugated polymer used in biosensor," *The Journal of Physical Chemistry B*, vol. 111, no. 43, pp. 12 418–12 426, 2007, pMID: 17918987. [Online]. Available: http://dx.doi.org/10.1021/jp070827g

[114] Y.-Q. Huang, Q.-L. Fan, X.-F. Liu, N.-N. Fu, and W. Huang, "Solvent- and ph-induced self-assembly of cationic meta-linked poly(phenylene ethynylene): Effects of helix formation on amplified fluorescence quenching and forster resonance energy transfer," *Langmuir*, vol. 26, no. 24, pp. 19 120–19 128, 2010, pMID: 21114280. [Online]. Available: http://dx.doi.org/10.1021/la103394c

[115] Y. Wang and B. Liu, "Silica nanoparticle assisted dna assays for optical signal amplification of conjugated polymer based fluorescent sensors," *Chem. Commun.*, pp. 3553–3555, 2007. [Online]. Available: http://dx.doi.org/10.1039/B705936A

[116] H. Xu, H. Wu, F. Huang, S. Song, W. Li, Y. Cao, and C. Fan, "Magnetically assisted dna assays: high selectivity using conjugated polymers for amplified fluorescent transduction," *Nucleic Acids Research*, vol. 33, no. 9, p. e83, 2005. [Online]. Available: http://nar.oxfordjournals.org/content/33/9/e83.abstract

[117] A. Najari, H. A. Ho, J.-F. Gravel, P. Nobert, D. Boudreau, and M. Leclerc, "Reagentless ultrasensitive specific dna array detection based on responsive polymeric biochips," *Analytical Chemistry*, vol. 78, no. 22, pp. 7896–7899, 2006, pMID: 17105186. [Online]. Available: http://dx.doi.org/10.1021/ac061650+

[118] C. Sun, B. S. Gaylord, J. W. Hong, B. Liu, and G. C. Bazan, "Application of cationic conjugated polymers in microarrays using label-free dna targets," *Nature protocols*, vol. 2, no. 9, pp. 2148–2151, 2007.

[119] M. Montesern, H. D. Burrows, A. J. M. Valente, R. Mallavia, R. E. Di Paolo, A. L. Maanita, and M. J. Tapia, "Interaction between poly(9,9-bis(6-n,n,n-trimethylammonium)hexyl)fluorene phenylene) bromide and dna as seen by spectroscopy, viscosity, and conductivity: Effect of molecular weights and dna secondary structure," *The Journal of Physical Chemistry B*, vol. 113, no. 5, pp. 1294–1302, 2009. [Online]. Available: http://dx.doi.org/10.1021/jp806353y

[120] J. Preat, D. Zanuy, E. A. Perpete, and C. Alemán, "Binding of cationic conjugated polymers to dna: Atomistic simulations of adducts involving the dickersons dodecamer," *Biomacromolecules*, vol. 12, no. 4, pp. 1298–1304, 2011.

[121] D. Zanuy and C. Alemán, "Dna-conducting polymer complexes: A computational study of the hydrogen bond between building blocks," *The Journal of Physical Chemistry B*, vol. 112, no. 10, pp. 3222–3230, 2008.

[122] N. S. Sariciftci, L. Smilowitz, A. J. Heeger, and F. Wudl, "Photoinduced electron transfer from a conducting polymer to buckminsterfullerene," *Science*, vol. 258, no. 5087, pp. 1474–1476, 1992. [Online]. Available: http://www.sciencemag.org/content/258/5087/1474.abstract

[123] B. Kraabel, J. C. Hummelen, D. Vacar, D. Moses, N. S. Sariciftci, A. J. Heeger, and F. Wudl, "Subpicosecond photoinduced electron transfer from conjugated polymers to functionalized fullerenes," *The Journal of Chemical Physics*, vol. 104, no. 11, 1996.

[124] C. J. Brabec, G. Zerza, G. Cerullo, S. D. Silvestri, S. Luzzati, J. C. Hummelen, and S. Sariciftci, "Tracing photoinduced electron transfer process in conjugated polymer/fullerene bulk heterojunctions in real time," *Chemical Physics Letters*, vol. 340, no. 34, pp. 232 – 236, 2001. [Online]. Available: http://www.sciencedirect.com/science/article/pii/S0009261401004316

[125] G. Yu, J. Gao, J. Hummelen, F. Wudl, and A. Heeger, "Polymer photovoltaic cells: Enhanced efficiencies via a the device structure consisted of a metal (ca

or al) contact on the surface of a blend network of internal donor-acceptor heterojunctions," *Science*, vol. 270, p. 1995, 1789.

[126] R. Service, "Solar energy. outlook brightens for plastic solar cells." *Science (New York, NY)*, vol. 332, no. 6027, p. 293, 2011.

[127] S. E. Shaheen, C. J. Brabec, N. S. Sariciftci, F. Padinger, T. Fromherz, and J. C. Hummelen, "2.5% efficient organic plastic solar cells," *Applied Physics Letters*, vol. 78, no. 6, pp. 841–843, 2001.

[128] R. Marcus, "On the theory of electrochemical and chemical electron transfer processes," *Canadian Journal of Chemistry*, vol. 37, no. 1, pp. 155–163, 1959.

[129] N. S. Sariciftci, D. Braun, C. Zhang, V. I. Srdanov, A. J. Heeger, G. Stucky, and F. Wudl, "Semiconducting polymerbuckminsterfullerene heterojunctions: Diodes, photodiodes, and photovoltaic cells," *Applied Physics Letters*, vol. 62, no. 6, 1993.

[130] R. Koeppe and N. Sariciftci, "Photoinduced charge and energy transfer involving fullerene derivatives," *Photochemical & Photobiological Sciences*, vol. 5, no. 12, pp. 1122–1131, 2006.

[131] F. Liu, Y. Gu, J. W. Jung, W. H. Jo, and T. P. Russell, "On the morphology of polymer-based photovoltaics," *Journal of Polymer Science Part B: Polymer Physics*, vol. 50, no. 15, pp. 1018–1044, 2012. [Online]. Available: http://dx.doi.org/10.1002/polb.23063

[132] H. Hoppe, M. Niggemann, C. Winder, J. Kraut, R. Hiesgen, A. Hinsch, D. Meissner, and N. S. Sariciftci, "Nanoscale morphology of conjugated polymer/fullerene-based bulk-heterojunction solar cells," *Advanced Functional Materials*, vol. 14, no. 10, pp. 1005–1011, 2004.

[133] H. Hoppe, T. Glatzel, M. Niggemann, A. Hinsch, M. C. Lux-Steiner, and N. Sariciftci, "Kelvin probe force microscopy study on conjugated polymer/fullerene bulk heterojunction organic solar cells," *Nano letters*, vol. 5, no. 2, pp. 269–274, 2005.

[134] H. Hoppe and N. S. Sariciftci, "Morphology of polymer/fullerene bulk heterojunction solar cells," *Journal of Materials Chemistry*, vol. 16, no. 1, pp. 45–61, 2006.

[135] D. A. Skoog and D. M. West, *Principles of instrumental analysis*. Saunders College Philadelphia, 1980, vol. 158.

[136] M. KHAN and B. SEMINAR, "Ultraviolet/visible absorption spectroscopy," 2009.

[137] G. D. Fasman, "Circular dichroism and the conformational analysis of biomolecules," 1996.

[138] L. K. Fraiji, D. M. Hayes, and T. Werner, "Static and dynamic fluorescence quenching experiments for the physical chemistry laboratory," *Journal of chemical education*, vol. 69, no. 5, p. 424, 1992.

[139] T. Tao, J. H. Nelson, and C. R. Cantor, "Conformational studies on transfer ribonucleic acid. fluorescence lifetime and nanosecond depolarization measurements on bound ethidium bromide," *Biochemistry*, vol. 9, no. 18, pp. 3514–3524, 1970.

[140] W. Goldburg, "Dynamic light scattering," *American Journal of Physics*, vol. 67, no. 12, pp. 1152–1160, 1999.

[141] B. J. Berne and R. Pecora, *Dynamic light scattering: with applications to chemistry, biology, and physics*. Courier Dover Publications, 2000.

[142] K. K. M. Hans-Jurgen, Butt; Graf, *Physics and chemistry of interfaces*, 2nd ed. Wiley-VCH, 2006.

[143] C. Zhu, L. Liu, Q. Yang, F. Lv, and S. Wang, "Water-soluble conjugated polymers for imaging, diagnosis, and therapy," *Chemical Reviews*, vol. 112, no. 8, pp. 4687–4735, 2012, pMID: 22670807. [Online]. Available: http://dx.doi.org/10.1021/cr200263w

[144] J. Sun, Y. Lu, L. Wang, D. Cheng, Y. Sun, and X. Zeng, "Fluorescence turn-on detection of dna based on the aggregation-induced emission of conjugated poly(pyridinium salt)s," *Polym. Chem.*, vol. 4, pp. 4045–4051, 2013. [Online]. Available: http://dx.doi.org/10.1039/C3PY00350G

[145] K. P. R. Nilsson and O. Inganäs, "Chip and solution detection of dna hybridization using a luminescent zwitterionic polythiophene derivative," *Nature materials*, vol. 2, no. 6, pp. 419–424, 2003.

[146] H. Song, B. Sun, K.-J. Gu, Y. Yang, Y. Zhang, and Q.-D. Shen, "Interactions between cationic conjugated polyelectrolyte and dna and a label-free method for dna detection based on conjugated polyelectrolyte complexes," *Journal of Applied Polymer Science*, vol. 114, no. 2, pp. 1278–1286, 2009. [Online]. Available: http://dx.doi.org/10.1002/app.30566

[147] Z. Liu, H.-L. Wang, and M. Cotlet, "Dna sequence-dependent photoluminescence enhancement in a cationic conjugated polyelectrolyte," *Chemical Communications*, vol. 50, no. 77, pp. 11 311–11 313, 2014.

[148] Y. Gao, C.-C. Wang, L. Wang, and H.-L. Wang, "Conjugated polyelectrolytes with ph-dependent conformations and optical properties," *Langmuir*, vol. 23, no. 14, pp. 7760–7767, 2007, pMID: 17559239. [Online]. Available: http://dx.doi.org/10.1021/la063536s

[149] Z. Liu, H.-L. Wang, and M. Cotlet, "Energy transfer from a cationic conjugated polyelectrolyte to a dna photonic wire: Toward label-free, sequence-specific dna sensing," *Chemistry of Materials*, vol. 26, no. 9, pp. 2900–2906, 2014.

[150] C.-C. Wang, Y. Gao, A. P. Shreve, C. Zhong, L. Wang, K. Mudalige, H.-L. Wang, and M. Cotlet, "Thermochromism of a poly (phenylene vinylene): untangling the roles of polymer aggregate and chain conformation," *The Journal of Physical Chemistry B*, vol. 113, no. 50, pp. 16 110–16 117, 2009.

[151] M. L. Davies, P. Douglas, H. D. Burrows, B. Martincigh, M. d. G. Miguel, U. Scherf, R. Mallavia, and A. Douglas, "In depth analysis of the quenching of three fluorenephenylene-based cationic conjugated polyelectrolytes by dna and dna bases," *The Journal of Physical Chemistry B*, vol. 118, no. 2, pp. 460–469, 2014, pMID: 24350588. [Online]. Available: http://dx.doi.org/10.1021/jp409491d

[152] C.-C. Wang, H. Tsai, H.-H. Shih, S. Jeon, Z. Xu, D. Williams, S. Iyer, T. C. Sanchez, L. Wang, M. Cotlet, and H.-L. Wang, "Synthesis and characterization of ethylene glycol substituted poly(phenylene vinylene) derivatives," *ACS Applied Materials and Interfaces*, vol. 2, no. 3, pp. 738–747, 2010, pMID: 20356275. [Online]. Available: http://dx.doi.org/10.1021/am900766s

[153] A. I. Karsisiotis, N. M. Hessari, E. Novellino, G. P. Spada, A. Randazzo, and M. Webba da Silva, "Topological characterization of nucleic acid g-quadruplexes by uv absorption and circular dichroism," *Angewandte Chemie*, vol. 123, no. 45, pp. 10 833–10 836, 2011.

[154] P. F. Barbara, A. J. Gesquiere, S.-J. Park, and Y. J. Lee, "Single-molecule spectroscopy of conjugated polymers," *Accounts of chemical research*, vol. 38, no. 7, pp. 602–610, 2005.

[155] G. Rossi, R. Chance, and R. Silbey, "Conformational disorder in conjugated polymers," *The Journal of Chemical Physics*, vol. 90, no. 12, pp. 7594–7601, 1989.

[156] Z. Xu, H. Tsai, H.-L. Wang, and M. Cotlet, "Solvent polarity effect on chain conformation, film morphology, and optical properties of a water-soluble conjugated polymer," *The Journal of Physical Chemistry B*, vol. 114,

no. 36, pp. 11 746–11 752, 2010, pMID: 20726542. [Online]. Available: http://dx.doi.org/10.1021/jp105032y

[157] H.-A. Ho, M. Boissinot, M. G. Bergeron, G. Corbeil, K. Dor, D. Boudreau, and M. Leclerc, "Colorimetric and fluorometric detection of nucleic acids using cationic polythiophene derivatives," *Angewandte Chemie International Edition*, vol. 41, no. 9, pp. 1548–1551, 2002. [Online]. Available: http://dx.doi.org/10.1002/1521-3773(20020503)41:9¡1548::AID-ANIE1548¿3.0.CO;2-I

[158] B. S. Gaylord, A. J. Heeger, and G. C. Bazan, "Dna detection using water-soluble conjugated polymers and peptide nucleic acid probes," *Proceedings of the National Academy of Sciences*, vol. 99, no. 17, pp. 10 954–10 957, 2002. [Online]. Available: http://www.pnas.org/content/99/17/10954.abstract

[159] ——, "Dna detection using water-soluble conjugated polymers and peptide nucleic acid probes," *Proceedings of the National Academy of Sciences*, vol. 99, no. 17, pp. 10 954–10 957, 2002. [Online]. Available: http://www.pnas.org/content/99/17/10954.abstract

[160] ——, "Dna hybridization detection with water-soluble conjugated polymers and chromophore-labeled single-stranded dna," *Journal of the American Chemical Society*, vol. 125, no. 4, pp. 896–900, 2003, pMID: 12537486. [Online]. Available: http://dx.doi.org/10.1021/ja027152+

[161] B. S. Gaylord, M. R. Massie, S. C. Feinstein, and G. C. Bazan, "Snp detection using peptide nucleic acid probes and conjugated polymers: applications in neurodegenerative disease identification," *Proceedings of the National Academy of Sciences of the United States of America*, vol. 102, no. 1, pp. 34–39, 2005.

[162] J. Wang, "Survey and summary from dna biosensors to gene chips," *Nucleic Acids Research*, vol. 28, no. 16, pp. 3011–3016, 2000.

[163] H. Song, B. Sun, K.-J. Gu, Y. Yang, Y. Zhang, and Q.-D. Shen, "Interactions between cationic conjugated polyelectrolyte and dna and a label-free method for dna detection based on conjugated polyelectrolyte complexes," *Journal of Applied Polymer Science*, vol. 114, no. 2, pp. 1278–1286, 2009. [Online]. Available: http://dx.doi.org/10.1002/app.30566

[164] Z. Xu, H. Tsai, H.-L. Wang, and M. Cotlet, "Solvent polarity effect on chain conformation, film morphology, and optical properties of a water-soluble conjugated polymer," *The Journal of Physical Chemistry B*, vol. 114, no. 36, pp. 11 746–11 752, 2010, pMID: 20726542. [Online]. Available: http://dx.doi.org/10.1021/jp105032y

[165] S. Wang, B. S. Gaylord, and G. C. Bazan, "Fluorescein provides a resonance gate for fret from conjugated polymers to dna intercalated dyes," *Journal of the American Chemical Society*, vol. 126, no. 17, pp. 5446–5451, 2004, pMID: 15113216. [Online]. Available: http://dx.doi.org/10.1021/ja035550m

[166] B. Wang, Q. Yang, L. Liu, and S. Wang, "Direct energy transfer from conjugated polymer to {DNA} intercalated dye: Label-free fluorescent {DNA} detection," *Colloids and Surfaces B: Biointerfaces*, vol. 85, no. 1, pp. 8 – 11, 2011, special Issue: Biointerfaces in China. [Online]. Available: http://www.sciencedirect.com/science/article/pii/S0927776510005916

[167] X. Shi, E. Borguet, A. Tarnovsky, and K. Eisenthal, "Ultrafast dynamics and structure at aqueous interfaces by second harmonic generation," *Chemical Physics*, vol. 205, no. 12, pp. 167 – 178, 1996, surface Reaction Dynamics. [Online]. Available: http://www.sciencedirect.com/science/article/pii/0301010495003738

[168] D. M. Kolpashchikov, "Binary malachite green aptamer for fluorescent detection of nucleic acids," *Journal of the American Chemical Society*, vol. 127, no. 36, pp. 12 442–12 443, 2005, pMID: 16144363. [Online]. Available: http://dx.doi.org/10.1021/ja0529788

[169] S. J. Culp and F. A. Beland, "Malachite green: A toxicological review," *International Journal of Toxicology*, vol. 15, no. 3, pp. 219–238, 1996. [Online]. Available: http://ijt.sagepub.com/content/15/3/219.abstract

[170] J. L. Seifert, R. E. Connor, S. A. Kushon, M. Wang, and B. A. Armitage, "Spontaneous assembly of helical cyanine dye aggregates on dna nanotemplates," *Journal of the American Chemical Society*, vol. 121, no. 13, pp. 2987–2995, 1999. [Online]. Available: http://dx.doi.org/10.1021/ja984279j

[171] M. Wang, G. L. Silva, and B. A. Armitage, "Dna-templated formation of a helical cyanine dye j-aggregate," *Journal of the American Chemical Society*, vol. 122, no. 41, pp. 9977–9986, 2000. [Online]. Available: http://dx.doi.org/10.1021/ja002184n

[172] H. Ihmels, K. Faulhaber, D. Vedaldi, F. Dall'Acqua, and G. Viola, "Intercalation of organic dye molecules into double-stranded dna. part 2: The annelated quinolizinium ion as a structural motif in dna intercalators," *Photochemistry and Photobiology*, vol. 81, no. 5, pp. 1107–1115, 2005. [Online]. Available: http://dx.doi.org/10.1562/2005-01-25-IR-427

[173] B. Nordn, F. Tjerneld, and E. Palm, "Linear dichroism studies of binding site structures in solution: Complexes between {DNA} and basic arylmethane

dyes," *Biophysical Chemistry*, vol. 8, no. 1, pp. 1 – 15, 1978. [Online]. Available: http://www.sciencedirect.com/science/article/pii/0301462278850182

[174] B. Nordn and T. Kurucsev, "Analysing dna complexes by circular and linear dichroism," *Journal of Molecular Recognition*, vol. 7, no. 2, pp. 141–155, 1994. [Online]. Available: http://dx.doi.org/10.1002/jmr.300070211

[175] A. Frstenberg, M. D. Julliard, T. G. Deligeorgiev, N. I. Gadjev, A. A. Vasilev, and E. Vauthey, "Ultrafast excited-state dynamics of dna fluorescent intercalators: new insight into the fluorescence enhancement mechanism," *Journal of the American Chemical Society*, vol. 128, no. 23, pp. 7661–7669, 2006, pMID: 16756323. [Online]. Available: http://dx.doi.org/10.1021/ja0609001

[176] K. M. Sovenyhazy, J. A. Bordelon, and J. T. Petty, "Spectroscopic studies of the multiple binding modes of a trimethinebridged cyanine dye with dna," *Nucleic Acids Research*, vol. 31, no. 10, pp. 2561–2569, 2003. [Online]. Available: http://nar.oxfordjournals.org/content/31/10/2561.abstract

[177] F. C. De Schryver, T. Vosch, M. Cotlet, M. Van der Auweraer, K. Mllen, and J. Hofkens, "Energy dissipation in multichromophoric single dendrimers," *Accounts of Chemical Research*, vol. 38, no. 7, pp. 514–522, 2005, pMID: 16028885. [Online]. Available: http://dx.doi.org/10.1021/ar040126r

[178] J. K. Hannestad, S. R. Gerrard, T. Brown, and B. Albinsson, "Self-assembled dna-based fluorescence waveguide with selectable output," *Small*, vol. 7, no. 22, pp. 3178–3185, 2011. [Online]. Available: http://dx.doi.org/10.1002/smll.201101144

[179] N. Tian, Y. Tang, Q.-H. Xu, and S. Wang, "Single base pair mismatch detection using cationic conjugated polymers through fluorescence resonance energy transfer," *Macromolecular Rapid Communications*, vol. 28, no. 6, pp. 729–732, 2007. [Online]. Available: http://dx.doi.org/10.1002/marc.200600855

[180] B. Wang, Q. Yang, L. Liu, and S. Wang, "Direct energy transfer from conjugated polymer to {DNA} intercalated dye: Label-free fluorescent {DNA} detection," *Colloids and Surfaces B: Biointerfaces*, vol. 85, no. 1, pp. 8 – 11, 2011, special Issue: Biointerfaces in China. [Online]. Available: http://www.sciencedirect.com/science/article/pii/S0927776510005916

[181] A. Pivrikas, N. S. Sariciftci, G. Juka, and R. sterbacka, "A review of charge transport and recombination in polymer/fullerene organic solar cells," *Progress in Photovoltaics: Research and Applications*, vol. 15, no. 8, pp. 677–696, 2007. [Online]. Available: http://dx.doi.org/10.1002/pip.791

[182] X. Yang and J. Loos, "Toward high-performance polymer solar cells: the importance of morphology control," *Macromolecules*, vol. 40, no. 5, pp. 1353–1362, 2007. [Online]. Available: http://dx.doi.org/10.1021/ma0618732

[183] F. Yakuphanoglu, "Photovoltaic properties of the organicinorganic photodiode based on polymer and fullerene blend for optical sensors," *Sensors and Actuators A: Physical*, vol. 141, no. 2, pp. 383 – 389, 2008. [Online]. Available: http://www.sciencedirect.com/science/article/pii/S0924424707007364

[184] H.-L. Wang, D. W. McBranch, R. J. Donohoe, S. Xu, B. Kraabel, C. LIAO-HAI, D. Whitten, R. Helgeson, and F. Wudl, "Highly efficient energy and charge transfer in thin self-assembled multilayered polymer films," *Synthetic metals*, vol. 121, no. 1-3, pp. 1367–1368, 2001.

[185] A. Garcia, R. Yang, Y. Jin, B. Walker, and T.-Q. Nguyen, "Structure-function relationships of conjugated polyelectrolyte electron injection layers in polymer light emitting diodes," *Applied Physics Letters*, vol. 91, no. 15, p. 153502, 2007.

[186] Y. I. Park, Y.-S. Park, J. Gao, J. K. Grey, C.-C. Wang, M. A. Johal, J. Park, H. Y. Woo, and H.-L. Wang, "Water-soluble ppv and c¡ sub¿ 60¡/sub¿ nanocomposite with enhanced miscibility and enhanced photo-induced charge transfer through ground state electrostatic interactions," *Polymer*, vol. 55, no. 3, pp. 855–859, 2014.

[187] B. S. Harrison, M. B. Ramey, J. R. Reynolds, and K. S. Schanze, "Amplified fluorescence quenching in a poly (p-phenylene)-based cationic polyelectrolyte," *Journal of the American Chemical Society*, vol. 122, no. 35, pp. 8561–8562, 2000.

[188] Z. Liu, H.-L. Wang, and M. Cotlet, "Dna sequence-dependent photoluminescence enhancement in a cationic conjugated polyelectrolyte," *Chemical Communications*, vol. 50, no. 77, pp. 11 311–11 313, 2014.

[189] P. P. Lee, T. Ngai, J.-D. Huang, C. Wu, W.-P. Fong, and D. K. Ng, "Synthesis, characterization, biodegradation, and in vitro photodynamic activities of silicon (iv) phthalocyanines conjugated axially with poly (ε-caprolactone)," *Macromolecules*, vol. 36, no. 20, pp. 7527–7533, 2003.

[190] D. Wang, J. Wang, D. Moses, G. C. Bazan, and A. J. Heeger, "Photoluminescence quenching of conjugated macromolecules by bipyridinium derivatives in aqueous media: charge dependence," *Langmuir*, vol. 17, no. 4, pp. 1262–1266, 2001.

[191] K. Campbell, A. Zappas, U. Bunz, Y. S. Thio, and D. G. Bucknall, "Fluorescence quenching of a poly (¡ i¿ para¡/i¿-phenylene ethynylenes) by c¡ sub¿ 60¡/sub¿ fullerenes," *Journal of Photochemistry and Photobiology A: Chemistry*, vol. 249, pp. 41–46, 2012.

[192] C. D. Geddes, "Optical halide sensing using fluorescence quenching: theory, simulations and applications-a review," *Measurement Science and Technology*, vol. 12, no. 9, p. R53, 2001.